Mechanical Properties of Titanium Foams Having Disordered and Ordered Cell Structures

不規則及び規則セル構造を有するポーラスチタンの機械的特性

Yue xue-zheng

Department of Aerospace Engineering

Graduate School of System Design

Tokyo Metropolitan University

January 2018

Mechanical Properties of Titanium Foams Having Disordered and Ordered Cell Structures

不規則及び規則セル構造を有するポーラスチタンの機械的特性

by

Yue xuezheng

Student ID 15991504

Submitted to the Department of Aerospace Engineering,
Graduate School of System Design,
in partial fulfillment of the requirements for the degree of
Doctor of Philosophy in Aerospace Engineering

at
TOKYO METROPOLITAN UNIVERSITY
December 2017

Certified by advisor

Professor Koichi Kitazono
Department of Aerospace Engineering
Graduate School of System Design
Tokyo Metropolitan University

Contents

Titanium and titanium alloy are metal material with high tensile strength to density ratio, high corrosion resistance, fatigue resistance, high crack resistance and so on. Metal foams have many advance properties for example: low densities and novel physical, mechanical, thermal, electrical and acoustic properties. Manufacturing titanium foams traditional method and additive manufacturing method are reviewed. The powder sinter process generally consists powder blending, die compaction, and sintering. Compaction is generally performed at room temperature, and the elevated-temperature process of sintering is usually conducted at atmospheric pressure and under carefully controlled atmosphere composition. This titanium foam of 60% porosity product was manufactured by powder metallurgy through compacting and pressure working. Additive manufacturing method builds a three-dimensional object from computer-aided design (CAD) model by laser or electron beam sintered titanium powder layer by layer. it has been widely expected to revolutionize the manufacturing of complex structure, from medical implants to aerospace engineering.

Outline of metal foam research obtained as followed：

Chapter 1： First chapter showed the introduction to physics properties of metal foams, applications of metal foam, many kinds of material（Al, Mg, Cu, Ti, Steel and so on）, Advantages of titanium, manufacture methods of titanium foam and comparison between traditional technology and additive manufacturing. Based on titanium foam, the motivation and objectives of this study are stated.

Chapter 2： Investigates the strain rate sensitivity of commercial pure titanium foam at elevated temperature. Uniaxial compression tests were performed to investigate the effects of temperature and strain rate on the plastic deformation of titanium foams are with high temperature. Stress-strain curves showed line are elastic, plateau and

densification regions which are typical characteristics of titanium foams. Both the flow stress and the energy absorption increase within creasing the strain rate and with decreasing the temperature. Apparent activation energy of the titanium foam was calculated. These results indicate that the thermally activated kinetics of the titanium foam mainly depends on the characteristics of the base material. In addition, XRD analysis showed the excellent oxidation resistance of the titanium foam.

Chapter 3： This chapter aimed to clarify the effects of cell geometry on compressive deformation of open-cell titanium foams. Truncated octahedron and rhombic dodecahedron cells were used as different unit cell geometries by designing a commercial 3D-CAD software. The open cell titanium was printed of 10 kinds of pore structure for energy absorbing application by the electron beam melting process. The nominal porosities of both truncated octahedron cell and rhombic dodecahedron cell are plotted as a function of the normalized edge length. Relationship between the normalized porosity and normalized cell diameter are plotted as a function. The compressive behavior depended on the porosity, cell geometry and the cell orientation. Titanium foams with truncated octahedron cells showed high strength compared to those of rhombic dodecahedron cells. the parallel and oblique cell edges against the compression direction are effective to increase the compressive strength.

Chapter 4: Investigated influence of heat treatment on microstructure, mechanical properties and energy absorption capacities for Ti-6Al-4V foams with octahedron structure by additive manufacturing. Ti-6Al-4V foams were heat treatment at 1173 K and 1323 K (recrystallization annealing) for 1 h cooling by argon atmosphere in furnace. Titanium foams were subjected to different annealing in order to evaluate possibilities to the mechanical properties and energy absorption capacities. The apparent microstructure

of Titanium alloy foams were studied through the SEM, XRD equipment. The Vickers hardness was discussion.

Chapter 5: summarizes the whole results in present. The remaining problems and future works are suggested in the fields of Titanium foam by powder metallurgy and additive manufacture.

Chapter 1: Introduction

1.1 Metal foam

Metal foams are a class of materials with low densities and novel physical, mechanical, thermal, electrical and acoustic properties. They are known for their interesting combinations of physical and mechanical properties such as high stiffness in conjunction with very low specific weight or high compression strengths combined with good energy absorption characteristics [1]. In closed-cell foams each cell is completely enclosed by a thin wall or membrane of metal, whilst in open-cell foams the individual cells are interconnected, allowing tissue to infiltrate the foam and anchor it into position. According to the pores structure, metal foam can be classified into open-cell metal foam (Fig. 1.2) and closed-cell metal foam (Fig. 1.1). The open-cell one has network structure and all the cells are connected, while the structure in closed-cell metal foam contains many airtight bubbles and the bubbles are isolated.

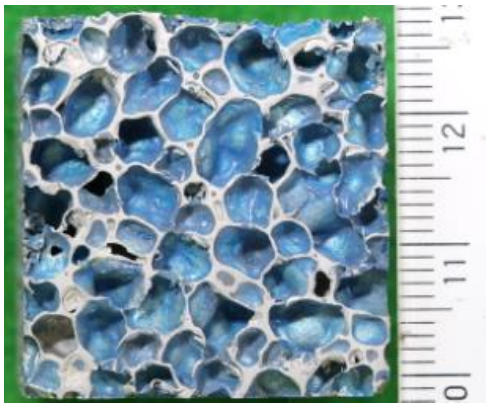

Fig. 1.1 Section of closed-cell aluminum foam

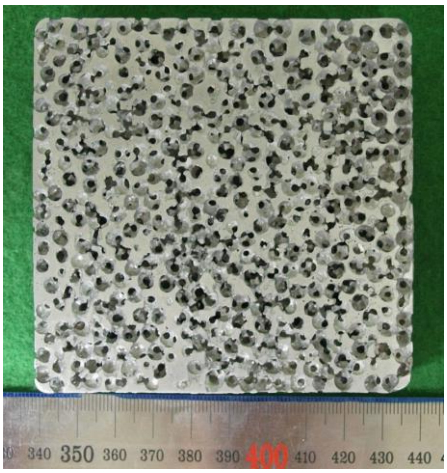

Fig. 1.2 Section of open-cell aluminum foam

To properly identify metallic foam, one has to distinguish:

(1) Cellular metals: the most general term, referring to a metallic body in which any kind of gaseous voids are dispersed. The metallic phase divides space into closed cells which contain the gaseous phase.

(2) Porous metals: a special type of cellular metal restricted to a certain type of voids. Pores are usually rounded and isolated from each other.

(3) (Solid) metal foams: a special class of cellular metals that originate from liquid-metal foams and, therefore, have a restricted morphology. The cells are closed, round, or polyhedral and are separated from each other by thin films.

(4) Metal sponges: morphology of a cellular metal, usually with interconnected voids [2].

1.2 Application of metal foam

Their potential applications of metal foams were in different fields, such as high energy absorption, sound/thermal insulation, heat exchangers, filters, and catalyst carriers.

1.2.1 Automobile industry

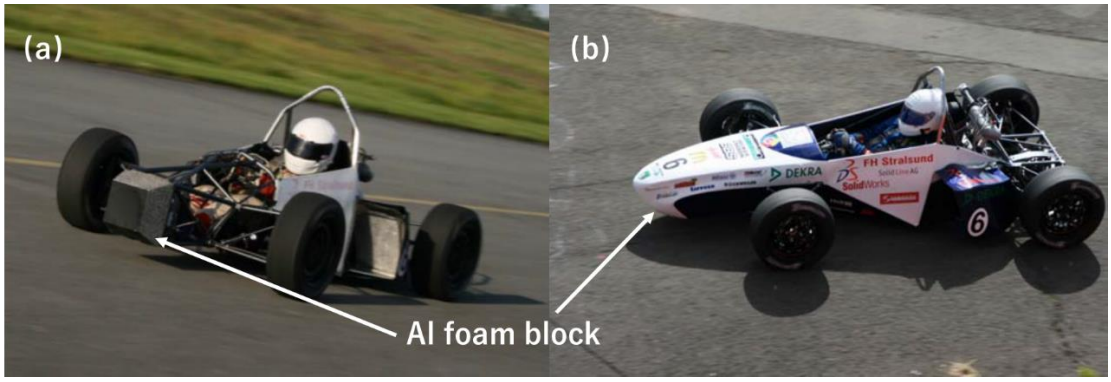

Fig. 1.3 (a) view of car with the front encasement taken off, (b) full view (Courtesy of Sönke Reinhardt).

In automobile industry, metal foams were used as protection materials during side impacts. Energy of frontal collisions was absorbed by deformation of metal foams.

According to the reported by Louis-Philippe Lefebvre, John Banhart and David C. Dunand [3], Alporas metal foam was used as crash protector in the front tip of the chassis of a racing car in Figure 1.3 at the University of Technology of Stralsund, Germany. This metal foam protector was shown to fulfil the requirements of a limitation of deacceleration at 7 m/s impact velocity for a vehicle weight of 300 kg. For electric automobiles, hybrid metal foams can protect the battery packs, it is helpful to cool the battery packs by hybrid metal foams in future.

1.2.2 High-speed trains

The area of high speed trains was also potential application by a typical sandwich structure which are composed of two layers of thin composite material plate or metal plate

and thick metallic foam core which includes grid, metal foam and lattice truss core. The absorb energy can also be used practically to protect vehicles or aircraft from explosions, shrapnel in the military industry.

1.2.3 Chemical industry

Open-cell metal foams, due to their permeable and porous structure, it's very large inner surface and their large ratio of surface area to volume, excellent thermal conductivity, their high thermal and chemical resistance were applications as catalysts in chemical engineering [4].

1.2.4 Aerospace industry

In addition, metal foams as lightweight materials were weight saving in the aerospace field, Aluminum Foam Sandwiches (AFS) was introduced experimentally in the nose cone of Ariane 5 (Fig. 1.4). Aluminum foam sandwich design of the cone comprising an upper ring and 12 Aluminum foam sandwich segments with integrated flange at the bottom [5].

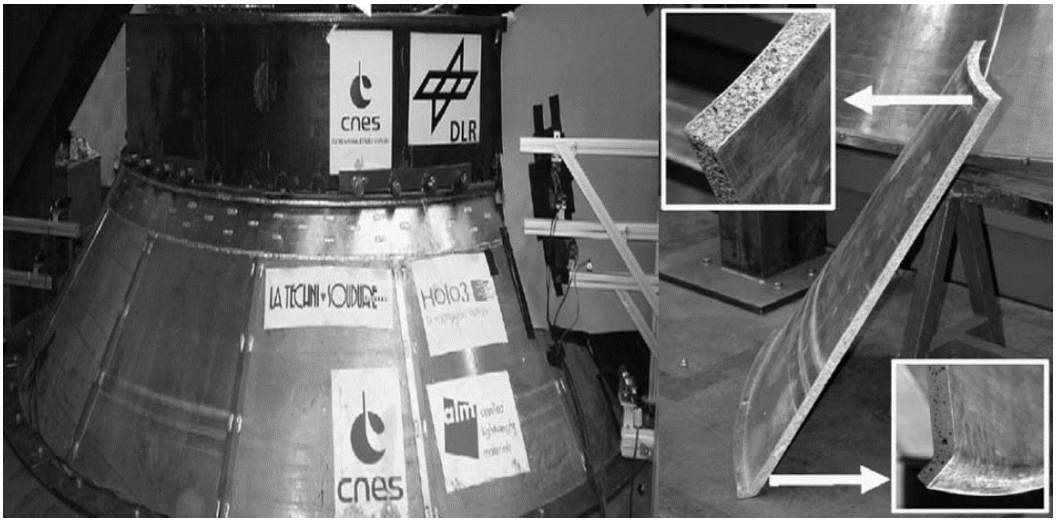

Fig. 1.4. Application of metal foam sandwich structure in the aerospace field.

High-strength light-weight porous metal materials play a significant role in achieving fuel efficiency goals for airplane in Fig. 1.5. They are yield strength and relatively high stiffness and achievable at low density. Some lattice metal was applied in Unmanned Aerial Vehicles (UAVs) to perform various military and civilian applications, for example surveillance of pipelines, attack missions, reconnaissance and interplanetary exploration. Lattice metal been developed and do tis contribution in UAV design and development [6].

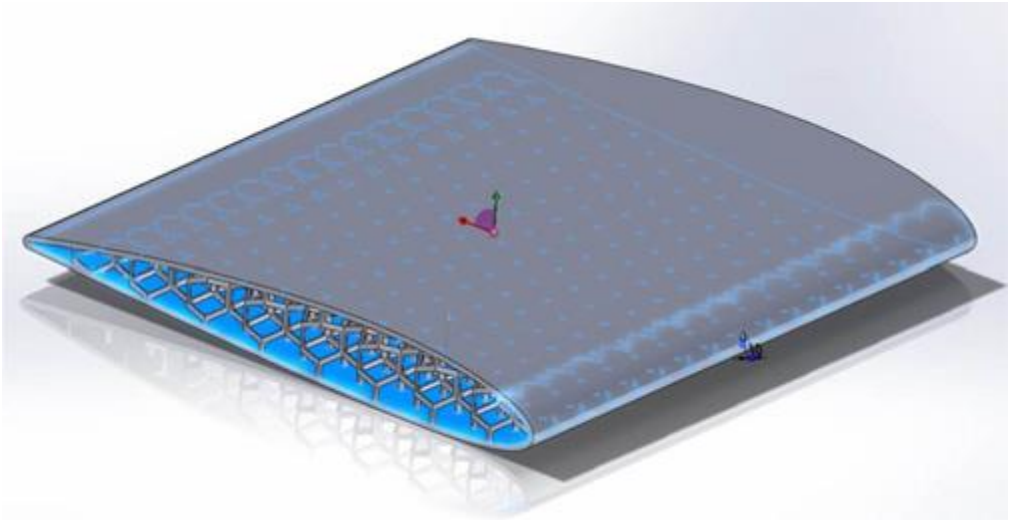

Fig. 1.5 The proposed CAD model of wing with light-weight high strength reinforcement [6].

1.2.5 Biological implant materials

Recently, biomedical open cell metallic materials become the widely used implant materials for hard tissues like dental roots, body-bone and knee. These porous materials are best suited for use as coatings since they do not readily have the required mechanical properties that would allow them to be used as bulk structural materials for implants, bone augmentation, or substitutes for bone graft [7]. Titanium and its alloys are widely used in oral medicine for its excellent mechanical property and biological safety, the research of the titanium-based implant materials is a hot topic. Biocompatible open cell and closed

cell magnesium alloys foam offer great potential as absorbable implant materials. Titanium foam coating uncemented stem for revision hip arthroplasty in figure 1.6 [8].

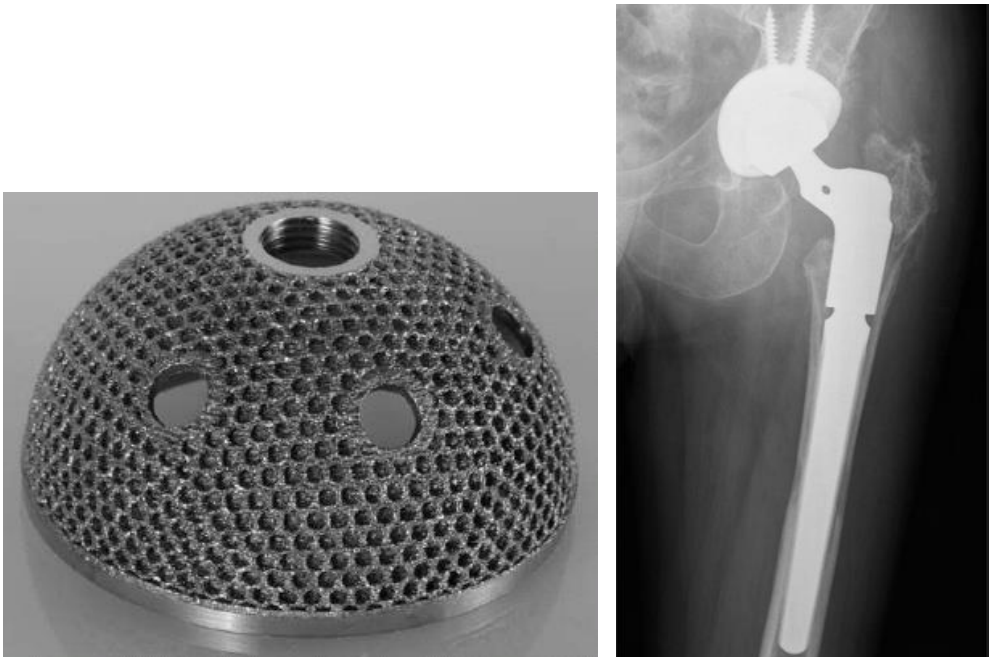

Fig. 1.6 Open-pore titanium foams ac biologic fixation of implant knee. The X ray shows osteointegration of the implant to host bone [8].

1.3 Different material metal foam

1.3.1 Gold material

In Figure 1.7, nanoporous Au was studied to oppose the mechanical properties and deformation behavior of ultra-fine grained nanoporous Au at elevated temperature by A. Leitner [9].

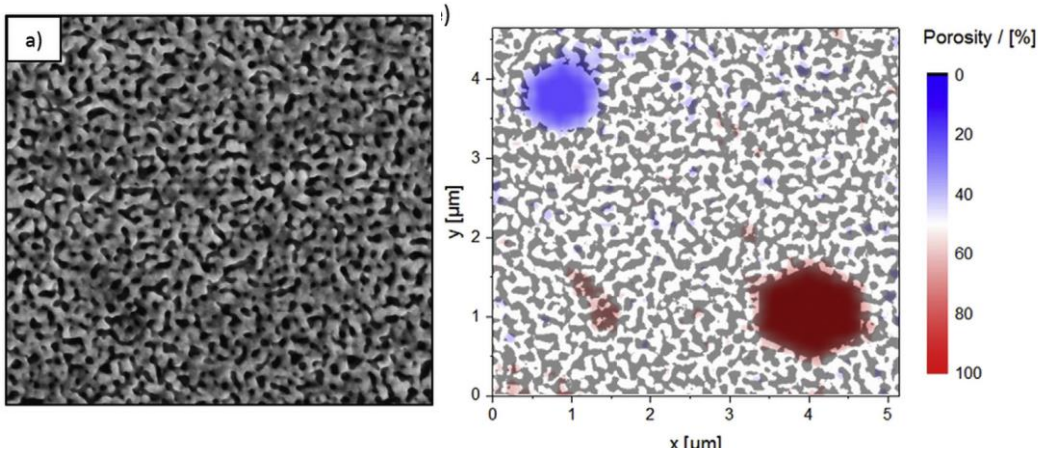

Fig. 1.7 Determination of localized porosity variations in NP Au. a) SEM micrograph of NP Au and e) Resulting porosity map with overlaid binary image which illustrates the local material porosity [9].

1.3.2 Magnesium material

A solid-state space holder method was used to fabricate open cell AZ31 metal foam samples shown in Fig. 1.8, effect of fluidity on the manufacturing of open cell magnesium alloy foams have reported by XZ Yue [10].

Fig. 1.8 The open cell AZ31 Mg alloy foam, sample with 1.70 mm Ø (30 mm*30 mm*30 mm).

1.3.3 Copper material

H. Nakajima [11] reported lotus-type porous copper used a continuous casting technique with long cylindrical pores aligned parallel to the solidification direction in a pressurized hydrogen atmosphere. Effect of transference velocity and hydrogen pressure on porosity and pore morphology of lotus-type porous copper was developed to fabricate technology in Fig 1.9.

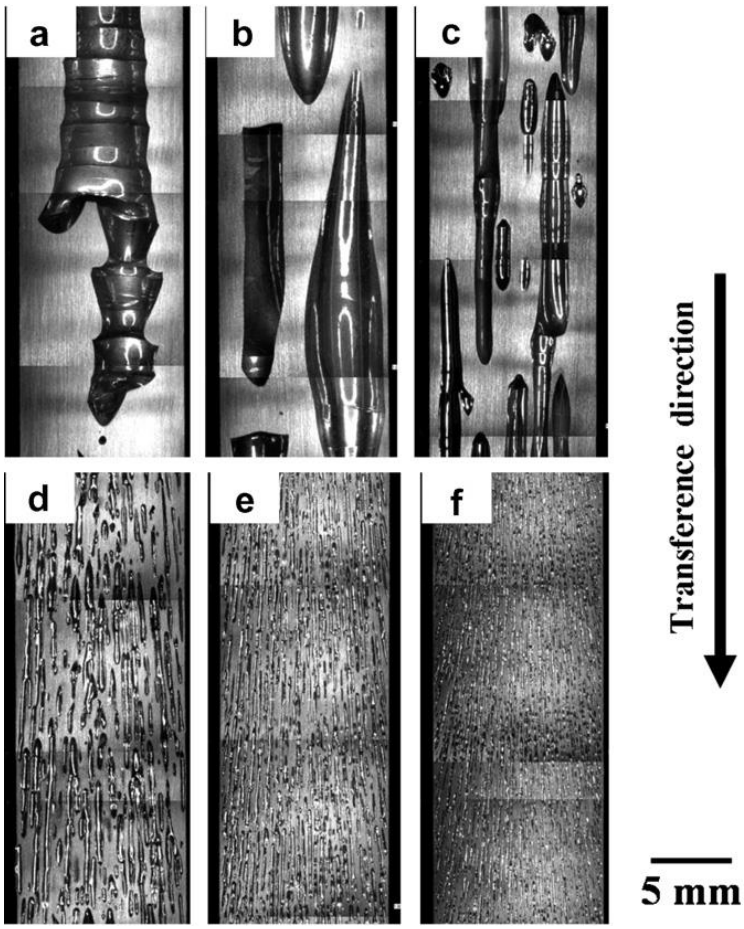

Fig. 1.9 Cross-sections parallel to transference direction of the lotus-type porous copper fabricated under hydrogen gas pressure of 1.0 MPa by the continuous casting technique. Transference velocities are: (a) 1 mm min^{-1}; (b) 5 mm min^{-1};
(c) 10 mm min^{-1}; (d) 20 mm min^{-1}; (e) 50 mm min^{-1} and (f) 100 mm min^{-1}[11].

1.3.4 Aluminum material

Casting-Dissolution Process was used to manufacture the open cell aluminum foams. To make the preform, NaCl particles were sieved to obtain controlled sizes of 2.0 mm, 1.0 mm and 0.5 mm. For Fig. 1.10, X-ray micro-computed tomography (μCT) was employed to obtain the required images [12].

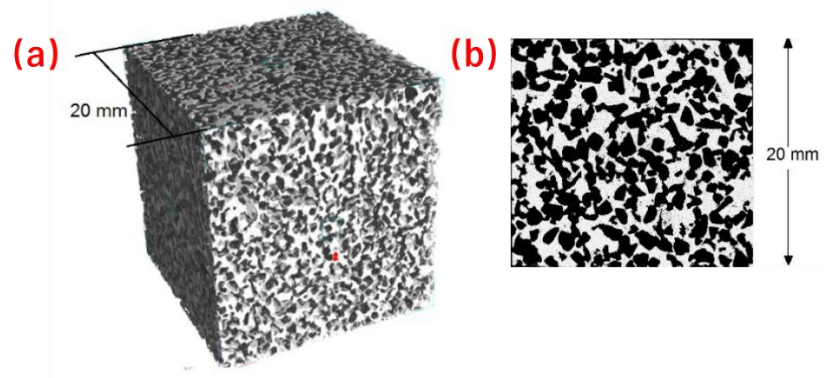

Fig. 1.10 Sample with 0.5 mm pore size: (a) 3D reconstruct using from X-ray micro-computed tomography (b) Sample from SEM.

Shinko Wire (Amagasaki, Japan) provided closed-cell Alporas aluminum foam for testing and evaluation. Relative densities of Alporas foams is approximate 7.4 and 15%. The cell size of these foams with approximately 4–7 mm was studied for the lower density foam, and the high-density foam was 2–3 mm. The macrostructures of closed cell are compared in Fig. 1.11 (a) and (b). The cell aspect ratio differed for the Alporas foams investigated [13].

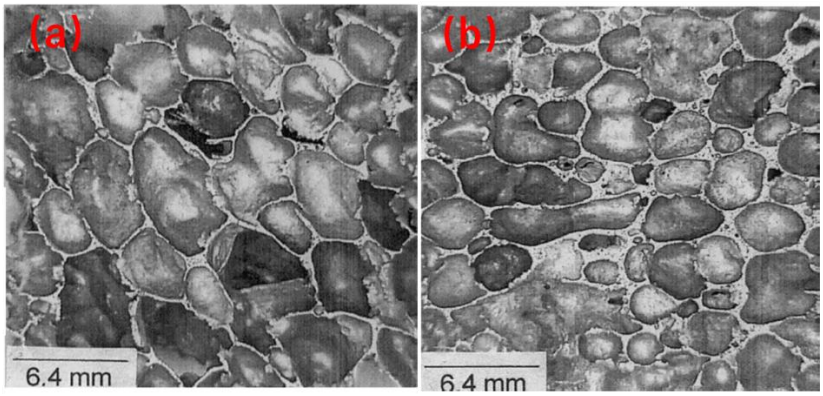

Fig. 1.11 Representative macrostructures: (a) Closed-cell Alporas foam, relative density is 0.07; (b) closed-cell Alporas foam, relative density is 0.15 [13].

1.3.5 Stainless steel material

Foamed steel intentionally introduces internal voids in steel, steel foam is emerging as a new structural material with intriguing properties: high stiffness-to-weight ratio, high energy absorption, and other advantages. Foaming steel increases bending rigidity. Steel hollow sphere foam is 18% relative density shown interior foam morphology through cut section in Fig. 1.12.

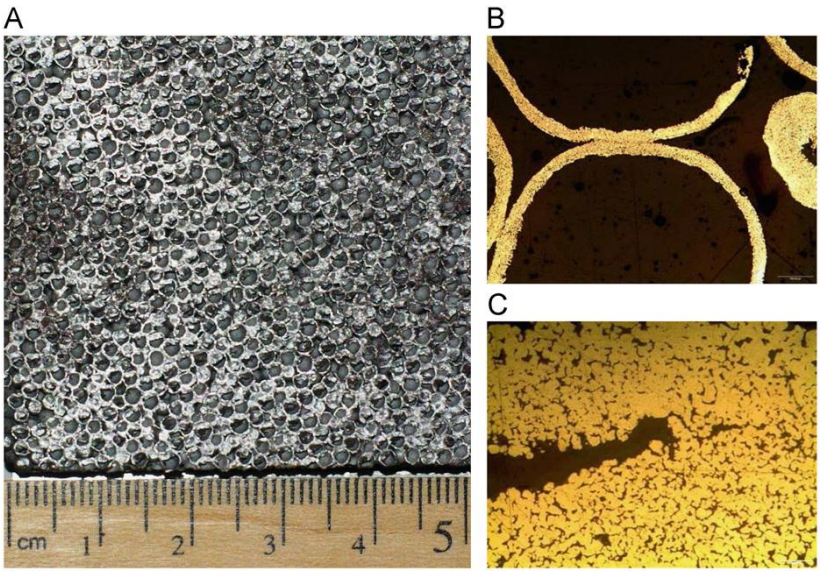

Fig. 1.12 Steel hollow sphere foam 18% relative density: (A)interior foam morphology through cut section, (B) contact between spheres as shown in cross-section, and (C) sphere walls are not fully dense [14].

1.3.6 Titanium material

Titanium alloys and commercial pure titanium have many applications in aerospace industry, for example: naval ships, spacecraft, aircraft, armor plating, and missiles [15] [16] and biology implant material. Due to high tensile strength to high corrosion resistance [15], high crack resistance [17], density ratio [18], fatigue resistance, and ability to withstand moderately high temperatures without creeping, in engine applications, titanium is used for rotors, compressor blades, hydraulic system components, and nacelles. The alloy accounts there are Ti-6AL-4V of almost 50% of titanium alloys used in aircraft industry [19]. Due to resistant to corrosion, titanium alloy used in sea water, some rigging, propeller shafts, and heat exchangers manufacture titanium produce in desalination plants [20].

Many studies have already investigated porous titanium and titanium alloy foam, Compressive and fatigue behavior of beta-type titanium porous structures fabricated by electron beam melting, the super-elastic property is improved with increasing porosity of Ti2448 porous samples, Ti2448 porous samples display only half of the Young's modulus of Ti-6Al-4V porous samples at same fatigue strength level were reported by Y.j.Liu [21]; The effect of surface alloying of Ti powder for vacuum plasma spraying of open porous titanium coatings, The coatings produced were ~1 mm thick and exhibited a porosity of 45–60% were researched by C.Jaeggi [22]; Self-propagating high temperature synthesis of nanostructured titanium aluminide alloys with varying porosity, Nanoscale aluminum (nAl) and nanoscale titanium (nTi) particles were mixed with either nanoscale aluminum passivated with a gasifying agent such as perfluoroalkyl carboxylic acid ($C_{13}F_{27}COOH$) or polytetrafluoroethylene (Teflon) $(C_2F_4)_n$ particles and pressed into pellets. were studied by Cory Farley [23]; Mechanical properties of directionally freeze-

cast titanium foams was published by Jessica C.Li and David C.Dunand [24], Increasing sintering times from 8 to 24 h and decreasing powder size from 20 to 10 μm resulted in improved densification within cell walls and decreased overall foam porosity, with a concomitant increase in compressive stiffness, yield strength and energy absorption; Wetting of porous titanium carbonitride by Al–Mg–Si alloys used the sessile drop experiment by G Levi [25]; Deviations from Weibull statistics in brittle porous materials was reported by Özgür Keleş [26]; Directionally freeze-cast titanium foam with aligned, elongated pores, titanium foams exhibited 57–67% aligned pores (~0.1 mm wide and several millimeters long) replicating the ice dendrites were studied by Yasumasa Chino and David C.Dunand [27]. Titanium with controllable pore fractions by thermoreversible gelcasting of TiH_2, incorporation of polypropylene and poly (methyl methacrylate) space-holder particles into the gel results in titanium with controlled porosities up to 44 vol.% and with low contamination by Kendra A.Erk [28]. Bonding features and associated mechanisms in kinetic sprayed titanium coatings studied by Gyuyeol Bae [29].

Surface and subsurface structural evolution during sliding wear of two in situ nitrided titanium alloys, β Ti–35Nb–7Zr–5Ta (TNZT) and α/β Ti–6Al–4V (Ti64), was studied by cross-sectional transmission electron microscopy coupled with precession electron diffraction [30]; Processing and characterization of porous Ti2AlC with controlled porosity and pore size was reported by Liangfa Hu [31]. A framework to link localized cooling and properties of directed energy deposition (DED)-processed Ti-6Al-4V was researched by Sarah J.Wolff [32]. Structure-processing correlations and mechanical properties in freeze-cast Ti-6Al-4V with highly aligned porosity and a lightweight Ti-6Al-4V-PMMA composite with excellent energy absorption capability was reported by Jordan S.Weaver [33]. Microstructure and deformation behavior of Ti-6Al-4V alloy by

high-power laser solid forming was studied, the post-fabricated heat-treated microstructure consists of coarse columnar prior-β grains (630–1000 μm wide) and α-laths (5–9 μm) under different scanning velocities (900 and 1500 mm/min), which caused large elongation (~18%) superior to the conventional laser additive manufacturing Ti-6Al-4V alloy [34].

Revival of pure titanium for dynamically loaded porous implants used additive manufacturing by Ruben Wauthle [35]. Mechanical properties and biocompatibility of porous titanium scaffolds applied for bone tissue engineering, Interconnectivity between pores is higher than 95% for porosity as low as 30%. The elastic moduli are 44.2 GPa, 24.7 GPa and 15.4 GPa for 30%, 40% and 50% porosity samples which match well to that of natural bone (4–30 GPa) by Yunhui Chen [36]. Commercially pure titanium (CP-Ti) and Ti–TiB composite parts with three different porosity levels (i.e. 10%, 17% and 37%) were produced by selective laser melting (SLM). The yield strength and elastic modulus of porous CP-Ti parts range 113–350 MPa and 13–68 GPa respectively, which are much lower than those for porous Ti–TiB counterparts (234–767 MPa and 25–84 GPa respectively) mainly due to the strengthening effect induced by TiB particles in Ti–TiB samples were published by H.Attar [37]. Tribocorrosion behavior of bio-functionalized highly porous titanium was studied by F.Toptan [38]. Ultrafine-grained porous titanium and porous titanium/magnesium composites fabricated by space holder-enabled severe plastic deformation [39]. Understanding long-term silver release from surface modified porous titanium implants by Anish Shivaram [40]. Powder metallurgical processing of low modulus β-type Ti-45Nb to bulk and macro-porous compacts were reported, macro-porous samples the use of additionally milled powder was beneficial for achieving increased strength values of ≈140 MPa [41].

Understanding compressive deformation behavior of porous Ti used finite element analysis with micro-CT and RVE based analysis, In vitro studies showed better cell proliferation with time on porous CP-Ti surfaces by Sandipan Roy [42]. An improved polymeric sponge replication method for biomedical porous titanium scaffolds, The scaffolds support growth of mesenchymal stem cells by Chunli Wang [43]. Application of porous titanium in prosthesis production using a moldless process: Evaluation of physical and mechanical properties with various particle sizes, shapes, and mixing ratios were published by Widyasri Prananingrum [44]. Surface modification of severe plastically deformed ultrafine grained pure titanium by plasma electrolytic oxidation by F.Reshadi [45]. On the influence of sintering protocols and layer thickness on the physical and mechanical properties of additive manufactured titanium porous bio-structures was studied by Ahmad Basalah [46]. On the effect of throughout layer thickness variation on properties of additively manufactured cellular titanium structures was reported by Esmat Sheydaeian [47]. Titanium foam scaffolds applied for dental applications by A. Nouri [48]. Dual properties of zirconia coated porous titanium for a stiffness enhanced bio-scaffold was studied by Han Lee [49]. Material process development for the fabrication of heterogeneous titanium structures with selective pore morphology by a hybrid additive manufacturing process was reported by Esmat Sheydaeian [50]. Various unit cells were used in the porous structure: (**a**) Cubic; (**b**) Diamond; (**c**) Truncated cube; (**d**) Truncated cuboctahedron; (**e**) Rhombic dodecahedron; (**f**) Rhombi cuboctahedron were review by S.M. Ahmadi [51].

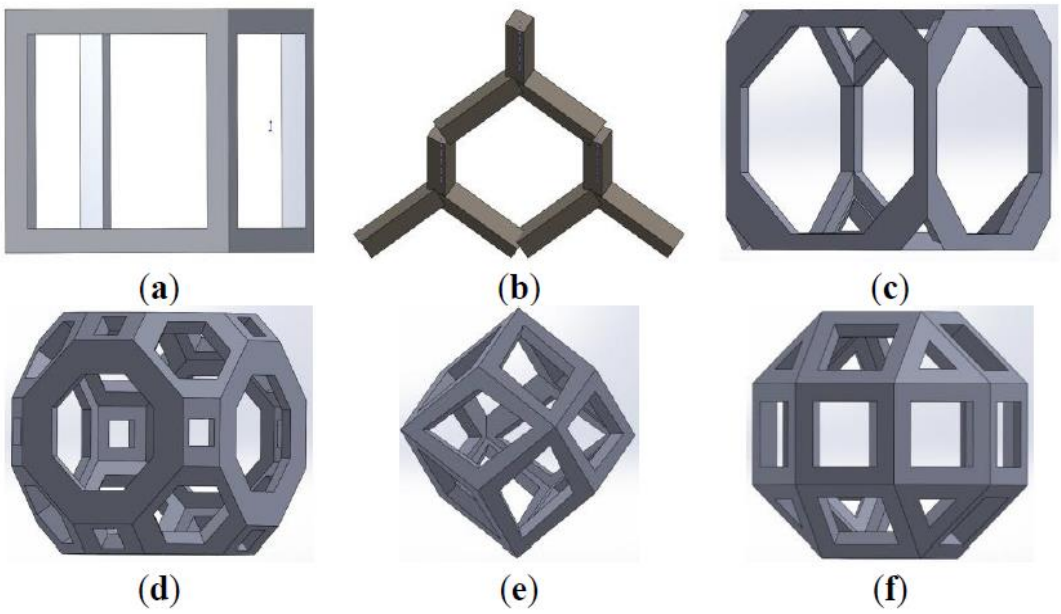

Fig. 1.13 Various unit cells were used for the porous titanium.

Reviews some new research results. Recently, researchers have attracted on 3D-printing or additive manufacturing, which is a hot spot. The microstructure of porous titanium alloy has been reported extensively by additive manufacturing technology. Most of the research articles were reported about titanium foam applications in implants that it will still subject of research and investigation.

1.4 Manufacture method

Metal foam was developed in the world about 30 years. There are many ways to fabricate metal foam, it can fall into five main classes:

1.4.1 Melt foaming method

Melt foaming method is one of cost-effective methods to make metal foam and it has been successfully applied to fabricate Al foam and Al alloy foams [52]. Meanwhile, some researchers have reported that Mg alloy foams [53] and Zn-22Al alloy [54] prepared by melt foaming method using titanium hydride as blowing agent have extraordinary coarse pore structures. Those methods include foaming by gas injection, foaming with blowing agents, gas–releasing particle decomposition in semi-solids, the solid-gas eutectic solidification,

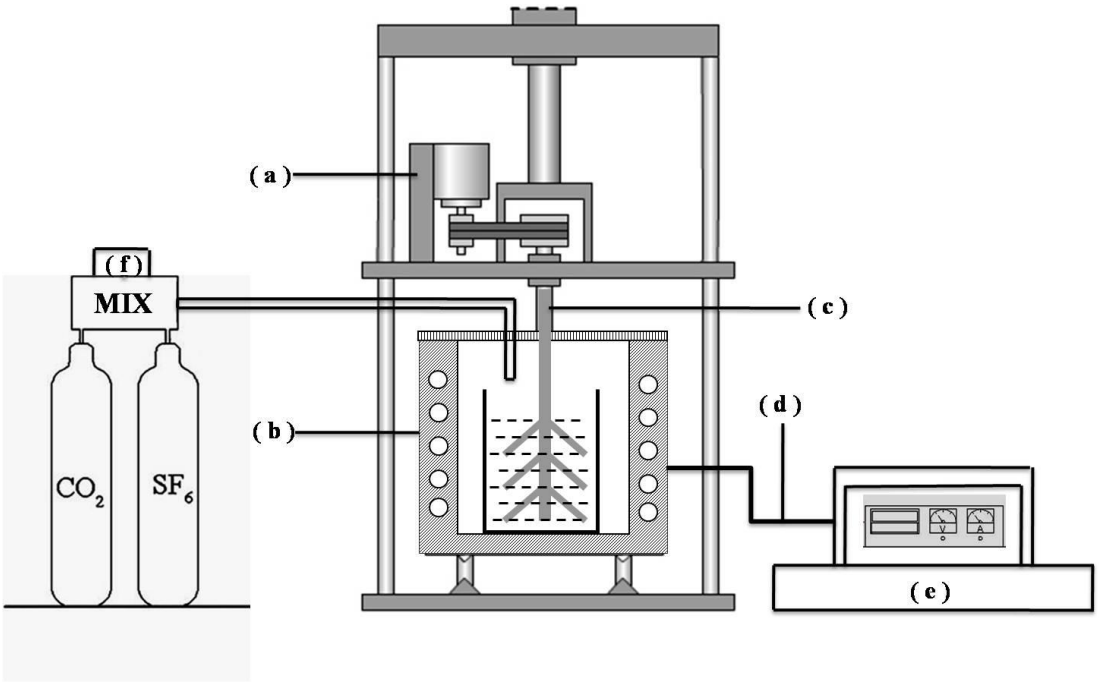

Fig. 1.13 Schematic diagram of apparatus for making metal foams [55];

(a) Motor (b) Furnace (melting, holing) (c) Impeller (d) Thermocouple (e) Power controller (f) Gas mixer

1.4.2 Casting method.

Many metal foam or porous metal can be used casting method to fabricate. A vacuum fluidity investment method has been driven for fabricating of open-cell foams via different infiltration pressures. In those foams, the pores shape is predominantly controlled by the initial shape of the space-holder particles that were used to producing the preform. Pores of the resulting foam “replicate” the initial shape of these space-holder particles.

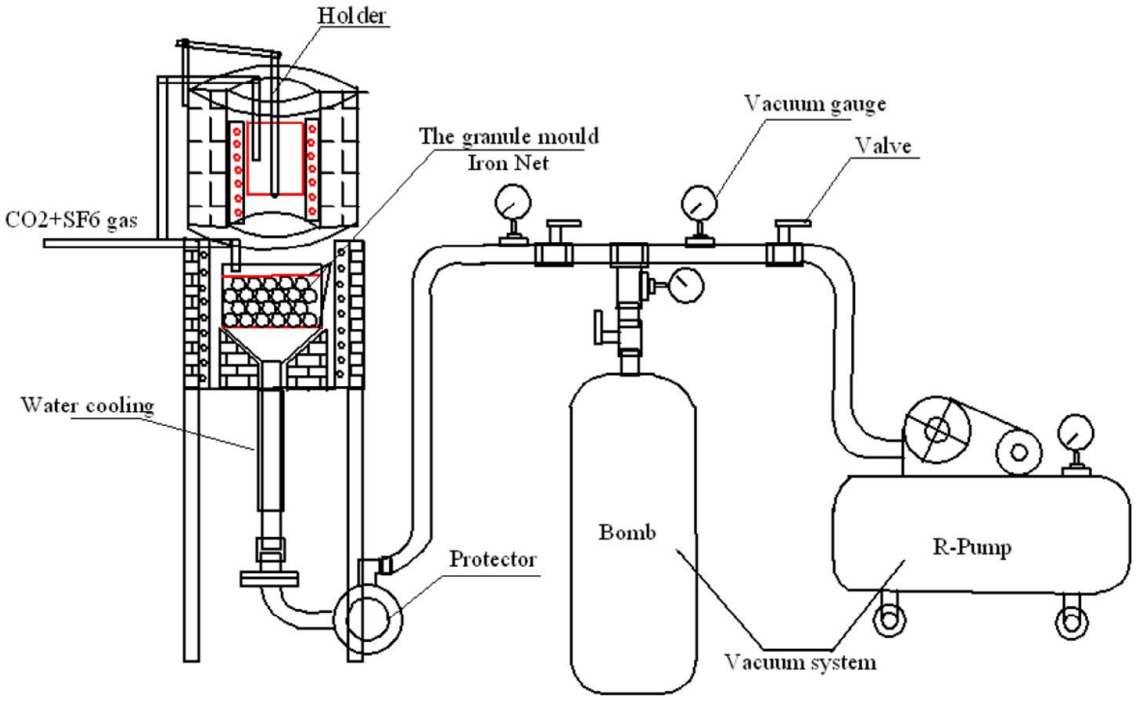

Fig. 1.14 Schematic diagram of apparatus for making open cell Mg alloy foams [56].

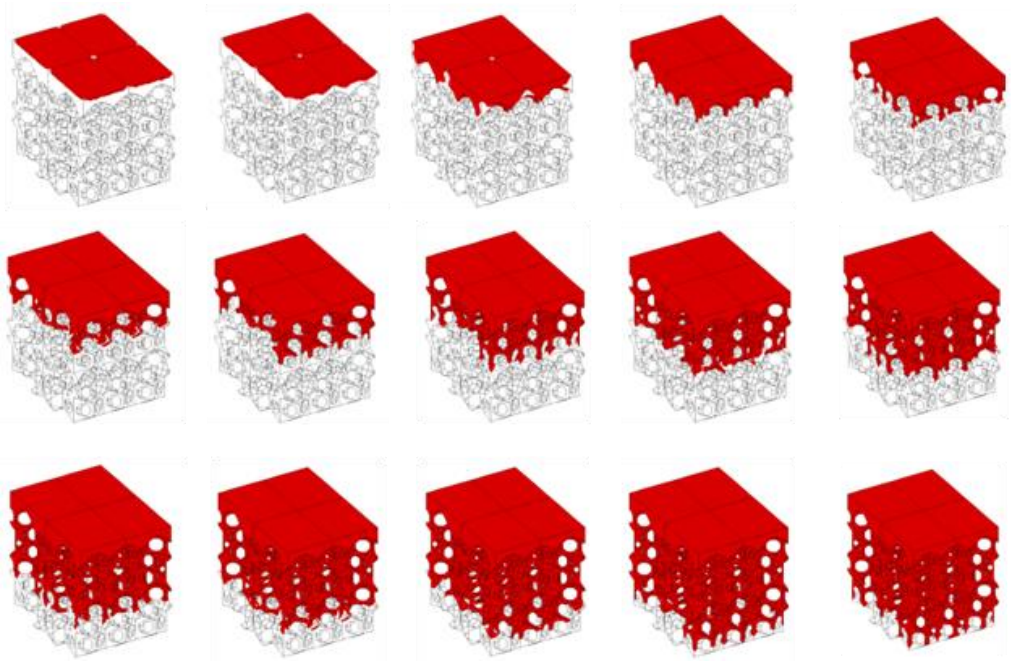

Fig. 1.15 Schematic diagram of Manufacture by vacuum flow casting

It mainly consists of two resistance furnaces, one furnace is preheated the granule mold, another furnace is melting the magnesium alloy, a stopper in the upper furnace and a steel crucible, the switch can control the molten Mg alloy into the bottom furnace. the upper furnace and the lower furnace were protected and supplies the inert gas by a gas system to in Fig. 1.14 [10]. high pressure infiltration process and investment casting used often for researcher, Fabrication of metal matrix composites by a high-pressure centrifugal infiltration process was reported by J Wannasin, MC Flemings [57].

1.4.3 Powder metallurgy.

Many report showed powder metallurgy process to fabricate metal foams for the production of metal foam sandwich panels, complex-shaped foam parts and foam filled hollow profiles [58].

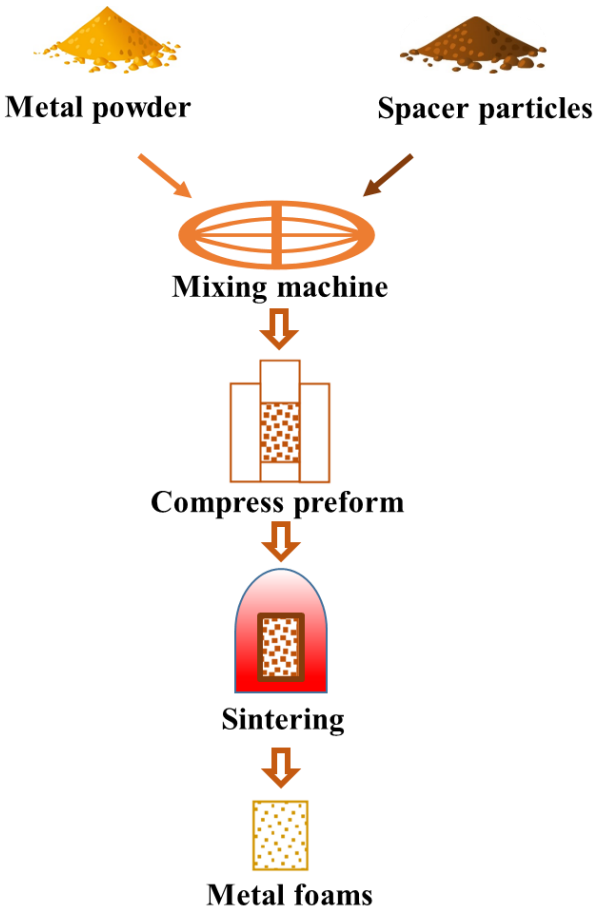

Fig. 1.16 Preparation process diagram for making metal foams by powder metallurgy process.

First, powder and space particles are weighing and calculating the volume ratio. It is important for control porosity of metal foam; Another geometry shape of particles determine the cell structure of metal foam. Second the mixing machine was used and made the metal powder and space particles homogenous distribution. Then, the preform was compressed and move to furnace for sintering. Finally remove the space particles from composites material, Metal foams were obtained in Fig. 1.15. Other methods include SDP (Sintering Dissolution Process) [59], SRF (Slip Reaction Foam Sintering Process) [60].

Titanium and titanium alloy fabricated by powder metallurgy (PM) processes, which can substantially broaden the field of application of titanium alloys. however, powder metallurgy (PM) processes make many productions more economically than by additive manufacturing.

1.4.4 Chemical or physical deposition of metal or plastic foams.

Metal deposition is the use of chemical or physical methods. Metal deposition in organic polymer materials of pore structure which is easily decomposed. After subsequent sintering or other processes, the polymer material can be remove and obtained porous metals. Deposition Physical deposition methods was used to make the porous metal by V Shapovalov [61]. This technically resemble chemical and electrochemical deposition.

Many types of cellular plastics or plastic foams were intended to be a source of practical information by AH Landrock [62], including, rubber-like and Elastomer foams are considered, the new structural plastic foams also.

1.4.5 3D Printing or additive manufacturing.

1.4.5.1 Classification of AM-additive manufacturing system

New products, complex structure material, leagues of artists, empowering, and hobbyists used 3D printing or additive manufacturing, that revolutionized the design company, prototype, present and manufacturer to create previously impossible for consumer demand. AM system often categorized in terms of energy source, the material feed stock, build volume, etc [63].

ASTM Standard	Industry Names	Vendors
Vat Photopolymerization	Stereolithography	3D Systems, EnvisionTEC, FormLabs
Powder Bed Fusion	Selective Laser Sintering, Laser Melting, Electron-Beam Melting	3D Systems, EOS, ARCAM, Renishaw
Material Extrusion	Fused Deposition Modeling	Stratasys, 3D Systems, Printrbot, etc.
Material Jetting	MultiJet Modeling, PolyJet	Stratasys, 3D Systems, Sanders
Binder Jetting	3D Printing	3D Systems, Ex One, VoxelJet
Directed Energy Deposition	Laser Engineered Net Shaping, Direct Metal Deposition	Optomec, DM3D, Sciaky, Insstek
Sheet Lamination	Laminated Object Manufacturing, Ultrasonic Consolidation	MCor Technologies, CAM-LEM, Fabrisonic, Solido

Table 1.1 Classification of AM process types [64]

1.4.5.2 Selective Laser Melting

Using of more powerful Laser for SLM is based on the DMLS and SLS. The Selective Laser Melting AM process that uses a laser beam to selectively fuse and sinter metallic powder or polymer particles. After each cross-section is scanned, the powder bed is lowered by one layer thickness, a new layer of material is spread on top, and the process is repeated until the part building is complete [65]. At the building spot, the density of energy is high enough to fully melt the powder. if the gap between the scanning paths is small enough, the parts manufactured have no or few porosities. It is crucial to obtain good surface quality from optimization of the parameters ([66], [67]). Due to thermal distortion at the higher temperature involved, shrinkage affects the parts [68].

1.4.5.3 Electron Beam Melting

Electron Beam Melting was fabricated commercial by Germany company of Arcam. It is difference and similar to SLM process on the nature of the energy source: a Laser was instead by an electron beam. It is up to several kilometers per second, due to the lack of moving parts to guide the melting spot determined high scanning speed possible. At the building spot, Moreover, the increase of the energy density makes the use of a many variety of metallic alloys. These two factors show the high melting speed. This process cannot require any specific curing operation also. Shrinkage takes place, due to the large quantity of energy absorbed by the part [68]. It is an important factor for scanning strategy proves to improve the part's quality and to minimize heat diffusion inside the powder bed [69].

Table 1.2 Manufacturer data (3D System, EOS GmbH, Arcam, POM) [68]

Technology	SLS	DMLS	SLM	EBM	DMD
Manufacturer	3D System – DTM Corp.	EOS GmbH	3D System - MTT	Arcam	POM - Easyclad
Maximal building volume* (in mm^3)	550x550x750	250x250x215	400x400x400	200x200x350	300x300x300
Building speed* (in cm^3/h)	10 – 100	7 – 70	5 – 20	55 – 80	10 – 70
Post-process operations	Cleaning Infiltration (Finishing)	Cleaning (Infiltration) (Finishing)	Cleaning (Finishing)	Cleaning (Finishing)	(Finishing)
Layer thickness*	20 – 150 µm	20 – 100 µm	20 – 100 µm	50 – 200 µm	-
Rugosity (in µm)	Ra 2 [5]	Ra 11 [5]	Ra 11 [5]	Ra 25 – 35*	Ra 10 – 25*
Dimensionnal quality*	0.2* mm	0.1 – 0.2* mm	0.2* mm	0.4* mm	0.3* mm
Available metallic	Any coated	Steels, Cobalt-	Steels, Cobalt-	Steels, Cobalt-	Steels, Inconel,
Materials	Material	Chrome, Aluminum, Bronze, Titanium.	Chrome, Aluminum, Bronze, Titanium.	Chrome, Aluminum, Bronze, Titanium, Inconel, Copper, Beryllium, Niobium,…	Copper, Titanium,…

1.4.5.4 Practical steps

3D printable models designed by computer aided design or another 3D software. An STL or X3D file were preparing by computer. additive manufacturing equipment obtained STL or stereolithography files (*.stl), however X3D output is primarily intended for communication and editing. Both STL and X3D output capabilities were studied for all three types of optimal structures for recently research. The output possibilities, in Fig. 1.16, as well as their intended purpose are summarized [70]. Recently, a new file format named AMF or Additive Manufacturing File (*.amf) was created to overcome the limitations of the STL format (ASTM ISO 2013) [71]. Finally, an object of desired 3-dimensional shape obtained by scanning cross-sections on the surface of a metallic powder bed layer-by layer based on a CAD model [65].

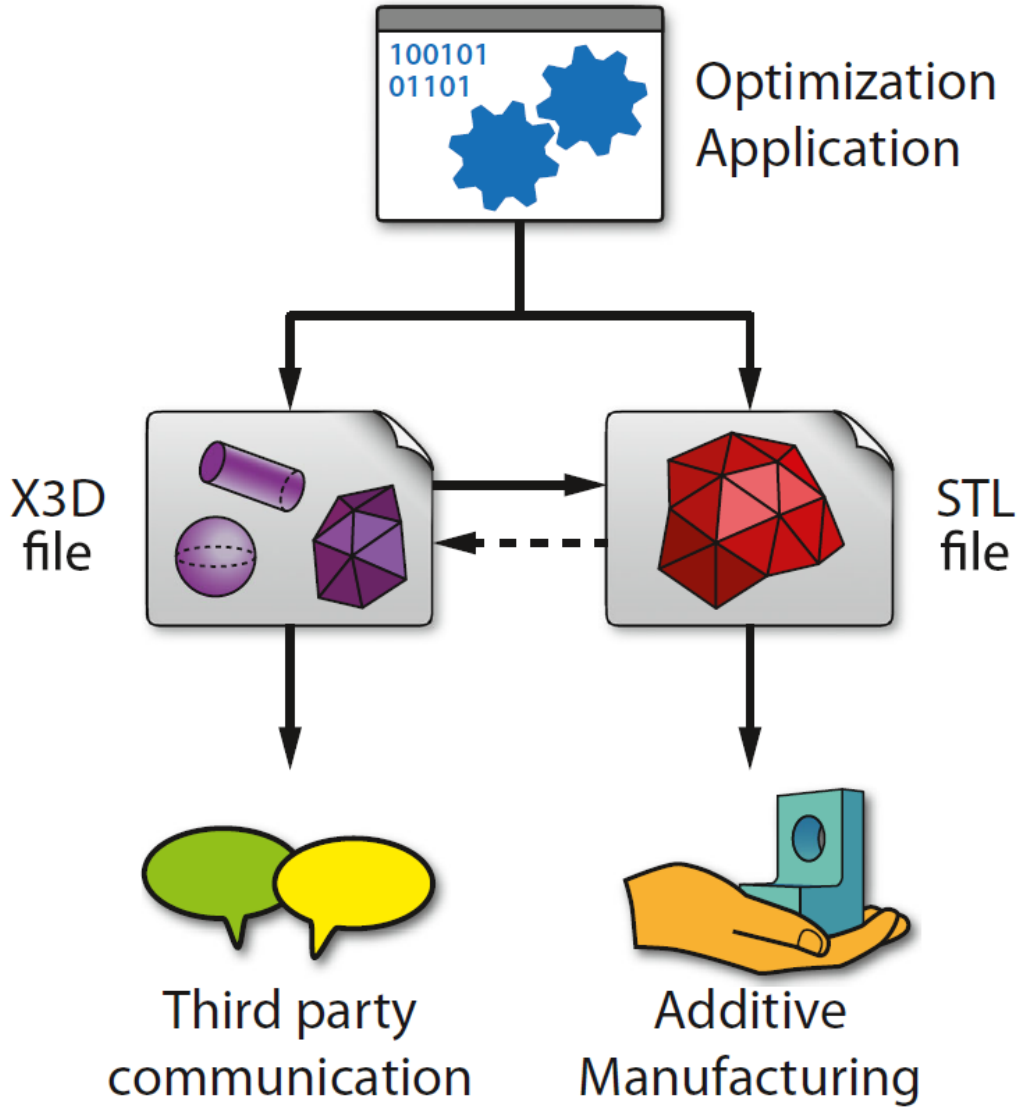

Fig. 1.17 Diagram illustrating the possible file outputs (X3D and STL) and their intended purpose [70]

1.5 Compare with traditional techniques and additive manufacturing.

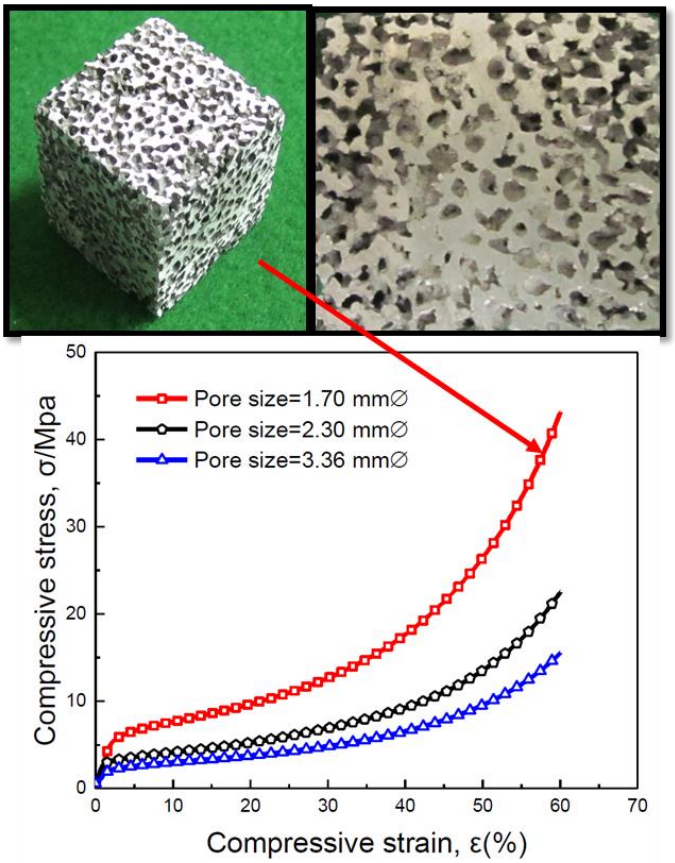

Fig. 1.18 Compressive stress-strain curves for AZ31 open cell Mg alloy foam [56]

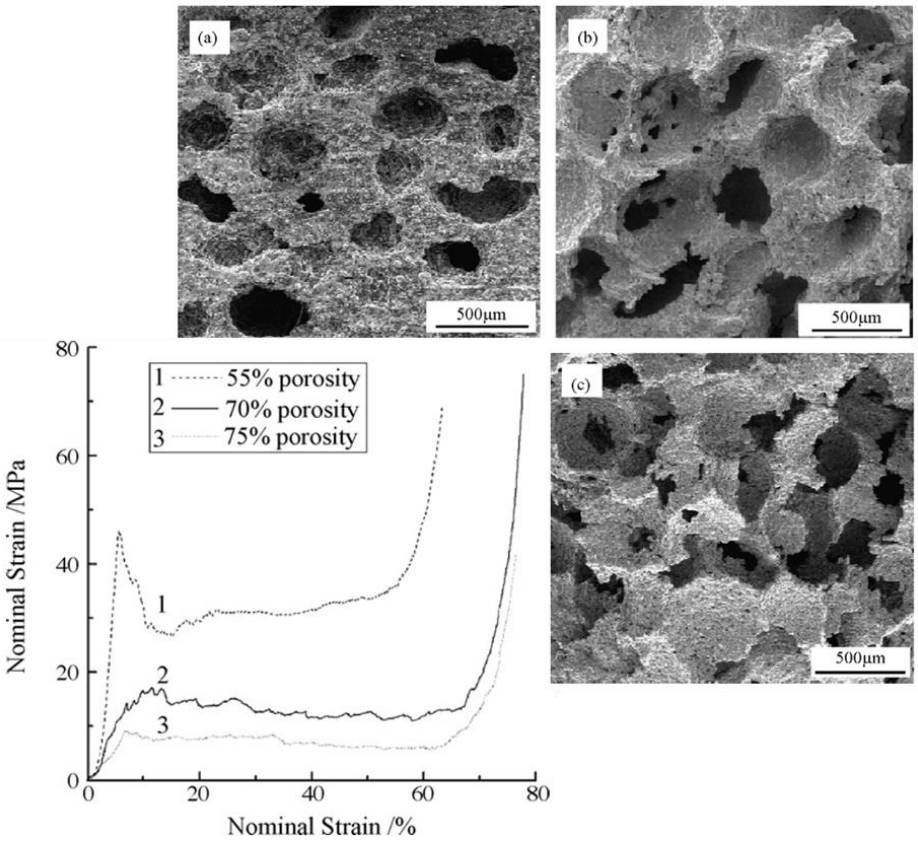

Fig. 1.19 Space holder technique and stress-strain curves of CP-Titanium foam [72].

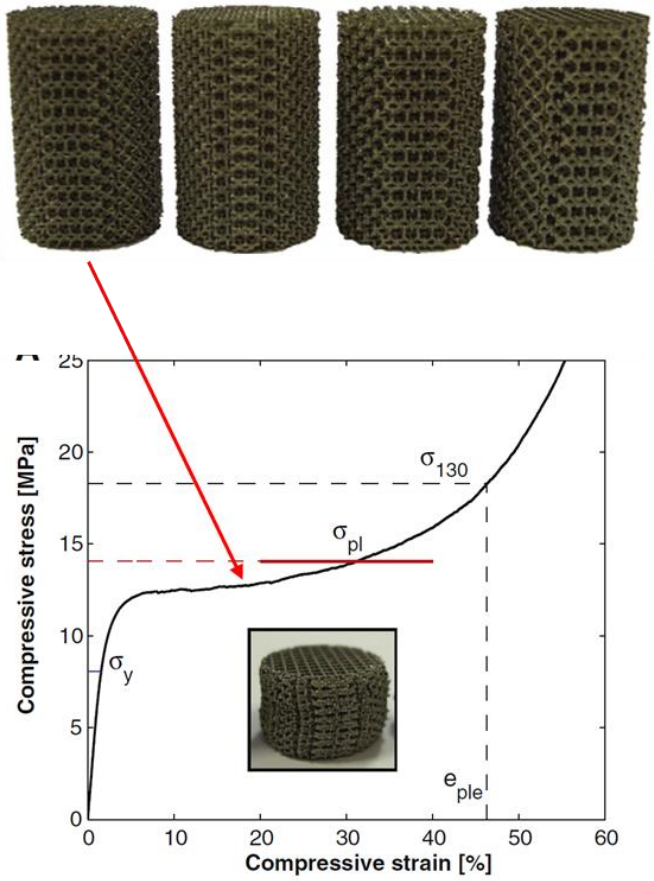

Fig. 1.20 Stress-strain curves of CP-Ti foams by SLM [73]

1.5.1 The Traditional melt foaming technology

1.5.1.1 Prepare process was as follows:

1 Melting

Melted in a crucible at proper temperatures.

2 Thickening

Thicken agent was introduced into the melted alloy by the impellor with a constant revolution speed. This process is usually considered to raise viscosity of liquid.

3 Foaming stage

Foaming agent was dispersed into the melt with the impeller revolution speed, , leading to the melt being foamed gradually. This time interval is defined as stirring foaming stage whose duration is defined as stirring time.

4 Holding

Immediately after stirring foaming stage, the melt is held in the furnace to let bubbles in the melt continuously grow until a certain cellular structure is formed. This time interval is defined as holding foaming stage whose duration is defined as holding time.

5 Cooling

The crucible is removed from the furnace and the melt, which has been foamed, is allowed to solidify by air blowing and water spraying immediately.

1.5.1.2 Pore structure and cell

The pore structure of metal foam has a close relation with blowing gas releasing rate. It was difficult to control blowing gas releasing rate and homogenous distribution, leads to some places are high porosity, some places have big size pore and some places are small size pore. During fabricating metal foam, pore structure and cell shape were random

forming by the random releasing gas until the end of liquid–solid reaction between melted and foaming gas.

1.5.1.3 Mechanical properties

Due to the pore structure and cell are random distribution, every time cut the 30*30*30 specimen which was different, every time experimental results were a little difference, Data repeatability was low. Closed-cell metal cell walls are connected with higher mechanical properties than open-celled metal.

That pores are spherical or irregular spherical for Al alloy by melting foam process. It is clear that the geometry shape of pore and pore structures are random distribution in Fig. 1.21. The pore sizes prepared using the method described above mainly distribute between 2 and 3 mm and the normal porosity is about 71–73%. Compared with the results of before corrosion (Fig. 1.21a), the engineering stress engineering strain curves after corrosion (Fig. 1.21b) significantly move to the negative direction of Y axis, meaning that the corrosion process substantially reduces the overall strength of the aluminum foams.

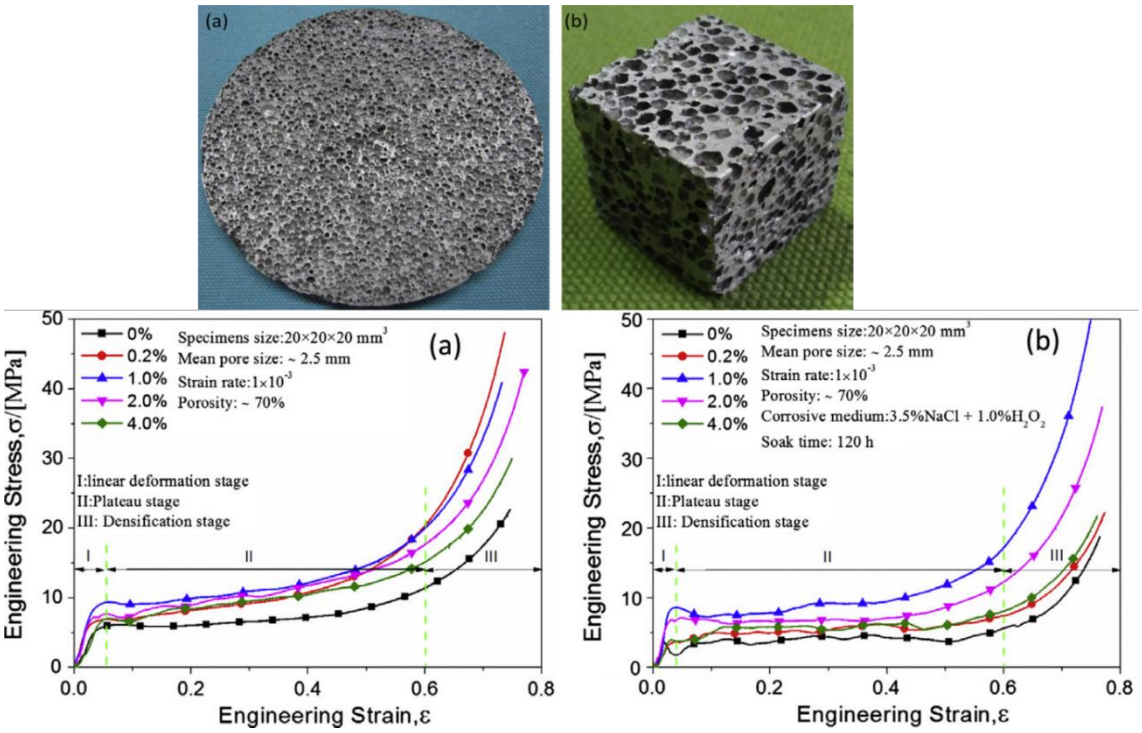

Fig. 1.21 Engineering stress–engineering strain curves of specimens before (a) and after (b) corrosion [74].

1.5.2 The Traditional vacuum flow casting

1.5.2.1 Prepare the granule mold (space holder)

Some same sizes of granule were arrangement in the granule mold. The pores shape was predominantly controlled by the initial shape of the space-holder granules that were used to produce the preforms. Pores of the resulting foam “replicate” the initial shape of these space-holder granules.

Preform granule mold need satisfies some points demands are:

(1) The property of heat resisting at 600℃-800℃

(2) Bear the infiltration pressures without deformation.

(3) The granules are easy to move away from the foam metal.

(4) The granular were prepared by a kind of economic and environmental friendly material.

1.5.2.2 Vacuum flow casting process

1. Ingot was melting in a steel crucible in the melting furnace

2. Infiltration of molten metal into the porous performs by Vacuum pump.

3. Solidification of the molten metal. metal/granules composite can be obtained.

4. Dissolution of the performs in a hot water. The ultrasonic machine was used with suitable water and many hours. The open-cell metal foam has been fabricated successfully by removing the preform granules.

AZ31 open cell magnesium foam was fabricated by vacuum flow casting in Fig. 1.19.

1.5.2.3 pore structure and cell

The appearance of the pores is directly related to the granules particles; However, the granule shape is smooth sphere, increasing infiltration pressure, many granules will be

cracked and flow channel will be blocked. Therefore, the whole open cell structure is uniform, due to space holder take thermal deformation or extrusion deformation, cell is random shape.

1.5.3 The Traditional powder metallurgy

Space holder was used to control the cell morphology in order to produce high performance metal foams. Porosity, pore size, shape and pore distribution were also depended on space holder. However, the composited material has to remove the space holder. There are many in crack cell wall showed in Fig. 1.19. The traditional powder metallurgy was similar with vacuum flow casting, the pore structure is homogeneous, cell morphology is random, Date repeatability is normal compared with others method. Due to defects and irregular cell morphology distribution, the mechanical properties were normal compared with other manufacture technology.

1.5.4 Additive manufacturing

(1) Design three-dimensional models to produce productions

Directly design by computer, any geometry shape of the three-dimensional CAD graphics generated physical products, the pore structure and geometry of cell was easy to control. Certainly, pore structure and cell can get uniform excellently.

(2) Pore structure and cell were easy to control

It can automatically, quickly, directly and more accurately transform the three-dimensional design of the computer into a physical model, or even directly manufacturing parts or molds, thus effectively shortening the product development cycle.

(3) Metal foam was fabricated at shorter time

3D printing can be shaped in hours, allowing designers and developers a leap from floor plan to solid;

(4) Mechanical properties of 3D printing technology

3D printed products compared with the traditional manufacture method of metal foam, once formed made it better mechanical properties.

Method:	Melt foaming method	Vacuum flow casting	Powder metallurgy	Additive Manufacturing
Structure and cell	Structure random Cell random	Structure uniform Cell random	Structure uniform Cell random	Uniform
Data Repeatability	Difficult	Normal	Normal	Excellent
Control Shape and structure	Difficult	Normal	Normal	Easy
Mechanical Properties	High	Normal	Normal	Excellent

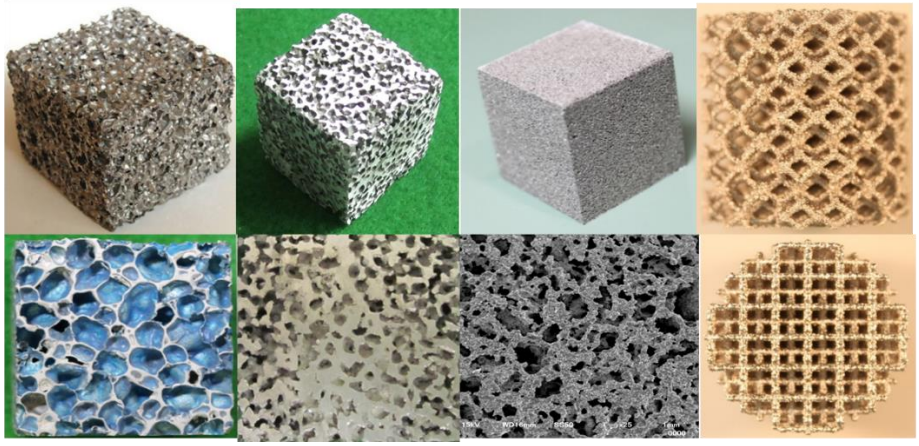

Figure 1.22 Comparison between traditional method and additive manufacturing (AM).

1.5.5 AM technology mainly has the following salient features:

(1) Directly forming. Raw materials of powder were directly forming as the production. The geometry shape can be any complex three-dimensional parts, directly across the traditional casting, forging, welding and other processes. It skips the roughing process, directly to the finished machining. This is AM The most important feature of technology.

(2) The short preparative time.

logistics links were less, it reduced period of manufacturing cycle.

(3) Green process.

The basic components are no longer being heat treatment or fast cooling in manufacturing process.

(4) Flexible.

It is freedom for designer who can design any geometry of the parts by AM technology, designers may full display own imagination.

(5) Digitization and Intellectualization.

It is possibility for change of the manufacturing industry. The AM technology makes development of the traditional production lines networking.

Therefore, this new technology is described as a direct, fast, green, flexible, digital, intelligent feature AM technology.

1.5.6 Disadvantages of AM technology

(1) High manufacturing costs.

(2) Low manufacturing efficiency.

(3) Product surface have some defects.

(4) Forming raw materials are only generally metal powders, including stainless steel, nickel-base super alloy, titanium alloy, cobalt-chromium alloy, high-strength aluminum alloy and refractory metals.

(5) Suitable for small size pieces.

(6) The mechanical properties of the formed parts are good, the general mechanical properties are better than the castings, however it is lower than forgings.

(7) Large-scale production with economies of scale is still more economical than 3D printing.

1.6 Theory

1.6.1 Porosity, pore size and pore distribution.

Porosity, pore size, pore size distribution and pore number are four most important parameters to describe the pore structures of metal foam. In this study, two kinds of porosities are mentioned to describe the porosity of titanium foam. One is bulk porosity, Pr_b, referring to the volume fraction of all the pores in a finished product of titanium foam, which can be calculated using the following equation

$$Pr_b=(Vs-(W/\rho))/Vs\times100\% \quad \ldots\ldots\ldots\ldots\ldots\ldots\ldots\ldots \quad (1.1)$$

Where Vs is the sample's volume, W is the foam weight and ρ stands for the density of titanium; another is plane porosity, Pr_p, referring to the area fraction of pores of a cross-section of a titanium foam sample, which can be expressed as

$$Pr_p=(\sum A_i)/A\times100\% \quad \ldots\ldots\ldots\ldots\ldots\ldots\ldots\ldots \quad (1.2)$$

Where A_i is a plane pore area measured by image analysis [75] and A is the measured section area. According to the Deless law [76], Pr_p is equal to Pr_b if the macroscopic structure is homogeneous. The Pr_p value displays the porosity of a sample at a selected position (height, level) and reflects the foaming condition at the selected level. The Pr_b value displays the whole foaming property of a sample and represents an average porosity of the entire foam block. There is only one Pr_b value for a foam block but there are several Pr_p values at different levels of the sample because the Pr_p values at different levels may

be different with each other. For a selected sample, its values of Pr_p should be dispersed around its Pr_b value. Small deviation between Pr_b and Pr_p values denotes good foaming result and vice versa. Apparently, this property can be used as a judgment to estimate the goodness of foaming situation by comparing the homogeneity of several samples. In this study, we use standard deviation S to reflect the homogeneity of plane porosity dispersion in foam, which is expressed as

$$S=\sqrt{\frac{\sum I\,(Pri-Pr)^2}{n-1}} \quad \text{.....(1.3)}$$

Where Pr_i denotes both plane porosity at level i and bulk porosity, Pr denotes arithmetic average of all plane porosities and bulk porosity and n denotes measurement times containing for measuring plane porosities and bulk porosity.

The plane pore size, pore number per unit area and pore size distribution are obtained after analyzing a cross-section of titanium foam to reflect its bulk pore structures [77]. The specific treatment process has been elaborated in Ref. [78]. Suppose the theoretical value porosity(Pr_b) are 53~95%，the theoretical value of density can be calculated using the following equation:

$$\rho_s=(1-Pr_b)/\rho_{Ti} \quad \text{.....(1.4)}$$

Where ρ_s is theoretical value of density and ρ_{Ti} is Ti and Ti alloy matrix density;

The ingot height, h_i, which can be calculated using the following equation:

$$h_i = W/(\pi r^2 \rho) \ldots\ldots\ldots\ldots\ldots\ldots\ldots\ldots\ldots\ldots (1.5)$$

And the expansion ratio (ER), η is defined as

$$\eta = (Vs-(w/\rho))/(w/\rho) \times 100\% \ldots\ldots\ldots\ldots\ldots\ldots\ldots\ldots (1.6)$$

1.6.2 Energy absorption

The energy absorption of the metal foam can be calculated by integrating the lower area of the stress-strain curve according to the following formula (1.7).

$$W = \int_0^{\varepsilon} \sigma(\varepsilon) d\varepsilon \ldots\ldots\ldots\ldots\ldots\ldots\ldots\ldots\ldots\ldots\ldots\ldots\ldots\ldots (1.7)\ [79]$$

Where W is energy absorption capacity, ε the compressive strain, and σ the compressive stress.

Energy absorption efficiency can be calculated using the following method:

$$W = \frac{\int_0^{e_0} \sigma(\varepsilon) de}{100} \ldots\ldots\ldots\ldots\ldots\ldots\ldots\ldots\ldots\ldots\ldots\ldots\ldots\ldots\ldots (1.8)$$

$$W_e = \frac{W}{\sigma_0 \times e_0} \times 10\text{^}4 \ldots\ldots\ldots\ldots\ldots\ldots\ldots\ldots\ldots\ldots\ldots\ldots\ldots\ldots\ldots (1.9)$$

Where W is the energy absorption per unit volume(MJ/m^3); W_e is the energy absorption efficiency (%); σ is compressive stress (N/mm^2); e_0 is upper limit of the compressive strain (%); σ_0 is the compressive stress at upper limit of the compressive strain (N/mm^2) [79].

1.7 Summary

1.7.1 Scope of the thesis

Metal foams are a class of materials with low densities and novel physical, mechanical, thermal, electrical and acoustic properties. They are known for their interesting combinations of physical and mechanical properties such as high stiffness in conjunction with very low specific weight or high compression strengths combined with good energy absorption characteristics. According to the pores structure, metal foam can be classified into open-cell metal foam and closed-cell metal foam. The open-cell one has network structure and all the cells are connected, while the structure in closed-cell metal foam contains many airtight bubbles and the bubbles are isolated. Their potential applications of metal foams were in different fields, such as high energy absorption, sound/thermal insulation, heat exchangers, filters, and catalyst carriers. In automobile industry, metal foams were used as protection materials during side impacts. Energy of frontal collisions was absorbed by deformation of metal foams. The area of high speed trains was also potential application by a typical sandwich structure. The absorb energy can also be used practically to protect vehicles or aircraft from explosions, shrapnel in the military industry.

Titanium and titanium alloy are metallic material with high tensile strength to density ratio, high corrosion resistance, fatigue resistance, high crack resistance and so on. Manufacturing titanium foams traditional method and additive manufacturing method are reviewed. Powder metallurgy is a term covering a wide range of ways in which materials or components are made from metal powders. The powder sinter process generally consists powder blending, die compaction, and sintering. Compaction is generally performed at room temperature, and the elevated-temperature process of sintering is usually conducted at atmospheric pressure and under carefully controlled atmosphere

composition. This titanium foam of 60% porosity product was manufactured by powder metallurgy through compacting and pressure working. 3D printing is also known as additive manufacturing (AM). Additive manufacturing method builds a three-dimensional object from computer-aided design (CAD) model or another electronic data source such as an Additive Manufacturing File (AMF) file. Stereolithography (STL) is one of the most common file types that 3D printers can read. Selective laser melting (SLM) is a particular rapid prototyping. SLM equipment use a high power-density laser to melt and fuse metallic powders together. Electron-beam additive manufacturing is a type of additive manufacturing, or 3D printing, for metal parts. Metal powder or wire is welded together using an electron beam as the heat source. Titanium foams made by laser or electron beam sintered titanium powder layer by layer. it has been widely expected to revolutionize the manufacturing of complex structure, from medical implants to aerospace engineering.

1.7.2 Outline of thesis

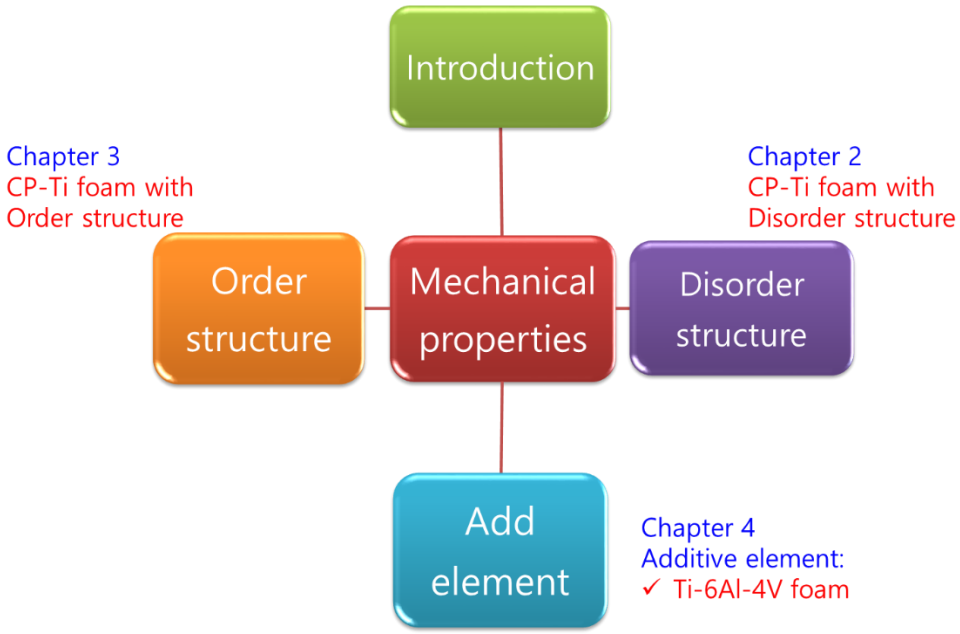

Outline of metal foam research obtained as followed：

Chapter 1：First chapter showed the introduction to physics properties of metal foams, applications of metal foam, many kinds of material（Al, Mg, Cu, Ti, Steel and so on）, Advantages of titanium, manufacture methods of titanium foam and comparison between traditional technology with disorder structure and additive manufacturing with order structure. Based on titanium foam, the motivation and objectives of this study are stated.

Chapter 2：This chapter presented the strain rate sensitivity of commercial pure titanium foam at elevated temperature. Uniaxial compression tests were performed to investigate the effects of temperature and strain rate on the plastic deformation of titanium foams are with high temperature. Stress-strain curves showed line are elastic, plateau and densification regions which are typical characteristics of titanium foams. Both the flow stress and the energy absorption increase within creasing the strain rate and with decreasing the temperature. Apparent activation energy of the titanium foam was calculated. Apparent activation energy of the titanium foam was 603 kJ/mol, which is comparable to Commercial pure titanium with 746 kJ/mol. These results indicate that the thermally activated kinetics of the titanium foam mainly depends on the characteristics of the base material. In addition, XRD analysis showed the excellent oxidation resistance of the titanium foam.

Chapter 3：This chapter aimed to clarify the effects of cell geometry on compressive deformation of open-cell titanium foams. Truncated octahedron and rhombic dodecahedron cells were used as different unit cell geometries by designing a commercial 3D-CAD software. The open cell titanium was printed of 10 kinds of pore structure for energy absorbing application by the electron beam melting process. The nominal porosities of both truncated octahedron cell and rhombic dodecahedron cell are plotted as

a function of the normalized edge length. Relationship between the normalized porosity and normalized cell diameter are plotted as a function. The compressive behavior depended on the porosity, cell geometry and the cell orientation. Titanium foams with truncated octahedron cells showed high strength compared to those of rhombic dodecahedron cells. the parallel and oblique cell edges against the compression direction are effective to increase the compressive strength.

Chapter 4: This chapter analyzed influence of heat treatment on microstructure, mechanical properties and energy absorption capacities for Ti-6Al-4V foams with octahedron structure by additive manufacturing. Ti-6Al-4V foams were heat treatment at 1173 K and 1323 K (recrystallization annealing) for 1 h cooling by argon atmosphere in furnace. Titanium foams were subjected to different annealing in order to evaluate possibilities to the mechanical properties and energy absorption capacities. The apparent microstructure of Titanium alloy foams was studied through the SEM, XRD equipment. The Vickers hardness was discussion.

Chapter 5: summarizes the whole results in present. The remaining problems and future works are suggested in the fields of titanium foam with disorder structure and order structure.

References

[1] M.F. Ashby AGE, N.A. Fleck, L.J. Gibson, J.W. Hutchinson and H.N.G. Wadley. Metal Foams : A Design Guide. Pergamon, Oxford 2000.

[2] Banhart J. Manufacture, characterisation and application of cellular metals and metal foams.pdf. Progress in Materials Science 2001;46: 559–632.

[3] Louis-Philippe Lefebvre JB, David C. Dunand. Porous Metals and Metallic Foams: Current Status and Recent Developments. Advanced Engineering Materials 2008; 10:775-87.

[4] Ettrich J. Fluid Flow and Heat Transfer in Cellular Solids. Dissertation, Karlsruher Institut für Technologie (KIT): KIT Scientific Publishing; 2014.

[5] Schwingel D, Seeliger H-W, Vecchionacci C, Alwes D, Dittrich J. Aluminium foam sandwich structures for space applications. Acta Astronautica 2007; 61:326-30.

[6] Moon SK, Tan YE, Hwang J, Yoon Y-J. Application of 3D printing technology for designing light-weight unmanned aerial vehicle wing structures. International Journal of Precision Engineering and Manufacturing-Green Technology 2015; 1:223-8.

[7] Ryan G, Pandit A, Apatsidis DP. Fabrication methods of porous metals for use in orthopaedic applications. Biomaterials 2006; 27:2651-70.

[8] Fabrizio Matassi AB, Luigi Sirleo, Christian Carulli, Massimo Innocenti. Porous metal for orthopedics implants. Clinical Cases in Mineral and Bone Metabolism 2013; 10:111-5.

[9] Leitner A, Maier-Kiener V, Jeong J, Abad MD, Hosemann P, Oh SH, et al. Interface dominated mechanical properties of ultra-fine grained and nanoporous Au at elevated temperatures. Acta Materialia 2016; 121:104-16.

[10] XZ Yue, K Kitazono, X-J Yue, B-Y Hur. Effect of fluidity on the manufacturing of open cell magnesium alloy foams. Journal of Magnesium and Alloys 2016; 4:1-7.

[11] Park JS, Hyun SK, Suzuki S, Nakajima H. Effect of transference velocity and hydrogen pressure on porosity and pore morphology of lotus-type porous copper fabricated by a continuous casting technique. Acta Materialia 2007; 55:5646-54.

[12] Melisa Cardona JAI, Juan Fernando Ramírez, Patricia Fernández-Morales. Pores distribution statistical analysis for metal foams obtained by casting-dissolution process. Revista Matéria 2016;21: pp.501-9.

[13] Kathryn A. Dannemann JLJ. High strain rate compression of closed-cell aluminium foams. Mater Sci Eng A 2000; A293:157-64.

[14] Szyniszewski S, Smith BH, Hajjar JF, Arwade SR, Schafer BW. Local buckling strength of steel foam sandwich panels. Thin-Walled Structures 2012; 59:11-9.

[15] Haynes WM. CRC handbook of chemistry and physics, 95th Edition. CRC PRESS 1947.

[16] Krebs RE. The history and use of our earth's chemical elements: a reference guide: Greenwood Publishing Group; 2006.

[17] Moiseyev VN. Titanium alloys: Russian Aircraft and Aerospace Applications: CRC press; 2005.

[18] O'Connor TF. The Columbia Encyclopedia. Reference & User Services Quarterly 2001; 40:297.

[19] Leyens C, Peters M. Titanium and titanium alloys. Fundamentals and Applications, John Wiley & Sons; 2003.

[20] Wikimedia. Titanium. 2017.

[21] Liu YJ, Wang HL, Li SJ, Wang SG, Wang WJ, Hou WT, et al. Compressive and fatigue behavior of beta-type titanium porous structures fabricated by electron beam melting. Acta Materialia 2017; 126:58-66.

[22] Jaeggi C, Frauchiger V, Eitel F, Stiefel M, Schmotzer H, Siegmann S. The effect of surface alloying of Ti powder for vacuum plasma spraying of open porous titanium coatings. Acta Materialia 2011;59: 717-25.

[23] Farley C, Turnbull T, Pantoya ML, Hunt EM. Self-propagating high-temperature synthesis of nanostructured titanium aluminide alloys with varying porosity. Acta Materialia 2011; 59:2447-54.

[24] Li JC, Dunand DC. Mechanical properties of directionally freeze-cast titanium foams. Acta Materialia 2011; 59:146-58.

[25] Levi G, Bamberger M, Kaplan WD. Wetting of porous titanium carbonitride by Al–Mg–Si alloys. Acta Materialia 1999; 47:3927-34.

[26] Keleş Ö, García RE, Bowman KJ. Deviations from Weibull statistics in brittle porous materials. Acta Materialia 2013; 61:7207-15.

[27] Chino Y, Dunand DC. Directionally freeze-cast titanium foam with aligned, elongated pores. Acta Materialia 2008; 56:105-13.

[28] Erk KA, Dunand DC, Shull KR. Titanium with controllable pore fractions by thermoreversible gelcasting of TiH2. Acta Materialia 2008; 56:5147-57.

[29] Bae G, Kumar S, Yoon S, Kang K, Na H, Kim H-J, et al. Bonding features and associated mechanisms in kinetic sprayed titanium coatings. Acta Materialia 2009; 57:5654-66.

[30] Mohseni H, Nandwana P, Tsoi A, Banerjee R, Scharf TW. In situ nitrided titanium alloys: Microstructural evolution during solidification and wear. Acta Materialia 2015; 83:61-74.

[31] Hu L, Benitez R, Basu S, Karaman I, Radovic M. Processing and characterization of porous Ti2AlC with controlled porosity and pore size. Acta Materialia 2012; 60:6266-77.

[32] Wolff SJ, Lin S, Faierson EJ, Liu WK, Wagner GJ, Cao J. A framework to link localized cooling and properties of directed energy deposition (DED)-processed Ti-6Al-4V. Acta Materialia 2017; 132:106-17.

[33] Weaver JS, Kalidindi SR, Wegst UGK. Structure-processing correlations and mechanical properties in freeze-cast Ti-6Al-4V with highly aligned porosity and a lightweight Ti-6Al-4V-PMMA composite with excellent energy absorption capability. Acta Materialia 2017; 132:182-92.

[34] Ren YM, Lin X, Fu X, Tan H, Chen J, Huang WD. Microstructure and deformation behavior of Ti-6Al-4V alloy by high-power laser solid forming. Acta Materialia 2017; 132:82-95.

[35] Wauthle R, Ahmadi SM, Amin Yavari S, Mulier M, Zadpoor AA, Weinans H, et al. Revival of pure titanium for dynamically loaded porous implants using additive manufacturing. Materials Science and Engineering: C 2015; 54:94-100.

[36] Chen Y, Frith JE, Dehghan-Manshadi A, Attar H, Kent D, Soro NDM, et al. Mechanical properties and biocompatibility of porous titanium scaffolds for bone tissue engineering. Journal of the Mechanical Behavior of Biomedical Materials 2017; 75:169-74.

[37] Attar H, Löber L, Funk A, Calin M, Zhang LC, Prashanth KG, et al. Mechanical behavior of porous commercially pure Ti and Ti–TiB composite materials manufactured by selective laser melting. Materials Science and Engineering: A 2015; 625:350-6.

[38] Toptan F, Alves AC, Pinto AMP, Ponthiaux P. Tribocorrosion behavior of bio-functionalized highly porous titanium. Journal of the Mechanical Behavior of Biomedical Materials 2017; 69:144-52.

[39] Qi Y, Contreras KG, Jung H-D, Kim H-E, Lapovok R, Estrin Y. Ultrafine-grained porous titanium and porous titanium/magnesium composites fabricated by space holder-enabled severe plastic deformation. Materials Science and Engineering: C 2016; 59:754-65.

[40] Shivaram A, Bose S, Bandyopadhyay A. Understanding long-term silver release from surface modified porous titanium implants. Acta Biomaterialia 2017; 58:550-60.

[41] Schmidt R, Pilz S, Lindemann I, Damm C, Hufenbach J, Helth A, et al. Powder metallurgical processing of low modulus β-type Ti-45Nb to bulk and macro-porous compacts. Powder Technology 2017; 322:393-401.

[42] Roy S, Khutia N, Das D, Das M, Balla VK, Bandyopadhyay A, et al. Understanding compressive deformation behavior of porous Ti using finite element analysis. Materials Science and Engineering: C 2016; 64:436-43.

[43] Wang C, Chen H, Zhu X, Xiao Z, Zhang K, Zhang X. An improved polymeric sponge replication method for biomedical porous titanium scaffolds. Materials Science and Engineering: C 2017; 70:1192-9.

[44] Prananingrum W, Tomotake Y, Naito Y, Bae J, Sekine K, Hamada K, et al. Application of porous titanium in prosthesis production using a moldless process: Evaluation of physical and mechanical properties with various particle sizes, shapes, and

mixing ratios. Journal of the Mechanical Behavior of Biomedical Materials 2016; 61:581-9.

[45] Reshadi F, Faraji G, Baniassadi M, Tajeddini M. Surface modification of severe plastically deformed ultrafine grained pure titanium by plasma electrolytic oxidation. Surface and Coatings Technology 2017; 316:113-21.

[46] Basalah A, Esmaeili S, Toyserkani E. On the influence of sintering protocols and layer thickness on the physical and mechanical properties of additive manufactured titanium porous bio-structures. Journal of Materials Processing Technology 2016; 238:341-51.

[47] Sheydaeian E, Fishman Z, Vlasea M, Toyserkani E. On the effect of throughout layer thickness variation on properties of additively manufactured cellular titanium structures. Additive Manufacturing 2017; 18:40-7.

[48] Nouri A. 5 - Titanium foam scaffolds for dental applications A2 - Wen, Cuie. Metallic Foam Bone: Woodhead Publishing; 2017. p. 131-60.

[49] Lee H, Liao J-D, Sivashanmugan K, Liu BH, Weng S-L, Juang Y-D, et al. Dual properties of zirconia coated porous titanium for a stiffness enhanced bio-scaffold. Materials & Design 2017; 132:13-21.

[50] Sheydaeian E, Sarikhani K, Chen P, Toyserkani E. Material process development for the fabrication of heterogeneous titanium structures with selective pore morphology by a hybrid additive manufacturing process. Materials & Design 2017; 135:142-50.

[51] Ahmadi S, Yavari S, Wauthle R, Pouran B, Schrooten J, Weinans H, et al. Additively Manufactured Open-Cell Porous Biomaterials Made from Six Different Space-Filling Unit Cells: The Mechanical and Morphological Properties. Materials 2015; 8:1871.

[52] Akiyama S, Ueno H, Imagawa K, Kitahara A, Nagata S, Morimoto K, et al. Foamed metal and method of producing same. Google Patents; 1987.

[53] Yang D-H, Hur B-Y, Yang S-R. Study on fabrication and foaming mechanism of Mg foam using CaCO 3 as blowing agent. Journal of Alloys and Compounds 2008; 461:221-7.

[54] Sekido K, Seo T, Kitazono K. Energy absorption capability of Zn-22Al superplastic alloy foam manufactured through melt foaming process. Key Engineering Materials: Trans Tech Publ; 2010. p. 287-90.

[55] Zhao R, Li Y, Jeong S-R, Yue X, Hur B-Y. Fabrication, Microstructure and Compression Properties of AZ31 Mg Foams. Korean Journal of Materials Research 2011; 21:314-9.

[56] Yue XZ, BY Hur. Fluidity and Mechanical Properties of Open Cell AZ31 Mg Alloy Foam, Journal of Korea Foundry Society. 2012; 3: 150-156.

[57] Wannasin J, Flemings M. Fabrication of metal matrix composites by a high-pressure centrifugal infiltration process. Journal of Materials Processing Technology 2005; 169:143-9.

[58] Yu C-J, Eifert HH, Banhart J, Baumeister J. Metal foaming by a powder metallurgy method: Production, properties and applications. Materials Research Innovations 1998; 2:181-8.

[59] Zhao Y, Han F, Fung T. Optimisation of compaction and liquid-state sintering in sintering and dissolution process for manufacturing Al foams. Materials Science and Engineering: A 2004; 364:117-25.

[60] Angel S, Bleck W, Scholz PF, Fend T. Influence of Powder Morphology and Chemical Composition on Metallic Foams produced by Slip Reaction Foam Sintering (SRFS)-Process. Steel Research International 2004; 75:483-8.

[61] Shapovalov V. Porous metals. Mrs Bulletin 1994; 19:24-8.

[62] Landrock AH. Handbook of plastic foams: types, properties, Manufacture and Applications: Elsevier; 1995.

[63] Frazier WE. Metal Additive Manufacturing: A Review. Journal of Materials Engineering and Performance 2014; 23:1917-28.

[64] Rosen DW. Additive Manufacturing Process Overview. 2014.

[65] Guo N, Leu MC. Additive manufacturing: technology, applications and research needs. Frontiers of Mechanical Engineering 2013; 8:215-43.

[66] Yadroitsev I, Gusarov A, Yadroitsava I, Smurov I. Single track formation in selective laser melting of metal powders. Journal of Materials Processing Technology 2010; 210:1624-31.

[67] Yadroitsev I, Bertrand P, Smurov I. Parametric analysis of the selective laser melting process. Applied Surface Science 2007; 253:8064-9.

[68] Vayre B, Vignat F, Villeneuve F. Metallic additive manufacturing: state-of-the-art review and prospects. Mechanics & Industry 2012; 13:89-96.

[69] Lu W, Lin F, Han J, Qi H, Yan N. Scan strategy in electron beam selective melting. Tsinghua Science & Technology 2009; 14:120-6.

[70] Zegard T, Paulino GH. Bridging topology optimization and additive manufacturing. Structural and Multidisciplinary Optimization 2016; 53:175-92.

[71] International A. ASTM ISO (2013) ASTM52915-13. Standard specification for additive manufacturing file format (AMF) Version 11. PA: West Conshohocken; 2013.

[72] Niu W, Bai C, Qiu G, Wang Q. Processing and properties of porous titanium using space holder technique. Materials Science and Engineering: A 2009; 506:148-51.

[73] Wauthle R, Ahmadi SM, Amin Yavari S, Mulier M, Zadpoor AA, Weinans H, et al. Revival of pure titanium for dynamically loaded porous implants using additive manufacturing. Materials science & engineering C, Materials for biological applications 2015;54:94-100.

[74] Xia X, Zhang Z, Wang J, Zhang X, Zhao W, Liao B, et al. Compressive characteristics of closed-cell aluminum foams after immersion in simulated seawater. Materials & Design 2015; 67:330-6.

[75] Jiejun W, Chenggong L, Dianbin W, Manchang G. Damping and sound absorption properties of particle reinforced Al matrix composite foams. Composites Science and Technology 2003; 63:569-74.

[76] Underwood EE. Quantitative Stereology: Reading, Mass., Addison-Wesley Pub. Co.; 1970.

[77] Olurin OB, Fleck NA, Ashby MF. Deformation and fracture of aluminium foams. Materials Science and Engineering: A 2000; 291:136-46.

[78] McCullough KYG, Fleck NA, Ashby MF. Uniaxial stress–strain behaviour of aluminium alloy foams. Acta Materialia 1999; 47:2323-30.

[79] Standard I. ISO 13314: 2011 (E) (2011) Mechanical testing of metals—ductility testing—compression test for porous and cellular metals. Ref Number ISO; 13314:1-7.

.

Chapter 2: Strain rate sensitivity of open-cell titanium foam at elevated temperature

2.1 Introduction

Titanium foam is of great importance material in many industrial applications dues to their highly attractive properties, such as: good deformability, low density, high specific strength and excellent corrosion resistance. In addition, the high melting point of titanium allows for the use of titanium foams in functional aerospace and transportation industries. In fact, the strain rate and temperature properties of titanium foam are most crucial in the design of pore structures subjected to compression, which can lead to a drastic change in deformation modes and failure mechanisms [80] [81] [82] [83]. It is generally accepted that the dependence of flow stress on deformation temperature and strain rate was initially presented by Sellars and Tegart [84]. Many factors could influence the compressive behavior of metal materials, such as deformation temperature, strain rate and deformation degree. The constitutive equation of material could express the relationship between the deformation temperature, flow stress and strain rate [85]. There are many researches on the high temperature deformation of titanium alloys. Flow stress, microstructure evolution and the processing map of titanium alloy was obtained by Guo et al. [86]. Commercially pure titanium (CP-Ti) was subjected to compression at temperatures ranging from 673 to 973 K [87]. Temperature and strain rate effected on the deformation of nanostructured pure titanium [88]. Poletti et al. [89] proposed a unified description of the softening behavior of beta-metastable and alpha+beta titanium alloys during hot deformation. The effect of pore structure on the compressive property of porous titanium produced by powder metallurgy technique was studied [90]. Titanium

foams with varying porosities were made using acrowax bits as a space holder through powder metallurgy route. Two types of titanium particles (angular and spherical) were used [91]. Dynamic freeze casting as a new manufacturing technique for producing porous titanium scaffolds was reported [92]. High temperature deformation processing is an important technology for open cell titanium foam production, which usually used in aerospace industry, however, very little research into high temperature deformation processing of open cell titanium has been conducted [93]. Mechanical properties of titanium foams often depend on the heterogeneous cell morphology of experimental samples, which causes scattered data. In the present study, test specimens having almost identical porosity within 1% and homogeneous pore size distribution are used for compression tests. Effects of temperature and strain rate on the plastic deformation of titanium foams are investigated through uniaxial compression tests with different crosshead speeds.

2.2 Experimental procedure

The titanium foams were supplied by Osaka Yakin Kogyo. Co. Ltd, Japan. They were manufactured from a mixture of commercially pure titanium powder. An ammonium hydrogen carbonate was used as spacer particle [94]. Sintering was carried out at 1673 K for 2 h in argon. The porosity was 60±1 % and the average pore size was 250 μm [Fig. 2.2]. Macrostructure of deformed samples were examined by SEM (JSM-6510A) techniques [Fig. 2.1].

The compressive strength of the titanium foams body was measured using a hot compression. testing machine (Concreto 2000X, Shimadzu Co., Japan). The compression experiments were at fixed crosshead speed of 0.1 mm/min to 10 mm/min. Testing

temperatures of 300, 473 and 673 K are measured and controlled by a K-type thermocouple. All temperatures are controlled within ±1 K. In order to examine the oxide formation during the compression tests at elevated temperature, X-ray diffraction (XRD) analysis was carried out after compression tests. A Rigaku Ultima IV multipurpose XRD system was used in this study.

Fig.2.1 Photograph of CONCRETO 2000X (Shimadzu Co., Japan)

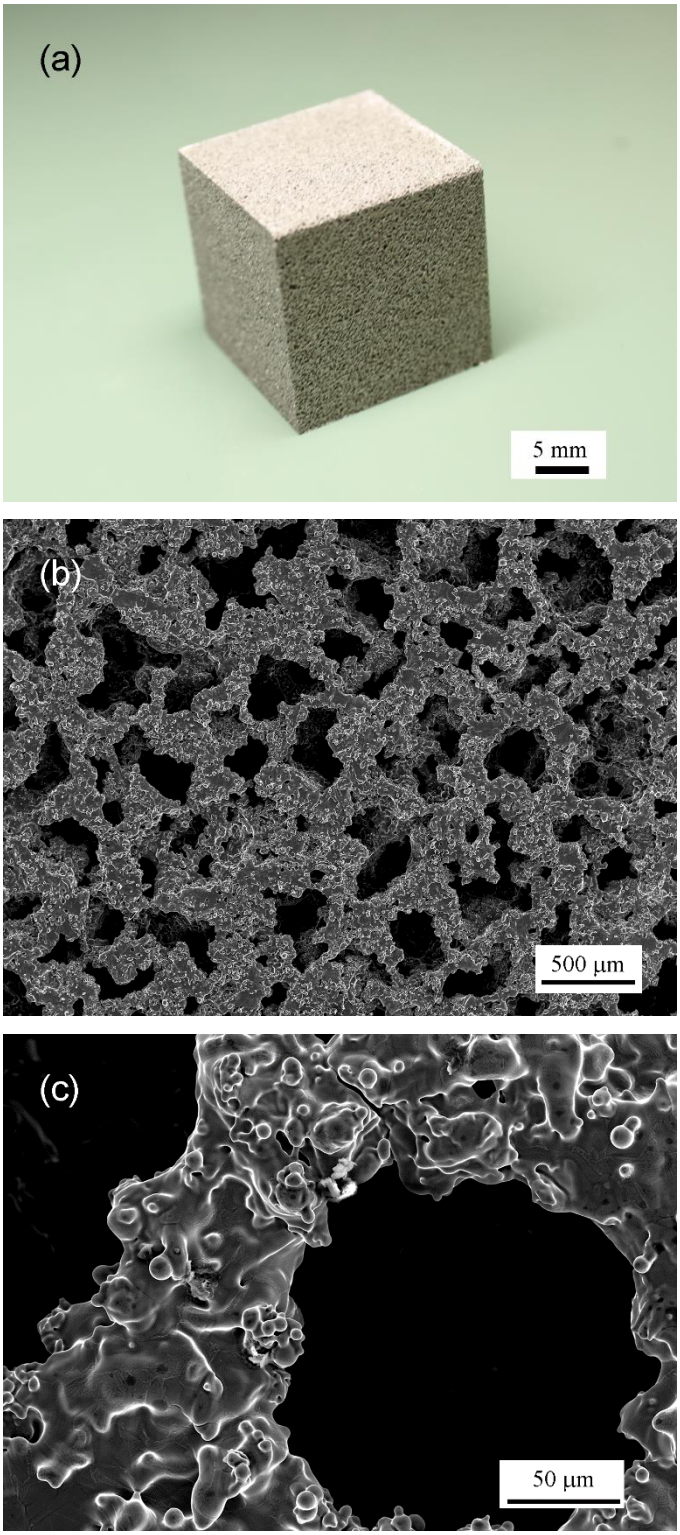

Fig.2.2 (a) Photograph of a cubic specimen of side 22 mm. Images (b) and (c) are SEM micrographs of titanium foam.

2.3 Results

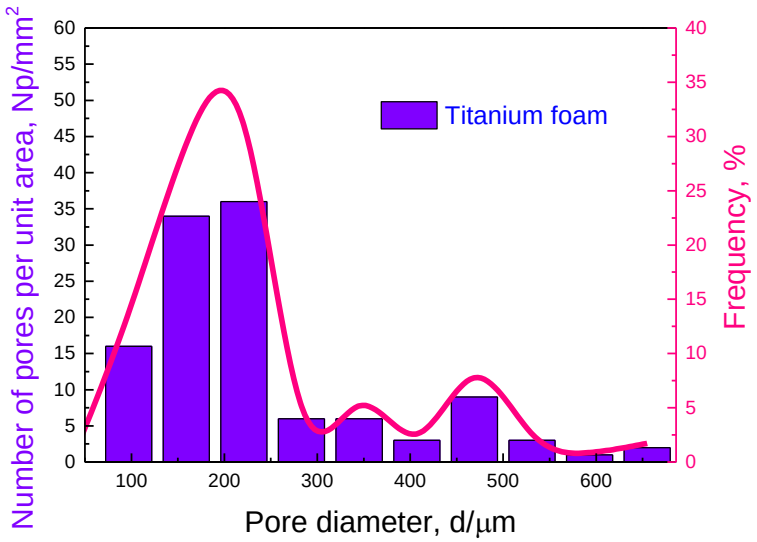

Fig. 2.3 Pore diameter distribution, number pores per unit area and frequency of titanium foam.

The varying trends of pore size against porosity distributions of the titanium foam specimen are shown in Fig. 2.3. Number of pores was measured using an image analysis software, ImageJ 1.48v. It is clear that all of the pores are distributed between 50 and 800 μm. However, for the titanium foams, the pores mainly distribute between 130 and 250 μm. The available camera and SEM were used to observe the macrostructure of the test material during compressive deformation for the initial sample in Fig. 2.4(a), the stage of material compaction is the plateau region at deformation 20% in Fig.2.4(c) and the densification region is at deformation 40% in Fig.2.4(e). Corresponding to Scanning Electronic Microscopy for the initial specimen in Fig. 2.4(b). Cracks appear in some of the cavities and structural walls of the samples for deformation 20% in Fig. 2.4(d). The

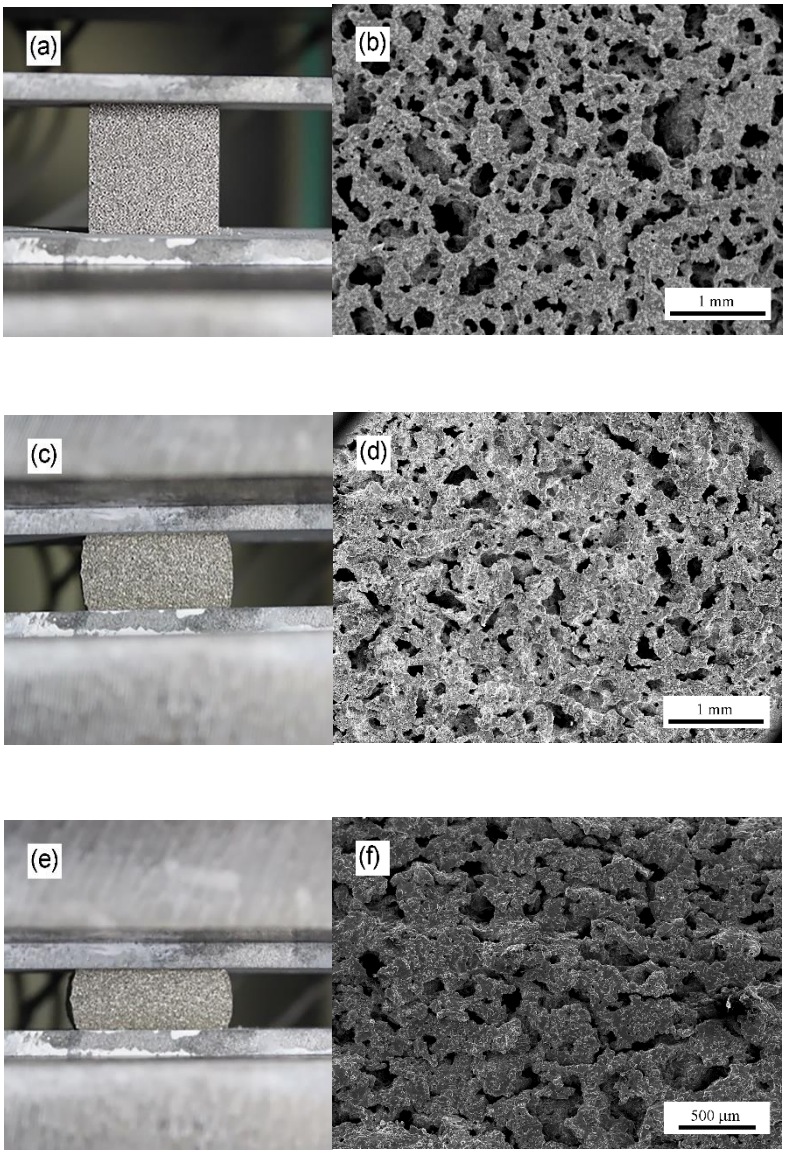

Fig. 2.4 Photographs (a), (c) and (e) show the cubic specimen after 0%, 20% and 40% compressive strain, respectively. Photographs (b), (d) and (f) show cell microstructures of (a), (c) and (e), respectively. Compressive test is carried out at room temperature and crosshead speed of 1 mm/min.

open cell structure gradually collapses and the sample reached the densification strain for deformation 40% in Fig. 2.4(f). The energy absorption of the metal foam, W, can be calculated by integrating the lower area of the stress-strain curve according to the following Eq. (2.1) [94],

$$W = \int_0^{\varepsilon} \sigma d\varepsilon, \qquad (2.1)$$

where ε is the compressive strain, and σ is the compressive stress. The relationship between the stress and the strain rate can be expressed as,

$$\sigma = K\dot{\varepsilon}^m, \qquad (2.2)$$

where m is the strain rate sensitivity exponent and K is the constant depending on the temperature.

The compressive deformation behavior is shown in Fig. 2.5. It is observed that the stress–strain curves of the investigated foams follow the general trend of stress–strain curves of metal foams. The stress strain curves depict three distinct regions: (i) linear elastic region, (ii) plateau region, where the stress oscillates about the average stress values with the increase in strain, and (iii) the densification region, where the stress increases sharply with strain due to densification of cells. The energy absorption by the foams is calculated from the stress–strain curves using Eq (2.1).

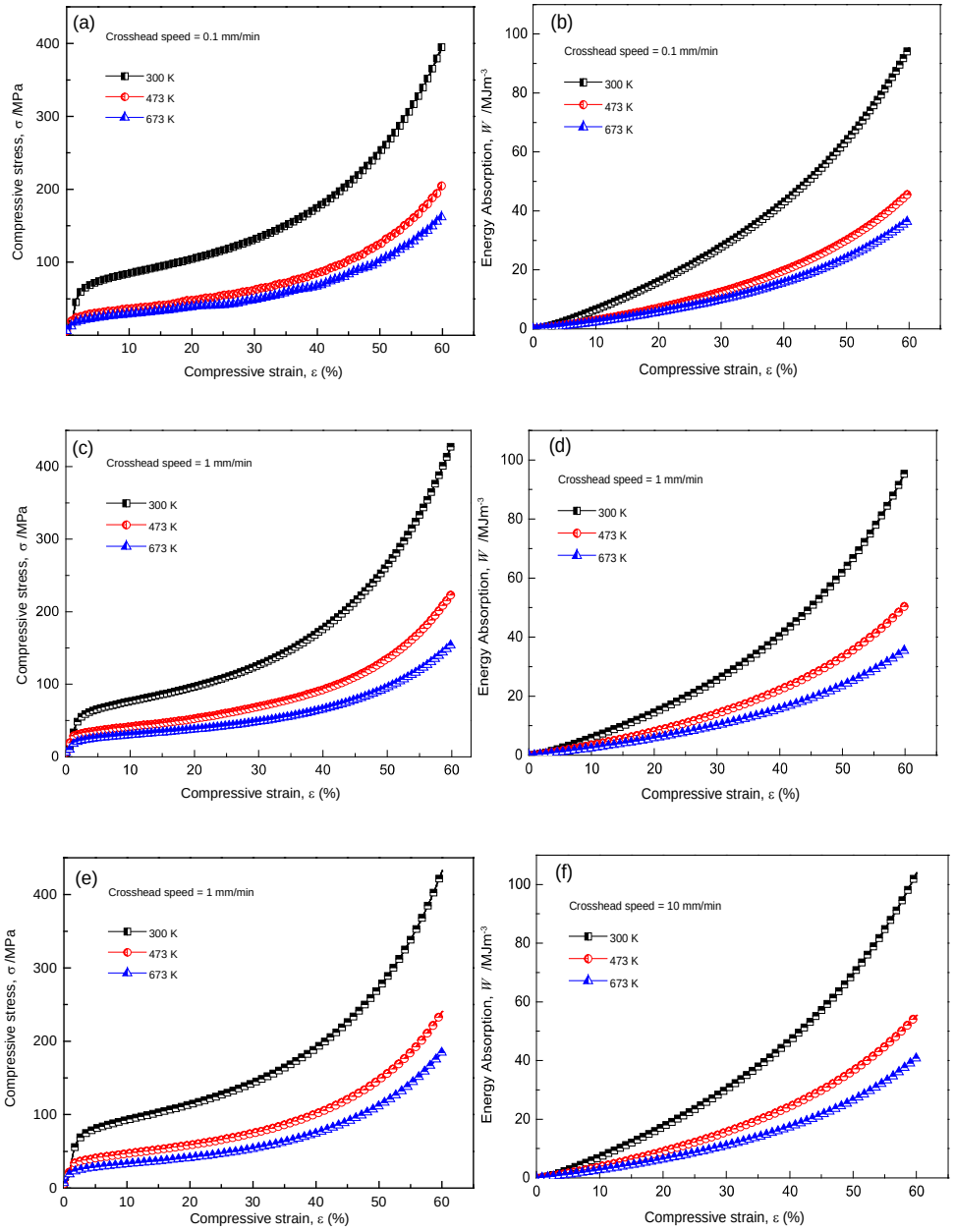

Fig. 2.5 Compressive stress-strain curves and energy absorption-strain curves of titanium foams in the range of 300 K to 673 K at the crosshead speed from 0.1 to 10 mm/min.

2.4 Discussion

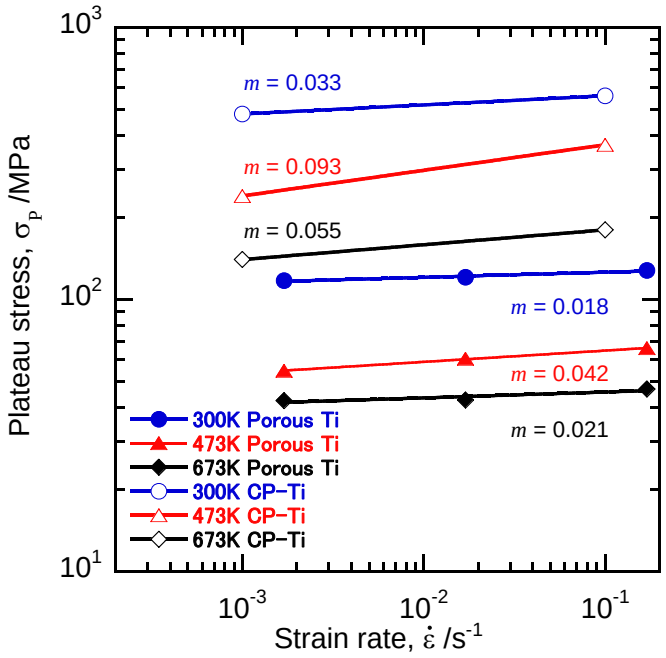

Fig. 2.6 Plateau stress is plotted as a function of strain rate with sensitivities of titanium foam and commercially pure titanium at different temperatures of 300, 473 and 673 K.

Plateau stress of titanium foams and flow stress of CP-Ti are plotted as a function of strain rate in Fig. 2.6. The slope in this figure corresponds to the strain rate sensitivity exponent (m-value) in Eq. (2.2). Titanium foams have m-values of 0.018, 0.021, 0.041 which is slightly smaller than those of CP-Ti (m = 0.033, 0.054, 0.093) in the range of 300 K-673 K. Inclusion of strain-rate sensitivity decreases by the gained plateau stress for the same density titanium foam or CP-Ti. It can be concluded that the strain rate sensitivity of titanium foams includes two factors: the deformation temperature caused by grain boundary sliding and the character of the base titanium material. For the

considered the porosity (p = 60%) titanium foam, the effect of the strain rate sensitivity outweighs the contribution of the deformation temperature.

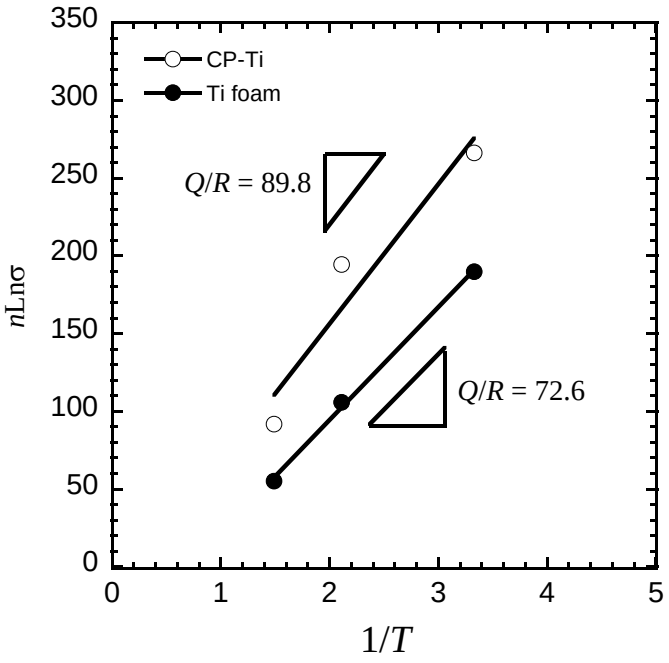

Fig. 2.7 Logarithm of the flow stress in titanium foam and CP-Ti is plotted against inverse temperature. The slopes indicate the activation energy.

$$\dot{\varepsilon} = \sigma^n \exp(-\frac{Q}{RT})$$

$$\sigma^n = \dot{\varepsilon} \exp(-\frac{Q}{RT})$$

$$\ln \sigma^n = \ln \dot{\varepsilon} \exp(-\frac{Q}{RT})$$

$$n \ln \sigma = \ln \dot{\varepsilon} + \frac{Q}{RT}$$

$\dot{\varepsilon}$ is strain rate(s^{-1}); σ is stress (MPa); n is stress index; T is deformation temperature (K), , where n is the stress exponent, Q is the apparent activation energy, R is the gas constant, T is absolute temperature.

In Fig. 2.7, flow stress at a constant strain rate is plotted as a function of 1/T. By regression analysis of the data, the deformation activation energy of CP-Ti can be calculated as 746 kJ/mol. The deformation activation energy of titanium foam can be determined as 603 kJ/mol. The value of titanium foam is comparable to the value of dense CP-Ti. Temperature is a highly influential factor in the resultant material strength during the high temperature deformation process. The thermal softening that occurs affects the fundamental stress–strain behavior of titanium foam. The variation of strain rate can be considered as dynamic strain aging and softening related to dynamic recovery.

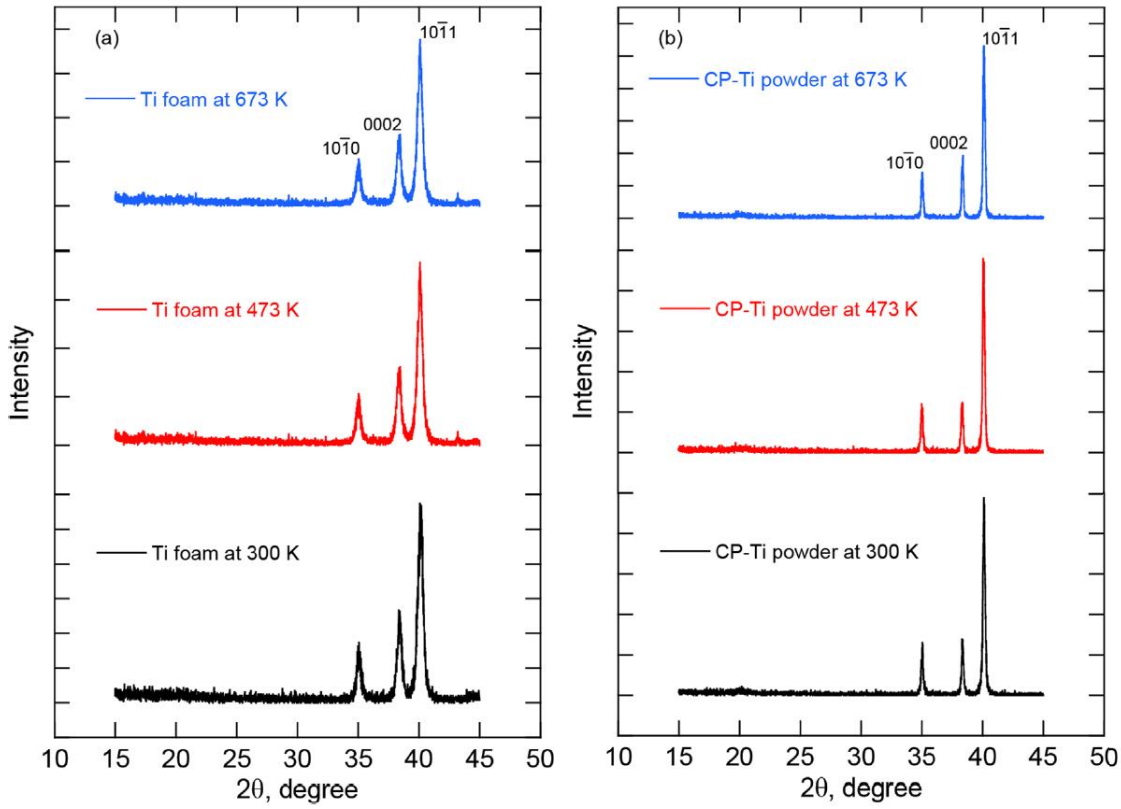

Fig. 2.8 (a) XRD patterns of titanium foams after compressive deformation at different temperatures of 300, 473 and 673 K. (b) XRD patterns of CP titanium powder after identical isothermal holding at 300, 473 and 673K.

Oxide formation at elevated temperature often gives negative effects on the mechanical properties. Results of XRD analysis are shown in Fig. 8. In addition, XRD analysis for CP titanium powder was carried out after isothermal holding at 300, 473 and 673K. Each XRD pattern possesses the peaks from hcp titanium. No XRD peak from TiO_2 oxide was observed in both Fig. 2.8(a) and(b). Experimental results indicate that oxide formation under 673 K is too less to influence on the mechanical properties of titanium foams. Furthermore, the excellent oxidation resistance has an advantage on the high temperature applications.

It is confirmed that the cell structure collapse during compressive deformation. Figure 2.9 shows the pore size distribution after 0%, 20% and 40% deformation. It can be seen that the deformation process has an important effect on the foams macrostructures and mechanical properties; the cell wall of the material suffers serious damage. Furthermore, many pores disappear on the cell walls, causing some of the pores to change from open-cell to close-cell. Generally, pore structures have a decisive influence on mechanical properties of metal foams. Under the same conditions, closed-cell foams possess a dense structure with much more attractive mechanical properties compared to open-cell foams. The mutual friction between the cell walls is reduced and disappears during the compression process, resulting in an increase of the compressive strength and yield strength. Furthermore, it has been confirmed that the energy absorption capacity of foam is mainly due to the yielding, buckling and friction of the cell walls. Because of the compression process, the strength, structural integrity and ductility of the cell walls increase, leading to the higher yielding, buckling and friction of the cell walls. In this way, the energy absorption capacity of the foams increases obviously.

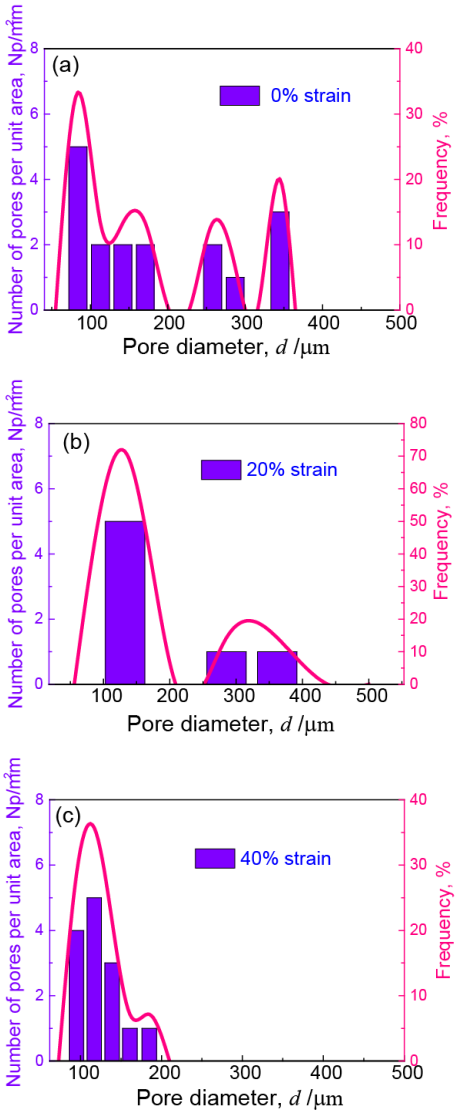

Fig. 2.9 Number pores per unit area and frequency of titanium foams are plotted after (a) 0%, (b) 20% and (c) 40% compressive strain.

2.5 Conclusions

In conclusion, the hot deformation behavior of open cell pure titanium was studied in temperature ranging from 300 K to 673 K and strain rates ranging from 0.1 to 10 mm/min. The porous structure deformation process has an important effect on porosity and pore macrostructure of titanium foams especially for the compressive properties, energy absorption capacity and yield strength. The compressive stress and energy absorbing capacity of titanium foams drop for increased temperature of the hot compression affected the fundamental stress–strain behavior of titanium foam. That deformation temperature has a great effect on material strength. In addition, the strain rate sensitivity increases at higher strain rates. The calculated activation energy for the titanium foams was 603 kJ/mol, which is comparable to commercially pure titanium with 746 kJ/mol. That demonstrated the potential for titanium foam in developing new applications in high temperature condition. Titanium foam will be helpful in automotive, aerospace and biomaterial applications even at elevated temperature up to 673 K.

References

[80] Murray N, Dunand D. Microstructure evolution during solid-state foaming of titanium. Composites science and technology 2003;63:2311-6.

[81] Dunand DC. Processing of titanium foams. Advanced engineering materials 2004;6:369-76.

[82] Kretz R, Hausberger K, Götzinger B. Energy-Absorbing Behavior of Aluminum Foams: Head Impact Tests on the A-Pillar of a Car. Advanced Engineering Materials 2002;4:781-5.

[83] Banhart J. Manufacture, characterisation and application of cellular metals and metal foams. Progress in materials Science 2001;46:559-632.

[84] Sellars CM, McTegart W. On the mechanism of hot deformation. Acta Metallurgica 1966;14:1136-8.

[85] Ashby MF. A first report on deformation-mechanism maps. Acta Metallurgica 1972;20:887-97.

[86] Guo W, HUI S-x, YE W-j, MI X-j. Hot compressive behavior of Ti–3.0 Al–3.7 Cr–2.0 Fe–0.1 B titanium alloy. Transactions of Nonferrous Metals Society of China 2012;22:2965-71.

[87] Zeng Z, Zhang Y, Jonsson S. Deformation behaviour of commercially pure titanium during simple hot compression. Materials & Design 2009;30:3105-11.

[88] Rodríguez-Galán D, Sabirov I, Segurado J. Temperature and stain rate effect on the deformation of nanostructured pure titanium. International Journal of Plasticity 2015;70:191-205.

[89] Poletti C, Germain L, Warchomicka F, Dikovits M, Mitsche S. Unified description of the softening behavior of beta-metastable and alpha+ beta titanium alloys during hot deformation. Materials Science and Engineering: A 2016;651:280-90.

[90] Li B, Wang C, Lu X. Effect of pore structure on the compressive property of porous Ti produced by powder metallurgy technique. Materials & Design 2013;50:613-9.

[91] Mondal D, Patel M, Jain H, Jha A, Das S, Dasgupta R. The effect of the particle shape and strain rate on microstructure and compressive deformation response of pure Ti-foam made using acrowax as space holder. Materials Science and Engineering: A 2015;625:331-42.

[92] Jung H-D, Yook S-W, Jang T-S, Li Y, Kim H-E, Koh Y-H. Dynamic freeze casting for the production of porous titanium (Ti) scaffolds. Materials Science and Engineering: C 2013;33:59-63.

[93] Kotan G, Bor AŞ. Production and characterization of high porosity Ti-6Al-4V foam by space holder technique in powder metallurgy. Turkish Journal of Engineering and Environmental Sciences 2007;31:149-56.

[94] Fujibayashi S, Takemoto M, Neo M, Matsushita T, Kokubo T, Doi K, et al. A novel synthetic material for spinal fusion: a prospective clinical trial of porous bioactive titanium metal for lumbar interbody fusion. European spine journal 2011;20:1486-95.

[95] Manmohan D, Matsagar VA, Gupta AK, Marburg S. Strain rate sensitivity of closed cell aluminium fly ash foam. Transactions of Nonferrous Metals Society of China 2013;23:1080-9.

[96] Christopher J, Choudhary B, Samuel EI, Srinivasan V, Mathew M. Tensile flow and work hardening behaviour of 9Cr–1Mo ferritic steel in the frame work of Voce relationship. Materials Science and Engineering: A 2011;528:6589-95.

[97] Wang S, Mi X, Yin X, Li Y. Deformation behavior of TiNiFe alloy in isothermal compression. Rare Metals 2012;31:323-7.

Chapter 3: Compressive behavior of open-cell titanium foams with different unit cell geometries

3.1 Introduction

Metal foams are a class of lightweight materials with novel physical, mechanical, thermal, electrical and acoustic properties. They offer potential for lightweight structures, energy absorption, and thermal management [98]. Titanium foams are used for structural applications or for bone-replacement implants because of their low density, high strength and excellent corrosion resistance [99, 93].

Powder metallurgical (PM) process with spacer materials has been used for manufacturing of magnesium [100] and titanium foams [56]. Due to the non-spherical shape of the spacer materials, the structure of porous metals becomes uniform, and the pore shape is anisotropic and random. Recently, additive manufacturing (AM) technology are focused on many industrial applications [80]. In the case of metallic parts, selective electron beam melting (EBM) [101], selective laser sintering (SLS) [102] and selective laser melting (SLM) [103-105] have enabled to produce highly porous interconnected structures. The arbitrary pore shapes and pore sizes in the range from 100 to 200 μm, which can create complex and uniform structure titanium foam that is distinguished from previous approaches [106-107].

AM process enables to manufacture open-cell geometry consisting of periodic space-filling polyhedrons. Though there are several space-filling polyhedrons, the present study focusses on two polyhedrons, truncated octahedron and rhombic dodecahedron. Truncated octahedron, which is one of Archimedean solids, has 14 faces (8 hexagons and 6 squares), 36 edges and 24 vertices. Rhombic dodecahedron, which is one of Catalan

solids, has 12 rhombic faces, 24 edges and 14 vertices. Of course, titanium foams with these polyhedron cell morphologies have been reported in the previous studied, for instance, cubic structure, normal octahedron structure (no rotation direction), diamond structure, normal rhombic dodecahedron (no rotation direction) and so on [108-110].

However, the relationship between the porosity, cell edge length, cell diameter and cell orientation has not been discussed systematically [111]. In the present study, mechanical properties of titanium foams with truncated octahedron and rhombic dodecahedron cells are investigated systematically. Optimal cell geometry for mechanical properties such as plateau stress and energy absorption is clarified through the compressive tests.

3.2 Experimental procedure

Periodic truncated octahedron and rhombic dodecahedron open-cell geometries are constructed by using a commercial 3D-CAD software. 3D images of the unit-cells are shown in Fig. 3.1. Octa_A and Octa_B are the truncated octahedron cells with the edge length of a. In the x-y-z orthogonal coordinate system, Octa_B has cell geometry after 54.7 deg rotation around y-axis and 45 deg rotation around z-axis of Octa_A. Dodeca_A, Dodeca_B and Dodeca_C are the rhombic dodecahedron cells with the edge length of a. In the x-y-z orthogonal coordinate system, Dodeca_B has cell geometry after 90 deg rotation around x-axis of Dodeca_A. Dodeca_C has cell geometry after 54.7 deg rotation around y-axis of Dodeca_A. Here, the compression direction is parallel to z-axis.

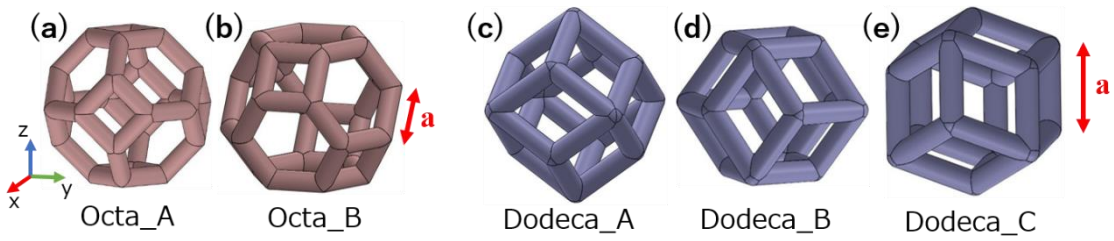

Fig. 3.1 3D-CAD images of two types of truncated octahedron unit cells, (a) and (b), and three types of rhombic dodecahedron unit cells, (c), (d) and (e). Compression direction is parallel to the *z*-axis.

In the case of truncated octahedron unit cell with the edge length, a, the volume is expressed as

$$V_0^{\mathrm{Octa}} = 8\sqrt{2}a^3 \tag{3.1}$$

By assuming the cylindrical shape of the cell edges, the volume of cell edges in the unit cell is calculated as

$$V_a^{\mathrm{Octa}} = \frac{\pi}{4}t^2 \times \frac{1}{3} \times a \times 36 = 3\pi a t^2 \tag{3.2}$$

where t is the diameter of cylindrical edges. Therefore, the nominal porosity, p_{N}, becomes

$$p_{\mathrm{N}}^{\mathrm{Octa}} = \frac{V_0^{\mathrm{Octa}} - V_a^{\mathrm{Octa}}}{V_0^{\mathrm{Octa}}} = 1 - \frac{3\sqrt{2}\pi}{16}\left(\frac{a}{t}\right)^{-2}. \tag{3.3}$$

In the case of rhombic dodecahedron unit cell with the edge length, a, the volume is expressed as

$$V_0^{\mathrm{Dodeca}} = \frac{16}{9}\sqrt{3}a^3. \tag{3.4}$$

By assuming the cylindrical shape of the cell edges, the volume of cell edges in the unit cell is calculated as

$$V_a^{\mathrm{Dodeca}} = \frac{\pi}{4} t^2 \times \frac{1}{3} \times a \times 24 = 2\pi a t^2 \qquad (3.5)$$

where t is the diameter of cylindrical edges. Therefore, the nominal porosity becomes

$$p_{\mathrm{N}}^{\mathrm{Dodeca}} = \frac{V_0^{\mathrm{Dodeca}} - V_a^{\mathrm{Dodeca}}}{V_0^{\mathrm{Dodeca}}} = 1 - \frac{3\sqrt{3}\pi}{8} \left(\frac{a}{t}\right)^{-2}. \qquad (3.6)$$

The nominal porosities of both truncated octahedron cell and rhombic dodecahedron cell are plotted as a function of the normalized edge length in Fig. 3.2(a). The normalized porosity increases with increasing the normalized edge length. The edge length of the rhombic dodecahedron unit cell is longer than that of the truncated octahedron unit cell.

When the volume of the unit cell is equivalent to the volume of sphere with the diameter of d, each nominal porosity is expressed as

$$p_{\mathrm{N}}^{\mathrm{Octa}} = 1 - 3^{\frac{5}{3}} \times 2^{-\frac{1}{2}} \times \pi^{\frac{1}{3}} \times \left(\frac{d}{t}\right)^{-2}, \qquad (3.7)$$

$$p_{\mathrm{N}}^{\mathrm{Dodeca}} = 1 - 3^{\frac{7}{6}} \times (2\pi)^{\frac{1}{3}} \times \left(\frac{d}{t}\right)^{-2}. \qquad (3.8)$$

The nominal porosities are plotted as a function of the normalized cell diameter in Fig. 3.2(b). Relationship between the normalized porosity and normalized cell diameter of two unit cells becomes almost the same. The nominal porosities of the present titanium foam specimens are 80% and 90%. Since the thickness of all cell edges are fixed at 1 mm, the cell diameters of specimens with 80% and 90% porosities are about 6 mm and 8 mm, respectively.

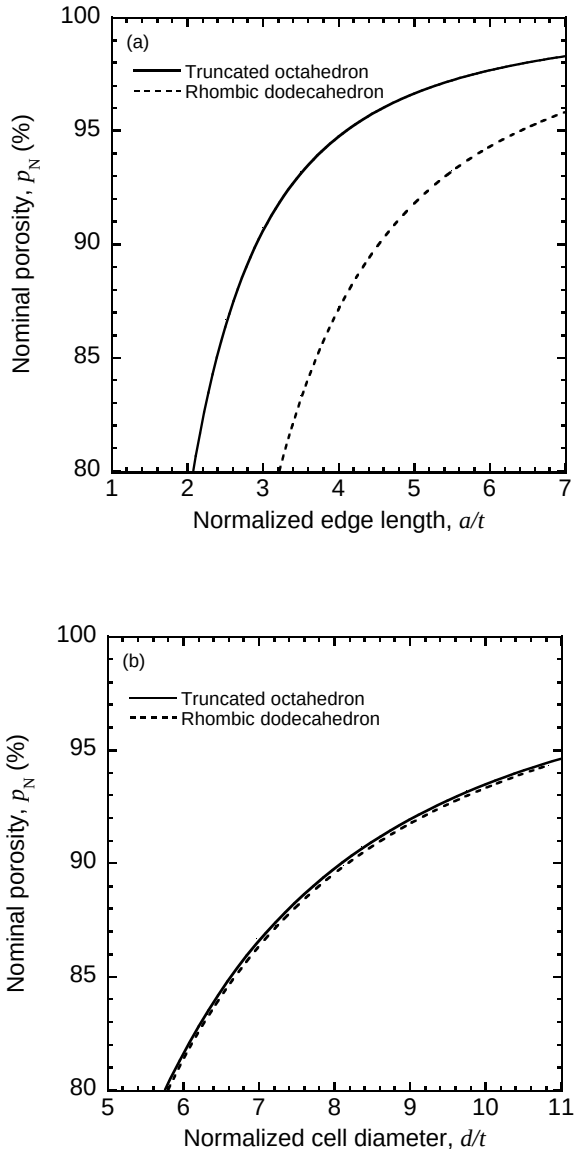

Fig. 3.2 Nominal porosities of truncated octahedron and rhombic dodecahedron unit cells are plotted as a function of (a) the normalized edge length and (b) the normalized cell diameter.

Fig. 3.3 Arcam A2X machine as electron beam melting process.

Open-cell titanium foams with different porosities and cell geometries were manufactured in vacuum through 3D EBM process. Arcam A2X machine (Fig. 3.3) designed for titanium alloys was used in this study. Commercially pure titanium, Grade 2, powder was used as a starting material. The chemical composition is shown in Table 3.1. The shape of the compressive specimens has cylindrical shape with 30 mm in diameter and 30 mm in height. Building direction is parallel to the cylindrical axis. No heat treatment was carried out after EBM process. Mechanical properties of the titanium foam specimens were examined by compressive tests at room temperature using a Shimadzu Autograph AG-50kNISD in Fig. 3.4. Crosshead speed was fixed at 10 mm/min [112].

Table 3.1 Chemical composition of commercially pure titanium, Grade 2, powder.

Element	C	Fe	O	N	H	Ti
mass%	0.02-0.08	0.07-0.3	0.14-0.25	0.02-0.03	0.002-0.015	Bal

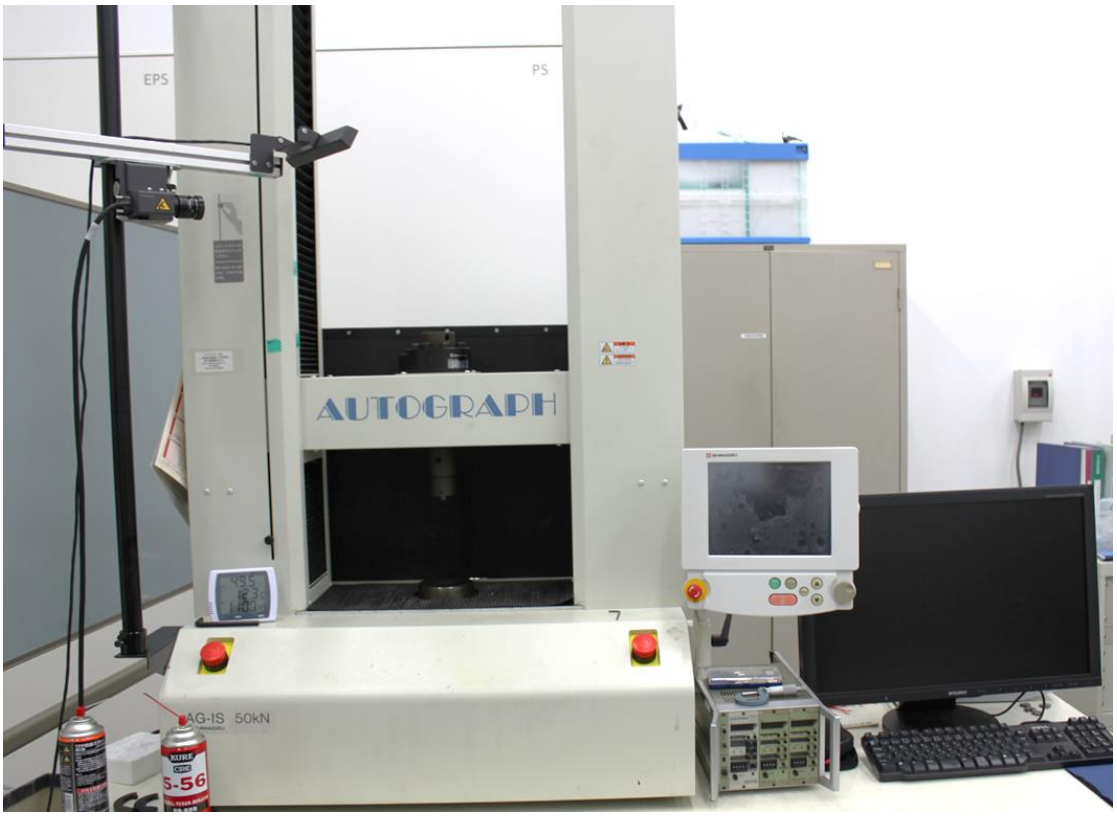

Fig. 3.4 titanium foam specimens were examined by compressive tests at room temperature using a Shimadzu Autograph AG-50kNISD.

3.3 Results

3.3.1 Effect of porosity

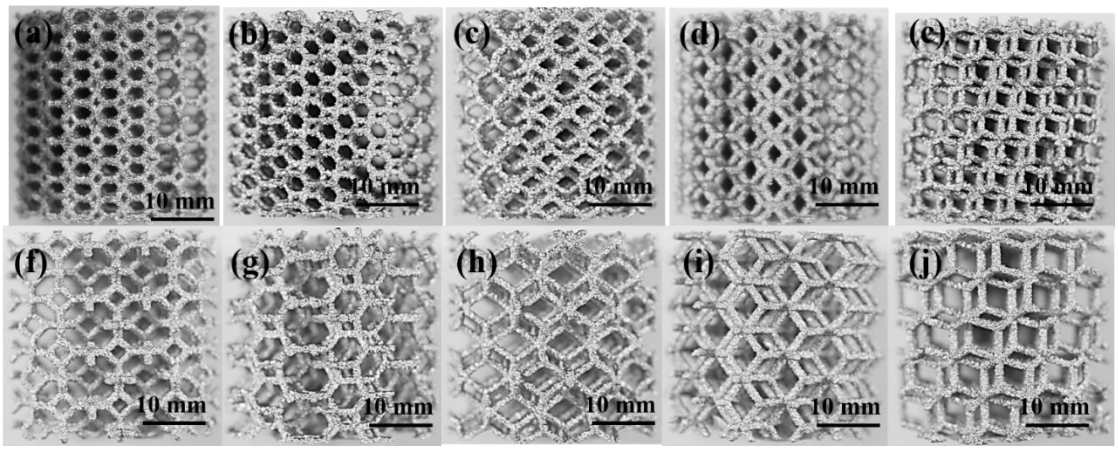

Fig. 3.5 Photographs of open-cell titanium foam specimens manufactured through EBM process. Octa_A (a,b), Octa_B (b,g), Dodeca_A (c,h), Dodeca_B (d,i), Dodeca_C (e,j). Each nominal porosity is 80% (a-e) and 90% (f-j).

Photographs of cylindrical titanium foam specimens are shown in Fig. 3.5. Vertical direction is parallel to the compression direction. Thickness of the cell edges is 1 mm in all specimens. It is noted that the cell diameters of truncated octahedron unit cells are the same as those of rhombic dodecahedron cells at the same porosity.

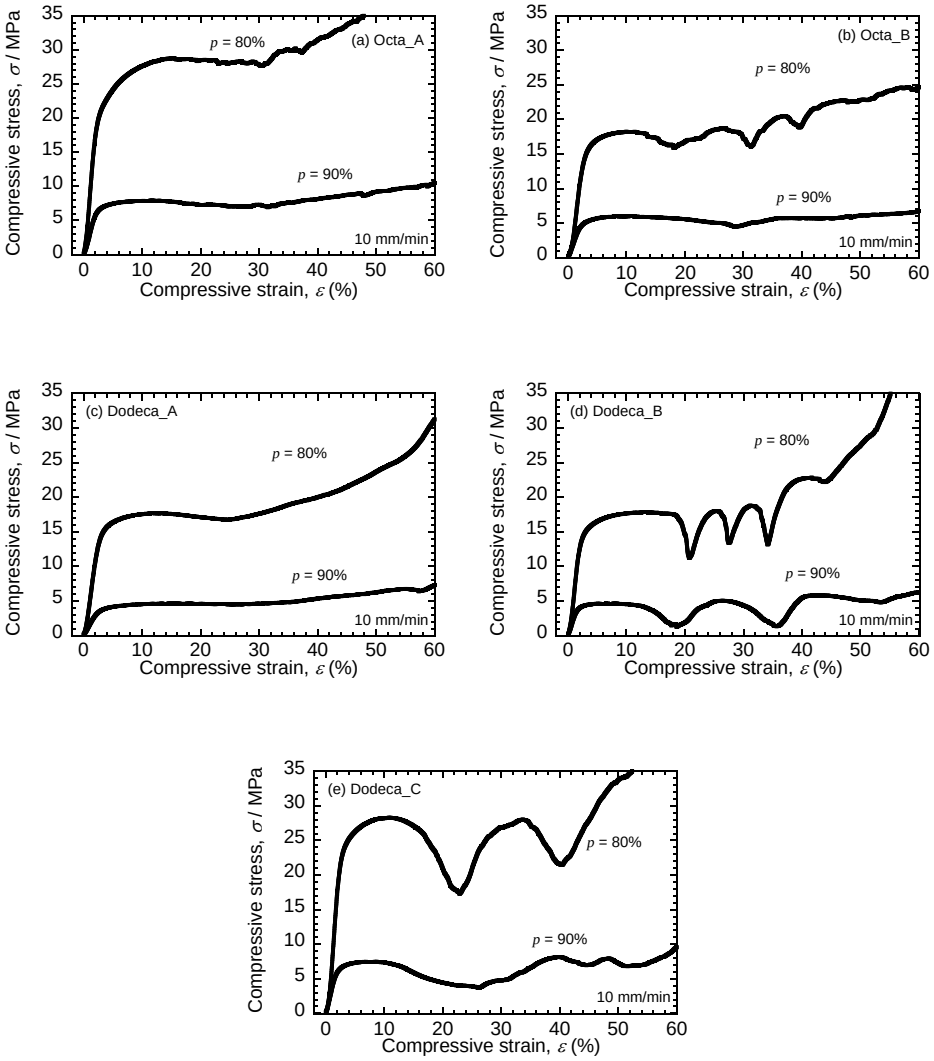

Fig. 3.6 Compressive stress-strain curves of open-cell titanium foams, (a) Octa_A, (b) Octa_B, (c) Dodeca_A, (d) Dodeca_B and (e) Dodeca_C with different porosities. The crosshead speed is fixed at 10 mm/min.

Compressive stress-strain curves of ten kinds of titanium foam specimens are shown in Fig. 3.6. The plateau stresses of Octa_A (80% and 90%) are 28.9 MPa and 7.4 MPa, respectively. The plateau stresses of Octa_B (80% and 90%) are 18.4 MPa and 5.3 MPa, respectively. The plateau stresses of Dodeca_A (80% and 90%) are 17.9 MPa and 4.7 MPa, respectively. The plateau stresses of Dodeca_B (80% and 90%) are 17.3 MPa and

3.7 MPa, respectively. The plateau stresses of Dodeca_C (80% and 90%) are 23.9 MPa and 5.4 MPa, respectively. Yield stress of dense Grade 2 titanium manufactured through 3D EBM process has been reported as 540 MPa, which was much higher than those of the present titanium foams. The absorbed energy up to 50% strain of Octa_A (80% and 90%) are 6.5 MJ/m^3 and 2.2 MJ/m^3, respectively. The absorbed energy of Octa_B (80% and 90%) are 4.1 MJ/m^3 and 1.6 MJ/m^3, respectively. The absorbed energy of Dodeca_A (80% and 90%) are 4.1 MJ/m^3 and 1.3 MJ/m^3, respectively. The absorbed energy of Dodeca_B (80% and 90%) are 4.1 MJ/m^3 and 1.2 MJ/m^3, respectively. The absorbed energy of Dodeca_C (80% and 90%) are 5.9 MJ/m^3 and 1.8 MJ/m^3, respectively. Both the plateau stress and absorbed energy of titanium foams with 80% porosity were higher than those of 90% porosity.

3.3.2 Effect of shape of unit cell

The plateau stresses of truncated octahedron cells were higher than those of rhombic dodecahedron cells. Energy absorption of truncated octahedron cells were also higher than those of rhombic dodecahedron cells. As shown in Fig. 3.2(b), the cell diameter of these cells is the same. Therefore, the difference is not due to the size effect.

3.3.3 Effect of compression direction

The plateau stress and the absorbed energy of Octa_A specimen were higher than those of Octa_B specimen. The plateau stress and the absorbed energy of Dodeca_C specimen were higher than those of Dodeca_A and Dodeca_B specimens. The plateau stress and the absorbed energy of Dodeca_A and Dodeca_B are almost the same. These differences were caused by the anisotropic deformation of open-cell titanium foams.

3.3.4 Macroscopic shear bands

Photographs of the titanium foam specimens at the compressive strain of 20% are shown in Fig. 3.7. Octa_A and Dodeca_A specimens showed relatively uniform deformation. On the other hand, the macroscopic shear bands are observed in Octa_B, Dodeca_B and Dodeca_C specimens. Oscillations of the stress-strain curves observed in these specimens [Fig. 3.6 (b), (d) and (e)] are due to the shear band formation.

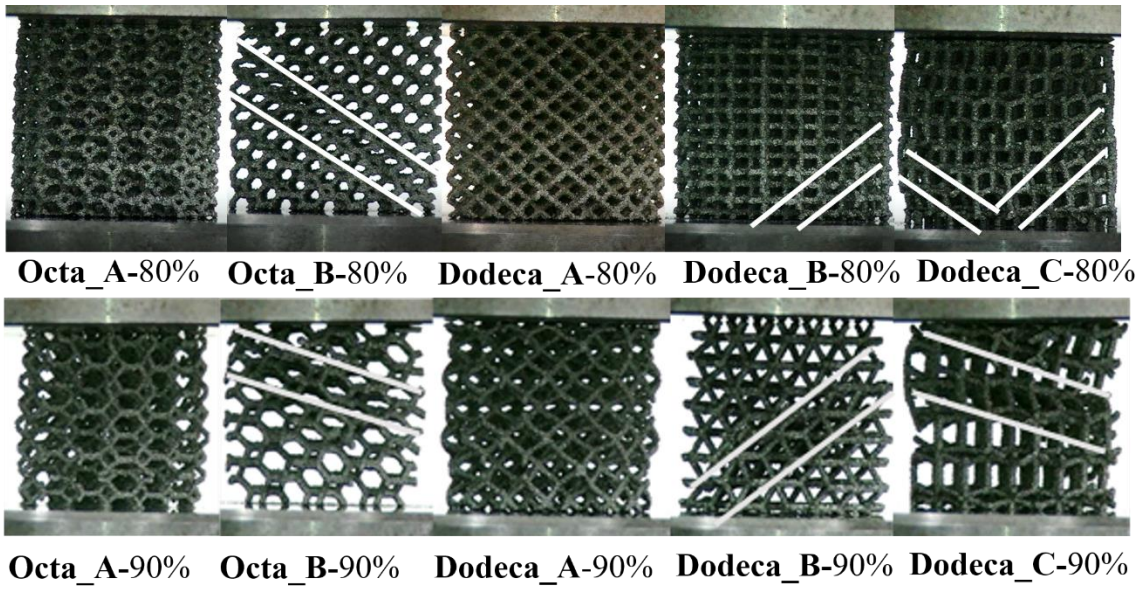

Fig. 3.7 Photographs of the compressive test specimens at the compressive strain of 20%. Macroscopic shear bands are observed in Octa_B, Dodeca_B and Dodeca_C specimens.

3.4 Discussion

Mechanical properties of the present titanium foam specimens are listed in Table 3.2. In many porous materials, the relationship between the plateau stress and the relative density has been expressed by

$$\sigma_P = C\sigma_S \left(\frac{\rho^*}{\rho_S}\right)^n. \quad (3.9)$$

where C is the constant, σ_s is the yield stress of the cell wall material, ρ^* is the density of the foam, ρ_s is the density of the cell wall material and n is the exponent. In the present open-cell titanium foams, the value of n is almost equal to two, which is independent of the cell geometry. If the porous material has completely plateau region, the relationship between the absorbed energy and the relative density becomes identical to that of plateau stress. However, the value of n in energy absorption was slightly smaller than that of plateau stress. This is due to the oscillation of stress-stain curves caused by the formation of macroscopic shear bands.

The strength of the present titanium foams depended on the cell geometry. Titanium foams with truncated octahedron cells showed higher strength than those with rhombic dodecahedron cells. This is due to the cell edge length. In the case of open-cell metal foams, the main mechanism of compressive deformation is the bending or buckling of the cell edges. According to the simple beam theory, the short beams shows high resistance to bending or buckling. As shown in Fig. 3.2(a), the cell edge length of the truncated octahedron cells is shorter than that of rhombic dodecahedron cells. Therefore, we can conclude that the truncated octahedron cell geometry is effective to increase the strength compared to the rhombic dodecahedron cell geometry.

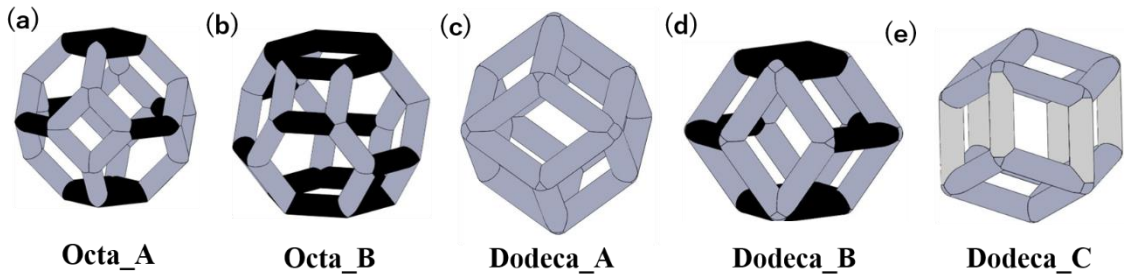

Fig. 3.8 Parallel, perpendicular and oblique cell edges against the compression direction are colored by light gray, black and dark gray, respectively. (a) Octa_A, (b) Octa_B and (d) Dodeca_B consist of perpendicular and oblique cell edges. (c) Dodeca_A consists of only oblique cell edges. (e) Dodeca_C consists of parallel and oblique cell edges.

The strength of the present titanium foams also depended on the compression direction. This is due to the orientation of the cell edges. Orientation of the cell edges are classified to three types: parallel, perpendicular and oblique cell edges against the compression direction (z-axis). These cell edges are illustrated as light gray, black and dark gray colors in Fig. 3.8. Difference between Octa_A and Octa_B specimens is due to the number of oblique edges, 24 oblique edges in Octa_A and 18 oblique edges in Octa_B [Table 3.2]. Oblique cell edges have high resistance to the compressive deformation compared to perpendicular cell edges. Therefore, Octa_A specimen consisting of many oblique cell edges showed high compressive strength compared to Octa_B specimen. On the other hand, Dodeca_C specimen has 6 parallel edges, which have highest resistance to compressive deformation. Therefore, Dodeca_C specimen showed the highest

compressive strength compared to Dodeca_A and Dodeca_B specimens, which have no parallel edges. Difference between Dodeca_A and Dodeca_B specimens is due to the same reason as octahedron specimens. Dodeca_A specimen consisting of many oblique edges, 24 oblique edges, showed high compressive strength compared to Dodeca_B specimen consisting of 12 oblique edges.

Present experimental results revealed that the cell geometry of Octa_A lattice was effective to increase the compressive strength and the absorbed energy. This result can be not only valid for titanium foams but also for other metal foams.

The formation of shear bands can be discussed. At initial period of linear elasticity, no shear band was formed. After the yielding, the shear band generated in the direction of the maximum shear stress of the cylindrical specimen. In the case of conventional metal foams such as ALPORAS aluminum foams, local deformation region like shear band generates in the perpendicular plane against the compression direction. The difference in the compressive deformation is probably due to two reasons. One is the ordered and homogeneous cell geometry in the present 3D EBM titanium foams. In the case of PM titanium foams with disordered cell geometry, no shear band formation has been observed. Present cell morphology is similar to the balk single crystal. Therefore, the shear band during the compression was formed in the direction of maximum shear stress. Another is the high buckling strength of the present titanium foams. Modulus and strength of titanium are higher than aluminum. Therefore, the local buckling was limited and the shear band was formed. It is recommended that the soft cell wall materials are effective to reduce the shear band formation. On the other hand, the shear band formation was limited in the titanium foams with 90% porosity against 80% porosity. In the case of high porosity, the local buckling occurred preferentially because of long cell edges.

Table 3.2 Cell geometry and mechanical properties in ten titanium foam specimens are summarized.

Unit cell	Number of			Nominal Porosity, p_N (%)	Cell diameter, d/t	Plateau stress, σ_P / MPa	Energy absorption, W / MJm^{-3}
	Parallel edges	Perpendicular edges	Oblique edges				
Octa_A	0	12	24	80	5.7	28.9	6.5
				90	8.0	7.4	2.2
Octa_B	0	18	18	80	5.7	18.4	4.1
				90	8.0	5.3	1.6
Dodeca_A	0	0	24	80	5.8	17.9	4.1
				90	8.2	4.7	1.3
Dodeca_B	0	12	12	80	5.8	17.3	4.1
				90	8.2	3.7	1.2
Dodeca_C	6	0	18	80	5.8	23.9	5.9
				90	8.2	5.4	1.8

3.4.1 Simulation for share band formation

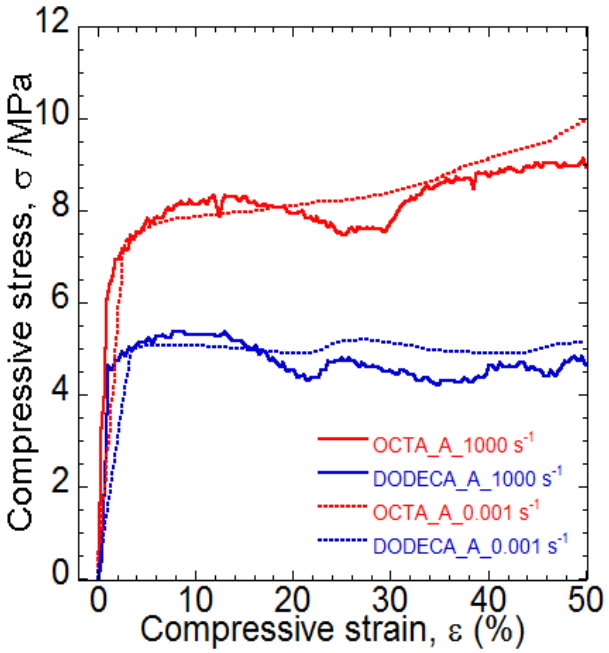

Fig 3.9 compressive stress- strain curve with experimental result and FEM data. Flow stress was cell transmitted to the cell column and the initial yield stress decreased

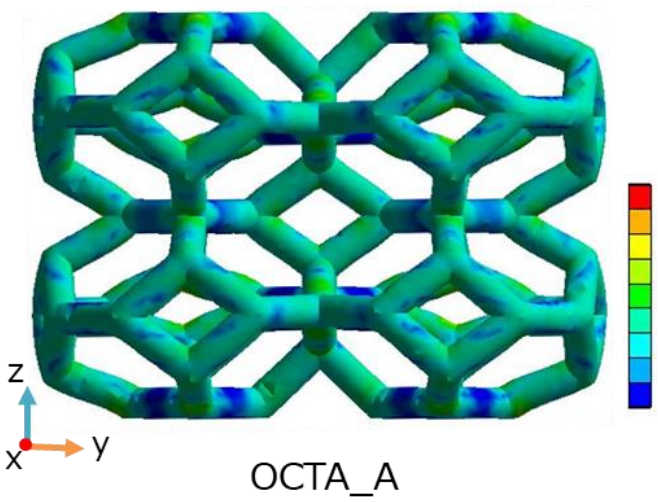

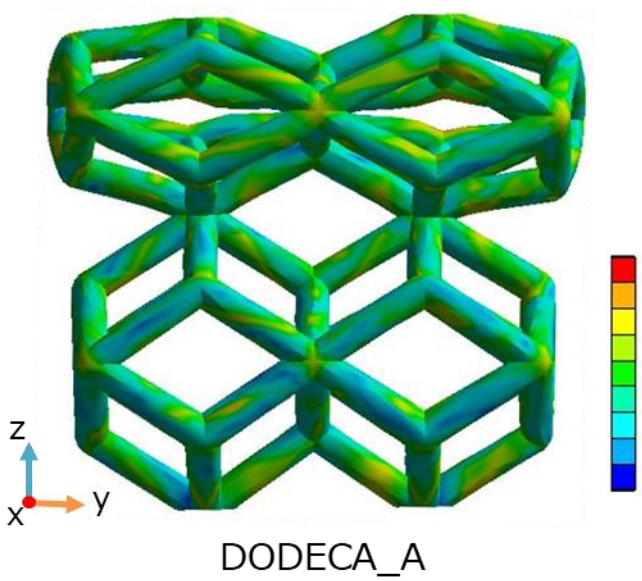

Fig 3.10 FEM for compressive deformation as Equivalent stress distribution at 20% strain.

There is no stress concentration and the distribution of stress on the whole for octahedron structure. However, Stress concentrates near the cell edge in dodecahedron structure in Fig 3.10. For the truncated octahedron structure of AlSi10Mg alloy foam with porosity of 97 %, a result of the plastic hinge generating load calculated by FEM for plastic hinge of

Centre crack model, Axial compressive model, buckling model were reported [127]. Deformation tends were occurring sequentially from Centre crack model, Axial compressive model to buckling model with the load increased. It is considered buckling model has biggest load for plastic hinge.

3.5 Conclusions

Open-cell titanium foams with different porosities and unit cell geometries were manufactured through 3D EBM process. Compressive tests at room temperature achieved the following experimental results.

Plateau stress and absorbed energy of open-cell titanium foams increased with decreasing the porosity.

Plateau stress and absorbed energy of the titanium foams with the truncated octahedron unit cells were higher than those of the titanium foams with rhombic dodecahedron unit cells. This is due to the short cell edges in truncated octahedron unit cells compared to in rhombic dodecahedron cells.

Plateau stresses of Octa_A and Dodeca_C specimens were higher than those of other specimens. The reason is due to the orientation of the cell edges. Parallel edges against the compression direction are effective to increase the initial flow stress.

Metal foams consisting of Octa_A lattice have a potential for energy absorbing applications.

In addition, the macroscopic shear bands were formed in some specimens. It caused the decrease in the absorbed energy. Mechanism of the shear band formation can be explained by both the ordered cell geometry and the buckling strength of the base material. Disordered cell geometry and soft material is probably effective to reduce the shear band formation. These results are not only valid for the present titanium foams but also for other metal foams such as aluminum foams.

References

[98] Ashby MF, Evans A, Fleck NA, Gibson LJ, Hutchinson JW, Wadley HN. Metal foams: a design guide: Butterworth-Heinemann, Oxford, UK, ISBN 0-7506-7219-6, Published 2000, Hardback, 251. Elsevier; 2002.

[99] Jian X, Hao C, Guibao Q, Yang Y, Xuewei L. Investigation on relationship between porosity and spacer content of titanium foams. Materials & Design 2015;88:132-7.

[100] Yue X-Z, Hur B-Y. Effect of the Holding Temperature and Vacuum Pressure for the Open Cell Mg Alloy Foams. Korean Journal of Materials Research 2012;22:309-15.

[101] Rafi H, Karthik N, Gong H, Starr TL, Stucker BE. Microstructures and mechanical properties of Ti6Al4V parts fabricated by selective laser melting and electron beam melting. Journal of Materials Engineering and Performance 2013;22:3872-83.

[102] Kruth J-P, Mercelis P, Van Vaerenbergh J, Froyen L, Rombouts M. Binding mechanisms in selective laser sintering and selective laser melting. Rapid Prototyping Journal 2005;11:26-36.

[103] Jiang Y, Wang Q. Highly-stretchable 3D-architected mechanical metamaterials. Scientific Reports 2016;6:34147.

[104] Heinl P, Körner C, Singer RF. Selective electron beam melting of cellular titanium: mechanical properties. Advanced Engineering Materials 2008;10:882-8.

[105] Traini T, Mangano C, Sammons R, Mangano F, Macchi A, Piattelli A. Direct laser metal sintering as a new approach to fabrication of an isoelastic functionally graded material for manufacture of porous titanium dental implants. Dental materials 2008;24:1525-33.

[106] Mullen L, Stamp RC, Brooks WK, Jones E, Sutcliffe CJ. Selective Laser Melting: A regular unit cell approach for the manufacture of porous, titanium, bone in-growth

constructs, suitable for orthopedic applications. Journal of Biomedical Materials Research Part B: Applied Biomaterials 2009;89:325-34.

[107] Salmi M, Paloheimo K-S, Tuomi J, Wolff J, Mäkitie A. Accuracy of medical models made by additive manufacturing (rapid manufacturing). Journal of Cranio-Maxillofacial Surgery 2013;41:603-9.

[108] SU X-b, YANG Y-q, Peng Y, SUN J-f. Development of porous medical implant scaffolds via laser additive manufacturing. Transactions of Nonferrous Metals Society of China 2012;22:s181-s7.

[109] Murr L, Esquivel E, Quinones S, Gaytan S, Lopez M, Martinez E, et al. Microstructures and mechanical properties of electron beam-rapid manufactured Ti–6Al–4V biomedical prototypes compared to wrought Ti–6Al–4V. Materials Characterization 2009;60:96-105.

[110] Xiao L, Song W, Wang C, Liu H, Tang H, Wang J. Mechanical behavior of open-cell rhombic dodecahedron Ti–6Al–4V lattice structure. Materials Science and Engineering: A 2015;640:375-84.

[111] Yue X-Z, Matsuo K, Kitazono K. Compressive Behavior of Open-Cell Titanium Foams with Different Unit Cell Geometries. Materials Transactions 2017;58:1587-92.

[112] Yue X-Z, Fukazawa H, Kitazono K. Strain rate sensitivity of open-cell titanium foam at elevated temperature. Materials Science and Engineering: A 2016;673:83-9.

[127] Yasutaka Satou, Masatsugu Otsuki, Mitsuhisa Baba, Hirobumi, Tobe, Kosei Ishimura, Koichi Kitazono, compressive behaviors of 3D additive manufactures truncated otcahedron for impact energy absorption of landing gear , 第 61 回宇宙科学技術連合講演会講演集, JSASS-2017-4356.

Chapter 4: Effect of heat treatment on mechanical properties of porous Ti-6Al-4V alloy manufactured by 3D selective laser melting

4.1 Introduction

Titanium foams have great potential for a number of application in the automotive, railway and aerospace industries. The open-cell foam has a complex macrostructure consisting of an interconnected network [113].

Titanium and titanium alloy has excellent mechanical properties, corrosion resistance and biological properties, titanium powder metallurgy (PM) offers the possibility of creating a porous titanium foams [114]. A rapid prototyping method named selective laser melting (short for SLM), 3D printing, or Additive Manufacturing (AM) technique. The high power-density laser was used to melt and fuse titanium powders together [115]. In the aerospace field, many studies have been on the mechanical properties of dense Ti - 6Al - 4V by the SLM method, it has been put to practical use for aircraft nozzles. The new technology for titanium foams is possible to directly manufacture free shapes, and solved randomness of pore shape and pore size of product by the traditional manufacturing method.

The 7075 and 6061 aluminum alloy foams [116] were studied with the aim of investigating the effect of heat treatment on their axial crushing behavior by Francesca Campana [117]. AA6061 foam were subjected to different heat treatments in order to evaluate possibilities to tailor mechanical properties reported by Dirk Lehmhus and john Banhart [118]. Effect of heat treatment on the compressive deformation behavior of Open

cell 6101 al foam was studied by J zhou [119]. Influence of heat treatment on the microstructure and mechanical behavior of open cell AlSi7Mg0.3 foams on different length scales were published by Paul Scchuler[120]. Effect of annealing on the mechanical propertied of Nano-copper reinforced open cell al/cu foams were discussed by Yi Sun [121]. An experimental study of the (Ti–6Al–4V)–xH phase diagram using in situ synchrotron XRD and TGA/DSC techniques was reported by Pei Sun in University of Utah [122]. A study of the microstructural evolution during selective laser melting of Ti–6Al–4V was discussed by Lore Thijs [123]. Heat treatment of Ti6Al4V produced on microstructure and mechanical properties by Selective Laser Melting was studied by Bey Vrancken [124]. Microstructure and mechanical behavior of porous Ti–6Al–4V parts published by E. Sallica-Leva [125]. The mechanical properties of titanium foams are able to improve by the different annealing conditions. There is important to investigate the effects of heat treatment on the mechanical properties of titanium alloy and titanium foams.

Recently many research forces on microstructure and mechanical properties of Ti-6Al-4V or the implant performance of Ti-6Al-4V. However, little studies have investigated effect annealing on energy absorption capacities of titanium foam with octahedron structure. In this paper, titanium alloy foam has been treated with annealing process. The annealing process was subjected to obtained stabilized mechanical properties. The quasi-static compressive experiments were carried out at room temperature. Compressive stress-strain curves were obtained at different porosity. Accordingly, the influence of annealing on the deformation behavior of titanium foams are to investigate. Furthermore, we aim to evaluate the compression characteristics and energy absorbing.

4.2 Materials and Methods

Table 4.1. Chemical composition of Ti-6Al-4V specimens, (%)

Ti	Al	V	Fe	C	O	N	H
Balance	5.5-6.5	3.5-4.5	0-0.25	0-0.08	0-0.13	0-0.05	0-0.012

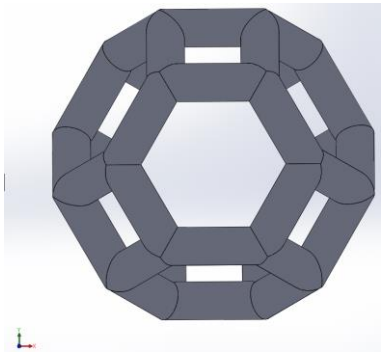

Fig. 4.1 Three-dimensional CAD image of a truncated octahedron unit cell with different location.

SLM is manufactured quickly in the production of various kinds of small quantities. Freedom of shaping is extremely high; however, it depends on equipment and materials, there are restrictions on the minimum thickness and allowable angle. Also, in order to remove internal powders after modeling, the porous material needs to have an open cell structure which vacancies are connected to each other. The Solidworks software was used to draw the uniform porous structure of truncated octahedron unit cell as shown in Fig. 4.1. The unit cells were same density and porosity in the two kinds of location. Titanium foams prepared by the SLM method which is a Three-dimensional layered

forming method was used. Ti - 6Al - 4V powder was used for preparation. The chemical composition is shown in Table 4.1. Production was carried out with Concept Laser M2 (Fig. 4.2) under a high-purity Ar atmosphere containing no more than 100 ppm oxygen. This specimen was designed a cylindrical shape of Φ 30 × h 30 mm and a thin plate has thickness of 1 mm on the top and bottom in order to secure a compression surface. Three sorts of porosity (90, 93, 96%) were prepared based on the lattice truncated octahedral. Cell edge average thickness of porosity (90, 93, 96%) were 0.63 mm, 0.58 mm, 0.57 mm, respectively.

Fig. 4.2 Selective Laser Melting from Concept Laser M2

Fig. 4.3 Photograph of SEM

Compressive character of Ti - 6Al - 4V foams were performed before and after heating treatment under constant crosshead speed of 10 mm/min by AUTOGRAPH (AG-50kNIS, Shimadzu). Specimens were performed grinding with SiC abrasive papers and polishing with 70% Hydrogen peroxide and 30% OP-S suspension mixed solution. Chemically etched was used 10% Fluoric acid, 5% Nitric acid and 85% H_2O mixed solution. Specimens were analysis by scanning electron microscope (JEOL JSM-6510A in Fig. 4.3). An RIGAKU Ultima IV X-ray diffractometer was used for structure characterization of Ti - 6Al - 4V foams.

4.3 Results

4.3.1 Macrostructure and Microstructure for specimen

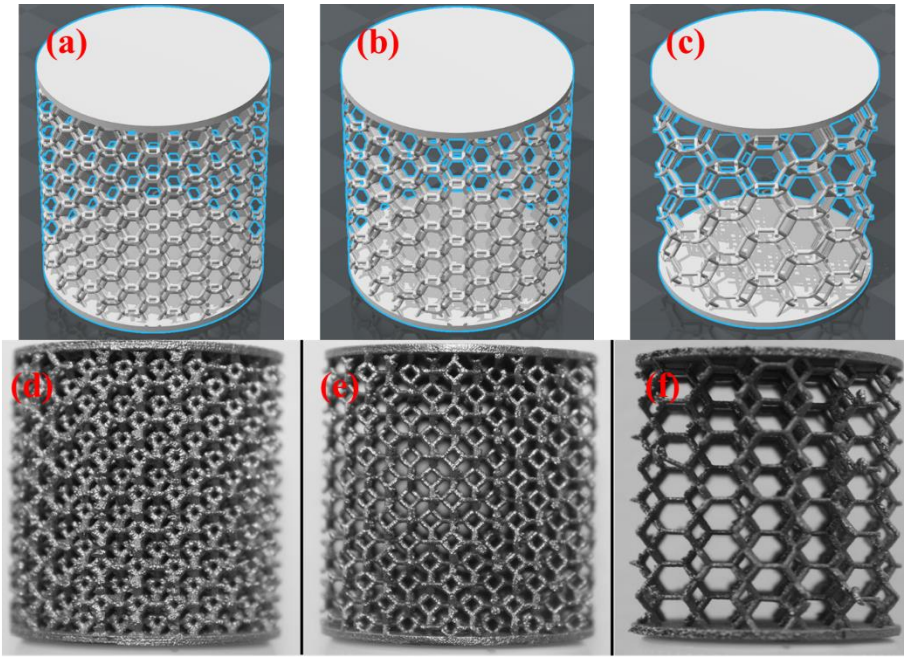

Fig. 4.4 Three-dimensional CAD image and photographs of cylindrical compression specimens with different nominal porosities of (a and d) 90%, (b and c) 93% and (c and f) 96%.

Model of lattice truncated octahedron with top and bottom plate were design by solidword software in [Fig. 4.4a, 4.4b and 4.4c]. Specimens of porosity (90, 93, 96%) were fabricated by 3D selective laser melting process in [Fig. 4.4d, 4.4e and 4.4f]. Relationship between the normalized porosity and normalized cell diameter were report as design rule [111].

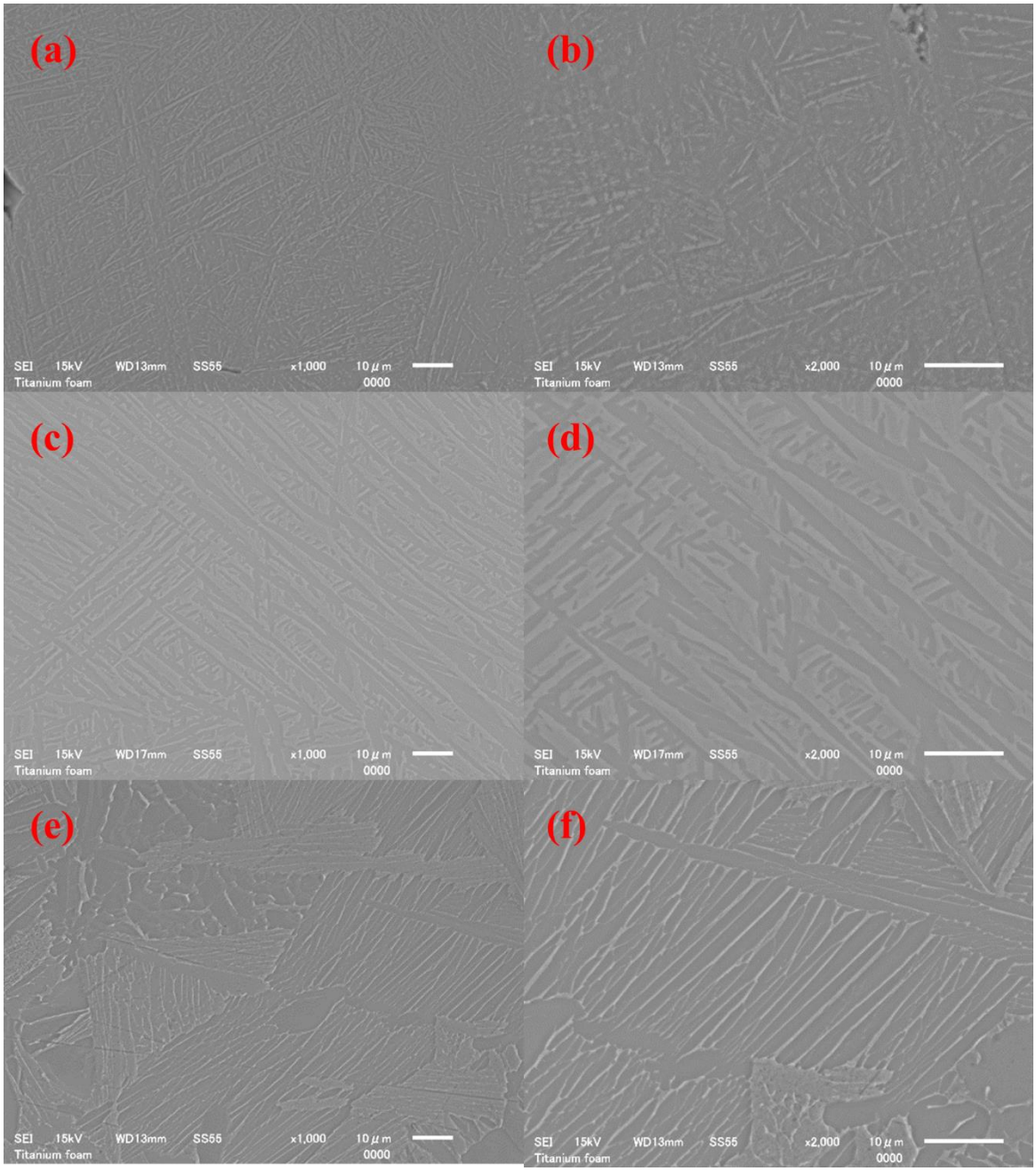

Fig. 4.5 SEM micrographs of cell edges in porous Ti-6Al-4V alloys. (a) and (b) As-build Ti-6Al-4V with x1000 and x2000; (c) and (d) are after annealing at HT 1173 K with x1000 and x2000, phase is α+β; (e) and (f) are after annealing at HT 1323 K with x1000 and x2000, phase is β phase, Lighter zones are beta phase, the dark phase is the alpha phase.

Fig. 4.5 are the phases composition of Ti-6Al-4V titanium foam with as-built, after annealing at 1173 K and 1323K. The cell edges microstructural photos of Ti-6Al-4V foams are shown in the three annealing conditions. Ti-6Al-4V foams with porosity of 90% annealed at 1173 K 1 hour. SEM be used by x20, x100, x1000 and x3000. The Ti-6Al-4V foams are tough metal material. Alpha phase is the dominant fraction even after heat treatment at 1323 K. XRD pattern analysis the hexagonal closed-packed (HCP) structure in Fig. 4.6 as predominantly the α-phase. It was not clearly detected body centered cubic (BCC) β-phase at peaks 2θ=38.5° and 2θ=69°. The peak 2θ=38.5° and 2θ=69° result were thought from the HCP α or martensitic α' phase via the transformed into β phase at 1323 K annealing temperatures. EDS analysis element map of porous Ti-6Al-4V alloys after annealing 1173 K in Fig 4.7(a). Used Image J software calculated As-built specimen has beta phase area fraction of 15.68%; For the annealing with HT 1173 K, this specimen has beta phase area fraction of 41.596%; For the annealing with HT 1323 K, this specimen has beta phase area fraction of 21.317% in Fig 4.7(b).

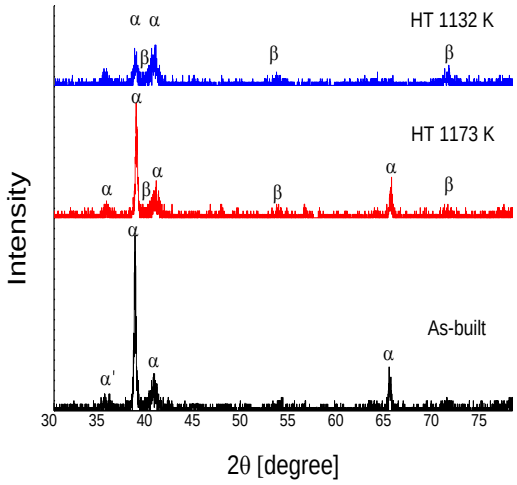

Fig. 4.6 Results of XRD analysis of porous Ti-6Al-4V alloys.

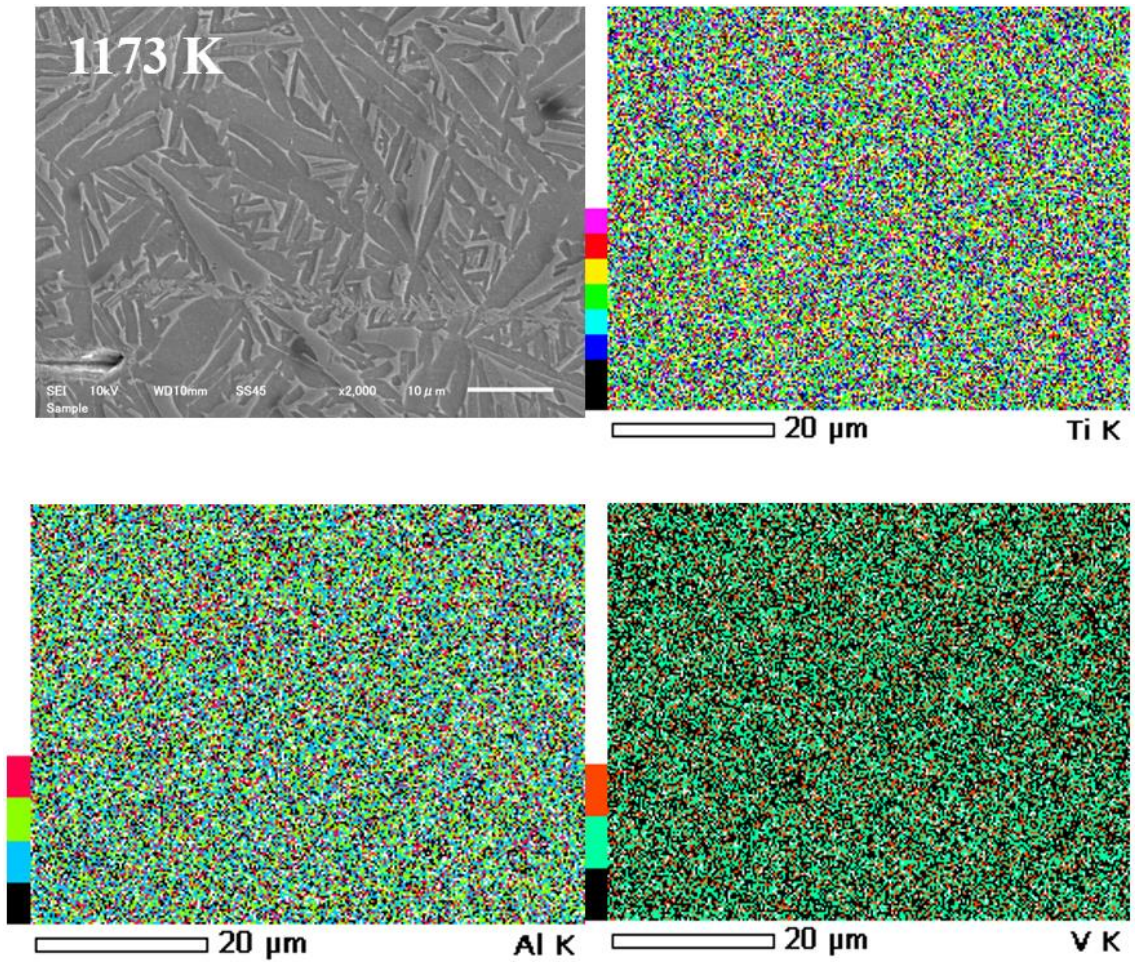

Fig 4.7(a). Results of EDS analysis element map of porous Ti-6Al-4V alloys after annealing 1173 K

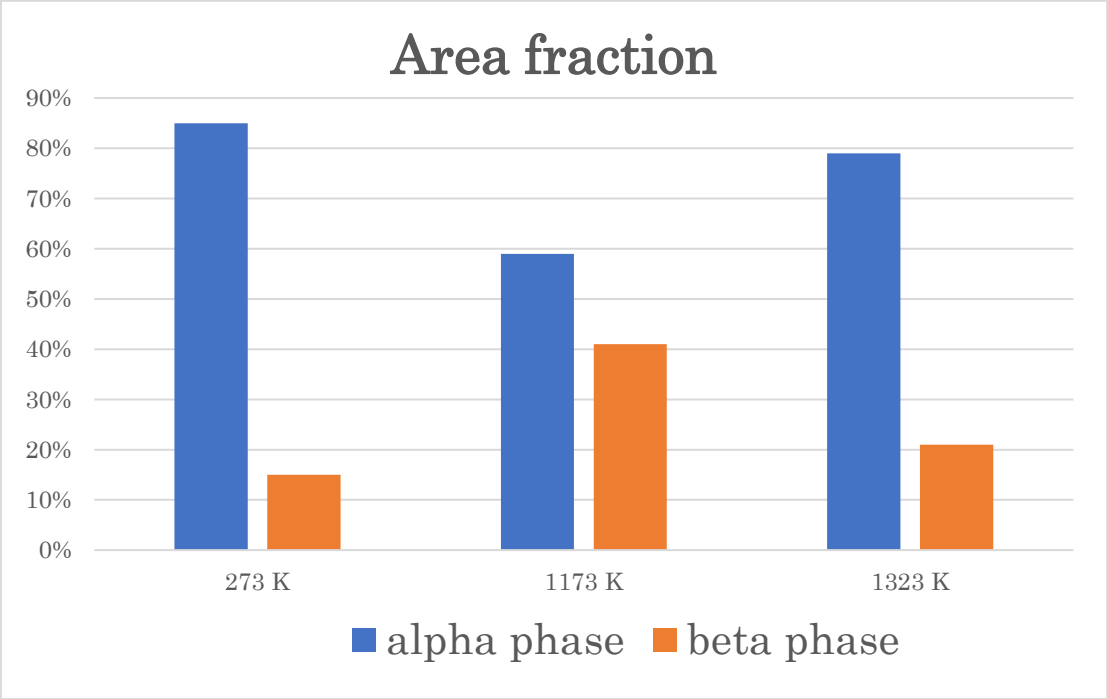

Fig 4.7(b) the result shows that the α phase decreases and β phase increases with the increase of annealing temperature.

4.3.2 Vickers hardness

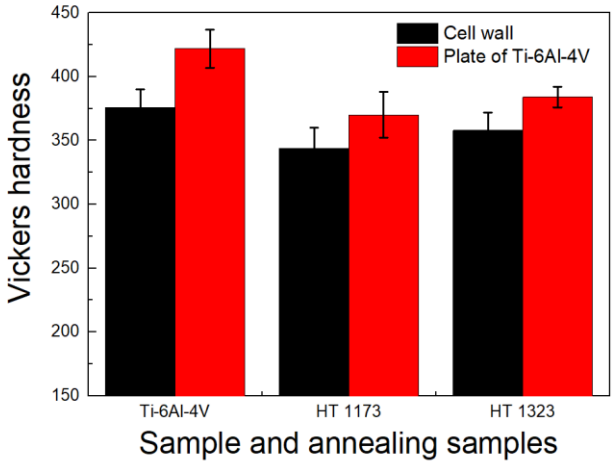

Fig. 4.8 Vickers hardness of dense Ti-6Al-4V alloys manufactured through 3D SLM process.

Titanium foam specimens prepared at different heat treatment temperatures for the Vickers hardness test. Titanium foam samples were polished by emery papers of 1000#, 1200#, 2000#, and 3 μm diamond. Vickers hardness test was conducted using Hardness Testing Machine (SHIMADZU, HMV-2T, Japan) in the cell wall of titanium foam. The effect of the heat treatment on the Vickers hardness of titanium foams are shown in Fig.4.8. Vicker hardness of Ti-6Al-4V foams are about 376 Hv, the hardness of 1173 K and 1323 K are about 344 Hv and 358 Hv. There is plate on top and bottom of Ti-6Al-4V foams, the Vicker hardness of plate are about 422 Hv, After heat treatment 370 HV of 1173 K and 384 Hv of 1323 K.

4.3.3 Compressive characterization

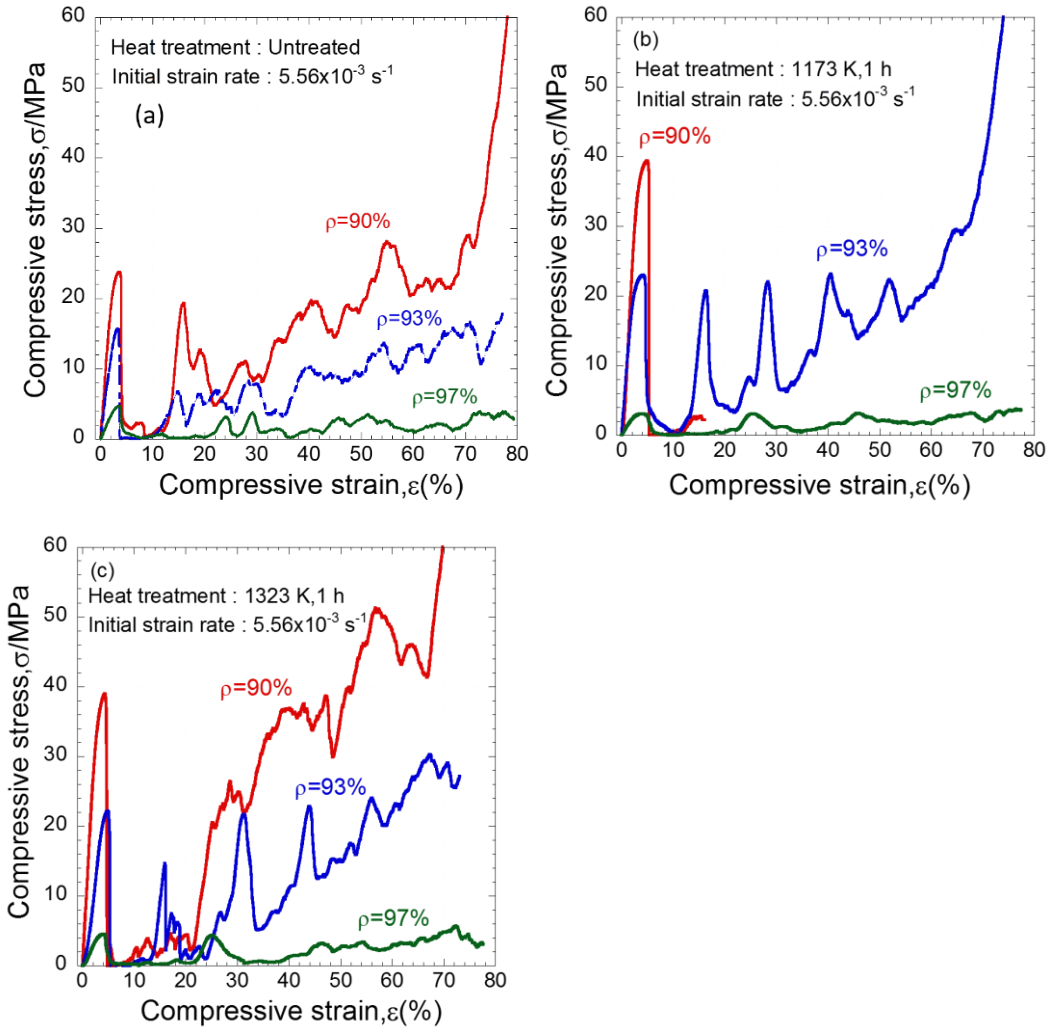

Fig. 4.9 Compressive stress-strain curves of porous Ti-6Al-4V alloys. (a) As-built, after annealing at (b) 1173 K and (c) 1323K.

The result shows that compression curve of titanium foam including linear elastic region, plateau region and densification region in Fig. 4.9. The heat treatment has a good effect on Ti-6Al-4V titanium foam shown. For porosity of 90%, yield strength of initial sample, sample with annealing 1173 K and sample with annealing 1323 K are 24 MPa, 40 MPa and 38.5 MPa, respectively. For porosity of 93%, yield strength of initial sample, sample with annealing 1173 K and sample with annealing 1323 K are 15 MPa, 22.5 MPa

and 23 MPa, respectively. For porosity of 97%, yield strength of initial sample, sample with annealing 1173 K and sample with annealing 1323 K are 4.8 MPa, 3 MPa and 4.5 MPa, respectively. The yield strength enhanced by the annealing process for porosity of 90% and 93%. Occurred a 45-degree (diagonal) shear fracture in beginning of strain 5.7% in Fig. 4.10. A 45-degree (diagonal) shear band for fracture surface from titanium foams shown in Fig. 4.11. Provide a more complete picture of the fracture mechanism. The compressed Ti alloy sample is found at the same place, cracks are distributed in the connecting of the cell wall. This is mainly because the Ti alloy foam have the brittle failure character with dense titanium alloy. The different porosity does not determiner the fracture surface. Thin cell wall is import reason for shear band. The Fracture surface show some dimples in the surface.

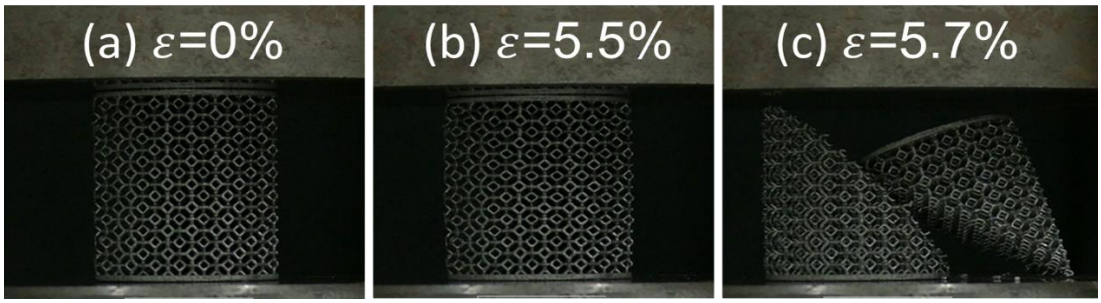

Fig. 4.10 Photographs of the porous Ti-6Al-4V specimen during the compression test.

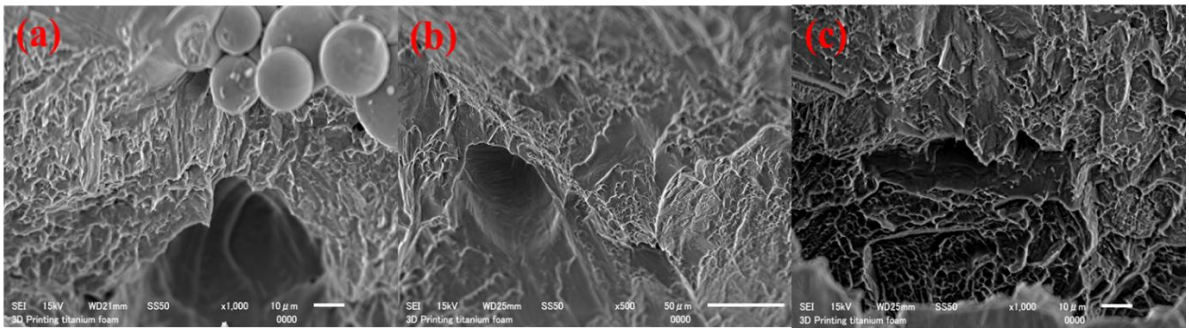

Fig. 4.11 SEM micrographs of the fracture surface of the cell edges. The nominal porosities are (a) 90%, (b) 93% and (c) 96%.

4.3.4 Energy absorption

The energy absorption capacity is determined the energy necessary to deform specimen to plateau end strain according to international standard ISO 13314:2011(E) [79]. Absorption energy capacity is W, compressive strain is ε, the area under the stress–strain curve is calculated using Formulae (4.1) as:

$$W = \int_0^{\varepsilon_0} \sigma(\varepsilon)\,\mathrm{d}\varepsilon \quad \text{..... (4.1)}$$

Energy absorption of Ti-6Al-4V titanium foam of 90%, 93%, 97% porosity at room temperature are 5.61 MJ/m^3, 2.84MJ/m^3, 0.66 MJ/m^3. After 1173 K heat treatment, Ti-6Al-4V titanium foam of 90% porosity show a diagonal shear band at a strain of 5.7% in Fig. 4.9. The energy absorption of 93% porosity and 97% are 5.33 MJ/m^3, 0.65 MJ/m^3 at 1173 K heat treatment. For 1323 K heat treatment, energy absorption of Ti-6Al-4V titanium foam of 90%, 93%, 97% porosity are 9.66 MJ/m^3, 4.14 MJ/m^3, 0.69 MJ/m^3, respectively. Compression properties of as-built and annealed porous Ti-6Al-4V alloy specimens, compared initial peak stress and absorbed energy capacity were showed by bar graphs in Fig. 4.12. We can see that the energy absorption increases with the porosity

decreases, for the yield stress decreases with the porosity, the area under the stress–strain curve also decreases.

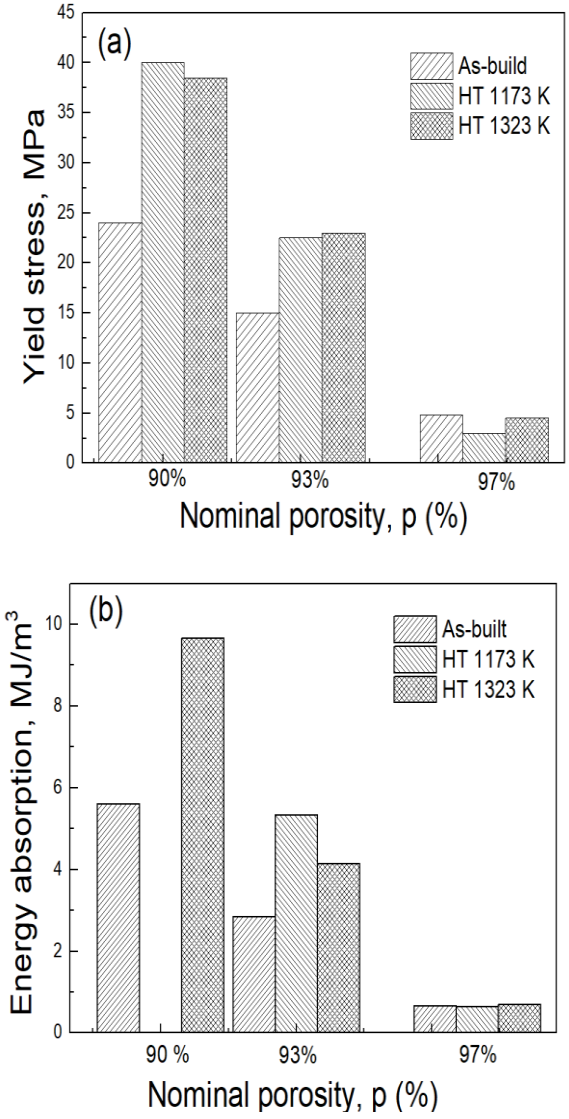

Fig. 4.12 Compression properties of as-built and annealed porous Ti-6Al-4V alloy specimens. Compare initial peak stress and absorbed energy by bar graphs.

4.4 Discussion

4.4.1 Microstructure and fracture surface

Titanium foams are cellular structure consisting of solid metal and pores, a strong effect of annealing on mechanical behavior of Ti-6Al-4V foams have revealed by stress-strain curves. The reason may be due to for laser sintering, a Widmanstätten structure composed of needle-like α-phase grains (acicular alpha) and α ' martensite phase which is a non-equilibrium phase were formed. Alpha phase is HCP, beta phase is BCC. At 1155 K, Alpha phase is beginning to slip, got beta phase. It is noted that α phase was detected, which proves that the solidification of titanium foam was same with the bulk titanium alloy. the movement of atoms has the effect of redistributing and eradicating the dislocations in titanium foams. The recrystallization annealing changed those grain deformed by internal stresses to new strain-free grains nucleate and made it grow.

The effective stress on the foams with uniform structure is more concentrated on 45-degree shear surface and propagated outward for Ti-6Al-4V foams which were deformation 5.7% will possess fracture. For the porous Ti-6AL-4V prepared by the SLM method, energy absorption efficiency was extremely low because of occurrence of shear fracture. Shear fracture is attributable to a regulated cell structure, it prevents shear fracture by preventing load concentration in the shear direction such as introduction of randomness into the cell structure and curved load surface, energy absorption efficiency can be expected.

4.4.2 Compressive characteristics

The quasi-static compressive stress–strain curves for various porosity titanium alloy foams have been studied using UTM. The compressive strength of foams not only depend on porosity but also depend on annealing temperature. The higher the foams porosities are implying lower yield stress. Due to the porosity is small and the cell wall is thick, collapse of the cell wall is gentle deformation. For titanium ally foams, macrostructure and microstructure of titanium alloy foams are in good combination. As the cell wall and skin microstructures can dramatically affect the mechanical response of metallic foams; in fact, the grain size and distribution of phases influence the material compressive performance. While the compressive deformation, it is important to evaluate the energy absorbed before the foam was compacted, because if the foam was compacted the buffering effect would be decreased seriously. Yield strength of Ti-6Al-4V in porosity of 90% was 24 MPa, yield strength of commercial pure titanium in porosity of 90% was 8 MPa, it has improved enormously compared to commercial pure titanium foam with Octahedron structure.

4.4.3 Energy absorption characteristics

The mechanisms properties of titanium foam depend on geometry structure of open cells and porous plastic or brittle material. Elastic deformation, plastic deformation or brittle deformation of porous titanium foam are related to energy absorption, the collapsed cell walls and the creation of surface appeared friction behavior. Energy absorption of open-cell titanium foams were bending and collapsing of the walls for interconnect cell structure, it mainly carried out in the steady stress plateau. The experimental results show that titanium alloy foams of different porosity exhibit different

energy absorption capacity. The porosity of titanium and titanium alloy foams decreased regularly along with the increase of energy absorption capacity and the energy absorption efficiency as strain of 50%, became insensitive to porosity. Therefore, it is important to know the annealing process improvement of mechanical properties and energy absorption capacity. Actual morphologies of cellular structure showed random unit cell and truncated octahedron, for some specific application, order pore structure is used for impact energy absorption capacity, it has been discussion in public paper [126]. Energy absorption capacity of Ti-6Al-4V in porosity of 90% was 5.6 MJ/m^3, Energy absorption of commercial pure titanium in porosity of 90% was 2.1 MJ/m^3, Energy absorption capacity of Ti-6Al-4V compared obviously with that of commercial pure titanium in porosity of 90% with octahedron structure.

4.5 Conclusion

In this report, the influence of different heat treatment on the mechanical behavior was investigated. The original sample was compared to the stress relief annealing and recrystallization annealing samples. Experimental and numerical analysis was conducted on titanium foam.

(1) Ti-6Al-4V foams have higher yield strength and stress-strain curve with lower porosity. Titanium and alloy foam are lower Vickers hardness with higher annealing temperature.

(2) Energy absorption capacities of titanium and alloy foams are distinctions after different annealing temperature. Ti-6Al-4V foams are higher available energy absorption capacity at 1173 K and 1323 K.

(3) Effect of temperature is important for recrystallization annealing process. Due to microstructure of titanium foam, Alpha phase is HCP, beta phase is BCC. At 1155 K, Alpha phase is beginning to slip, got beta phase.

(4) At Porosity of 90 %, specimen of Ti-6Al-4V foam as annealing 1173 K appeared shear fracture mainly in at 45-degree compression direction.

As described above, problems have been discovered for the metal foams by SLM method, in future changing the unit cell geometry and the shape of specimens, application as an excellent impact absorbing member can be expected.

References

[113] Izzati NF, Nazri M. Effect Of Yeast Content As Foaming Agent On The Mechanical Properties Of Titanium Foam. 2015.

[114] Arifin A, Sulong AB, Muhamad N, Syarif J, Ramli MI. Material processing of hydroxyapatite and titanium alloy (HA/Ti) composite as implant materials using powder metallurgy: a review. Materials & Design 2014;55:165-75.

[115] Zhu C, Liu T, Qian F, Chen W, Chandrasekaran S, Yao B, et al. 3D printed functional nanomaterials for electrochemical energy storage. Nano Today 2017;15:107-20.

[116] Mirbagheri SMH, Vali H, Soltani H. Heat Treatment of Closed-Cell A356 + 4 wt.%Cu + 2 wt.%Ca Foam and Its Effect on the Foam Mechanical Behavior. Journal of Materials Engineering and Performance 2017;26:14-27.

[117] Campana F, Pilone D. Effect of heat treatments on the mechanical behaviour of aluminium alloy foams. Scripta Materialia 2009;60:679-82.

[118] D LEHMHUS JB. Properties of heat-treated aluminium foams [J]. Materials Science and Engineering: A 2003;349:98-110.

[119] Zhou J, Gao Z, Cuitino A, Soboyejo W. Effects of heat treatment on the compressive deformation behavior of open cell aluminum foams. Materials Science and Engineering: A 2004;386:118-28.

[120] Schüler P, Frank R, Uebel D, Fischer SF, Bührig-Polaczek A, Fleck C. Influence of heat treatments on the microstructure and mechanical behaviour of open cell AlSi7Mg0. 3 foams on different lengthscales. Acta Materialia 2016;109:32-45.

[121] Sun Y, Burgueño R, Wang W, Lee I. Effect of annealing on the mechanical properties of nano-copper reinforced open-cell aluminum foams. Materials Science and Engineering: A 2014;613:340-51.

[122] Sun P, Fang ZZ, Koopman M, Paramore J, Chandran KR, Ren Y, et al. An experimental study of the (Ti–6Al–4V)–xH phase diagram using in situ synchrotron XRD and TGA/DSC techniques. Acta Materialia 2015;84:29-41.

[123] Thijs L, Verhaeghe F, Craeghs T, Van Humbeeck J, Kruth J-P. A study of the microstructural evolution during selective laser melting of Ti–6Al–4V. Acta Materialia 2010;58:3303-12.

[124] Vrancken B, Thijs L, Kruth J-P, Van Humbeeck J. Heat treatment of Ti6Al4V produced by Selective Laser Melting: Microstructure and mechanical properties. Journal of Alloys and Compounds 2012;541:177-85.

[125] Sallica-Leva E, Jardini A, Fogagnolo J. Microstructure and mechanical behavior of porous Ti–6Al–4V parts obtained by selective laser melting. Journal of the Mechanical Behavior of Biomedical Materials 2013;26:98-108.

[126] Liang C-C, Shi Z-L, He C-T, Tan J, Zhou H-D, Zhou H-L, et al. Engineering of Pore Geometry for Ultrahigh Capacity Methane Storage in Mesoporous Metal–Organic Frameworks. Journal of the American Chemical Society 2017;139:13300-3.

Chapter 5: Conclusions and future works

5.1 Conclusions

Based on the results of present investigation, the following conclusions can be drawn:

5.1.1 Strain rate sensitivity of open-cell titanium foam at elevated temperature

The hot deformation behavior of open cell pure titanium was studied in temperature ranging from 300 K to 773 K and strain rates ranging from 0.1 to 10 mm/min. Strain rate sensitivity exponent of the titanium foam was low and close to that of dense CP titanium. Deformation behavior of the titanium foam at relatively low strain rates can be controlled by the mechanical properties of the base titanium.

5.1.2 Compressive behavior of open-cell titanium foams with different unit cell geometries

Different compression direction was in order to estimate mechanical properties of open cell Titanium. Unit cell geometries of open cell titanium foam was studied. Plateau stress and absorbed energy of open-cell titanium foams increased with decreasing the porosity. Plateau stress and absorbed energy of the titanium foams with the truncated octahedron unit cells were higher than rhombic dodecahedron unit cells. Plateau stresses of Octa_A and Dodeca_C specimens were higher than those of other specimens. The reason is due to Parallel edges against the compression direction are effective to increase the initial flow stress.

5.1.3 Effect of heat treatment on mechanical properties of porous Ti-6Al-4V alloy manufactured by 3D selective laser melting

Influence of annealing on the mechanical behavior was investigated. Microstructure and simple fracture surface were obtained. Ti-6Al-4V foams have higher yield strength and stress-strain curve with lower porosity. Compression deformation of Ti-6Al-4V is influenced by the annealing temperature remarkably, Titanium and alloy foam are lower Vickers hardness with higher annealing temperature. Energy absorption capacities of titanium and alloy foams are distinctions after different annealing temperature. Ti-6Al-4V foams are higher available energy absorption capacity at 1173 K and 1323 K. Thin cell wall is import reason for shear band. The Fracture surface show some dimples in the surface.

5.1.4 Discussion about order and disorder cell Structure

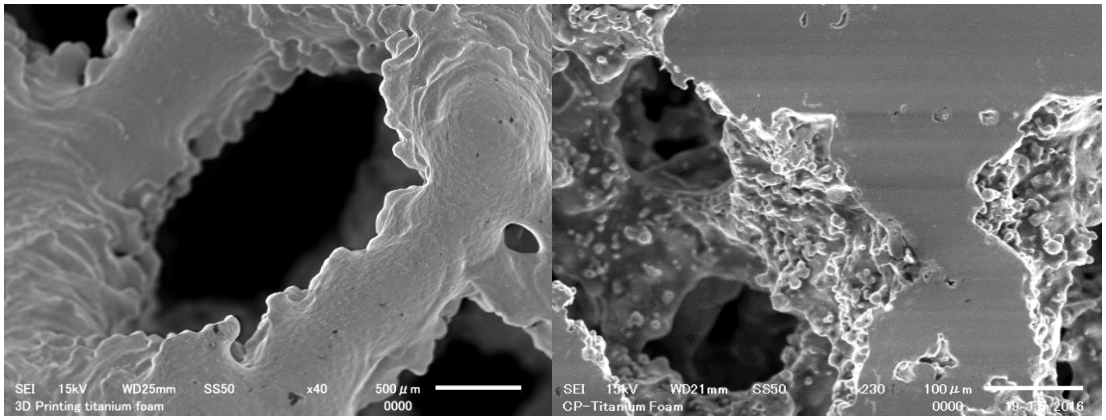

Order cell structure **Disorder cell structure**

Fig 5.1 Compare cell wall of order structure and cell wall disorder cell structure

Order cell structure has same thickness, length, same cell distribution, however for disorder cell structure, cell wall is Random. Order cell structure is easier to shape

control, with repeatability and stable mechanical properties. Titanium foam with Order cell structure could solve the specific needs.

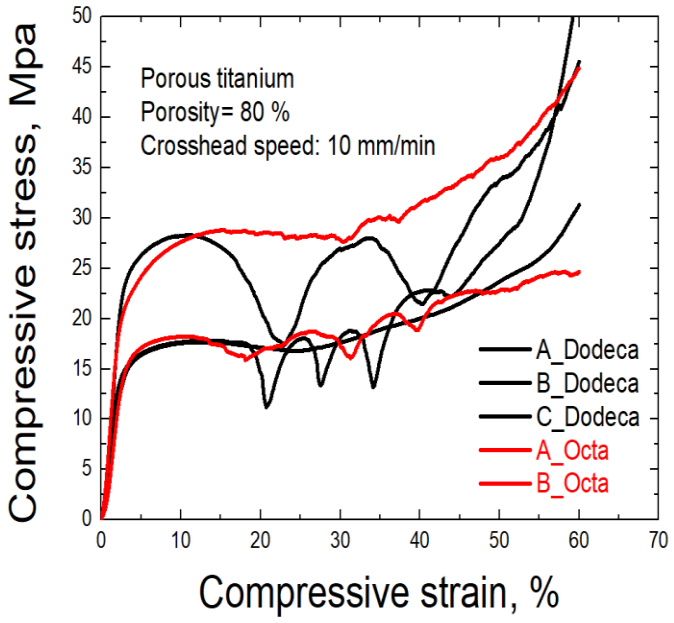

Fig 5.2 (a) Titanium foam with ordered cell structure

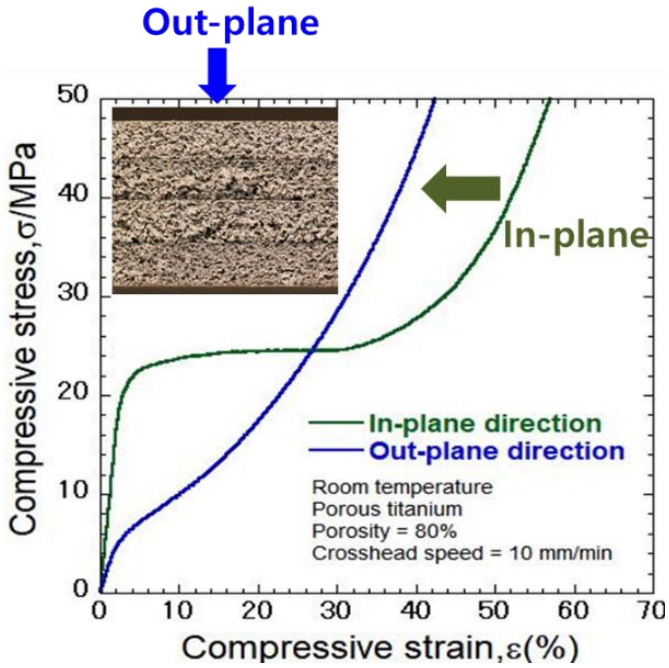

Fig 5.2 (b) Titanium foam with disordered cell structure

Specimens made by additive manufacturing in Fig 5.2(a), Stress-strain curves of ordered cell structure have double and multi peak curve, due to some shear band formation in deformation process. However, for disordered cell structure by traditional method (powder metallurgy) in Fig 5.2(b), Stress-strain curves is smooth curve. No obvious shear band is observed. Disordered and Ordered cell are able to fabricate by additive manufacturing, however it is difficult to make order cell structure by traditional method. the yield stress of sample is lower than octahedron structure specimen. The reason is the appearance of some defect were in remove space holder for traditional method. There are shear band formation in compressive deformation of ordered cell structure specimens, hence disordered cell structure using additive manufacturing was recommend in future research.

5.2 Suggestions for future work

5.2.1 Finite element method for dynamic properties of open cell titanium foam by additive manufacturing

This future research illustrates various dynamic characteristics of open cell 3D-printing titanium foams. The foam is obtained from the selective laser melting(SLM) process. Open-cellular 3D printing titanium foam and related complex structures, where porosity and associated mechanical behavior, including Young's modulus or elastic modulus can be controlled by several truncated octahedron and rhombic dodecahedron unit cell formats and models.

In parallel to experimental measurements, finite element method (FEM) have been performed to study the stress distribution globally and locally around the designed pores.

Consistent with FEM, a high elastic modulus was recorded with the rhombic dodecahedron unit cell.

5.2.2 Effect of voronoi cell structures on mechanical properties of titanium foams

The effects of voronoi geometry on the mechanical properties of high-porosity cellular titanium foam fabricated by Selective Laser Melting (SLM) were examined at room temperature. SEM was used to investigate the edge thickness of titanium foam, the yield strengths of voronoi materials produced by SLM were comparable with different porosity specimens, energy absorption of specimens were subjected.

Appendix

Appendix A. Publications

Parts of this work have been published or have submitted for the publication in the following papers:

1. Xue-Zheng Yue, Keiji Matsuo, Koichi Kitazono, Compressive behaviors of open-cell titanium foams with different unit cell geometries, Material Transaction, 2017；58: 1587-1592.

2. XZ Yue, K Kitazono, Strain rate sensitivity of open-cell titanium foam at elevated temperature, Mater. Sci. Eng. A, 2016; Vol 673: 83-9.

3. XZ Yue, K Kitazono, X-J Yue, B-Y Hur. Effect of fluidity on the manufacturing of open cell magnesium alloy foams. Journal of Magnesium and Alloys 2016; 4 :1-7.

4. XZ Yue, Bo-Young Hur,,Effect of the Holding Temperature and Vacuum Pressure for the Open Cell Mg Alloy Foams, Kor. J. Mater. Res, v.22, no.6, pp.309-315, 2012, 6

5. XZ Yue, Bo-Young Hur, Fluidity and Mechanical Properties of Open Cell AZ31 Mg Alloy Foam, Journal of the Korean Foundrymen's Society, 2012.5

6. Xue zheng Yue, Hiroshi Fukazawa, Kazuya Maruyama, Keiji Matsuo, Koichi Kitazono, Effect of heat treatment on the mechanical properties of open cell titanium foam, Additive Manufacturing, paper in progress.

Appendix B. Conferences and Presentations

Parts of this work have been presented in the following conference.

International conference proceedings:

1. XZ. Yue, K. Matsuo, K. Kitazono, Effects of cell geometry on compressive deformation of open-cell titanium foams, Metfoam2017, Nanjing, China, September 2017, in press

2. XZ. Yue, H. Fukazawa, K. Kitazono, Strain rate sensitivity of open-cell titanium foam at elevated temperature, PRICM9, Kyoto, Japan, August 2016, P 823-828.

Japanese conference proceedings

XZ. Yue, H. Fukazawa, K. Kitazono High temperature deformation of titanium foams, 第 161 回超塑性研究会, Japan, Feb 2017, No.1

Award

Yue xuezheng, Strain rate sensitivity of open-cell titanium foam at elevated temperature, Excellent poster award for young scientist, PRICM9, 2016-8-4